MONTE CARLO SIMULATION OF INDIRECT DAMAGE TO
BIOMOLECULES IRRADIATED IN AQUEOUS SOLUTION--
THE RADIOLYSIS OF GLYCYLGLYCINE

By

WESLEY EMMETT BOLCH

A DISSERTATION PRESENTED TO THE GRADUATE SCHOOL
OF THE UNIVERSITY OF FLORIDA IN PARTIAL FULFILLMENT
OF THE REQUIREMENTS FOR THE DEGREE OF
DOCTOR OF PHILOSOPHY

UNIVERSITY OF FLORIDA

1988

ii

research. The author would like to thank both Dr. Rufus Ritchie for developing the electron thermalization scheme used in this dissertation and Dr. Hiroko Yoshida for her experimental data which supported the computer simulations of this research. In addition, the author expresses his appreciation to Dr. Warren M. Garrison for his comments and suggestions.

Finally, the author wishes thank his wife, parents, and family for their continued and steadfast support.

TABLE OF CONTENTS

MONTE CARLO SIMULATION OF INDIRECT DAMAGE TO
BIOMOLECULES IRRADIATED IN AQUEOUS SOLUTION--
THE RADIOLYSIS OF GLYCYLGLYCINE

By

WESLEY EMMETT BOLCH

AUGUST 1988

Chairman: Charles E. Roessler
Major Department: Environmental Engineering Sciences

The objective of this dissertation is to determine the feasibility

of studying indirect damage to biological molecules irradiated in

aqueous solution using detailed Monte Carlo computer simulations. The

molecule glycylglycine is chosen for this study primarily because its

radiation chemistry is reasonably well characterized, thus limiting the

number of unknowns in the modeling effort. Good agreement between

calculated and measured yields of radiolysis products supports this

calculational technique and its usefulness in investigating more complex

molecules, such as DNA.

The study involves three major tasks. First, a Monte Carlo

computer code is developed for simulating the radiolysis of

glycylglycine in both oxygenated and deoxygenated aqueous solution.

Second, this model is used to calculate the yields of various products in solutions irradiated either by 250-kVp X-rays or by ^{60}Co gamma rays. Third, calculated product yields are compared to measured yields where available.

The Monte Carlo computer codes used in this study are modified and extended versions of three existing simulation codes, written at the Oak Ridge National Laboratory (ORNL), which simulate irradiations of pure liquid water. The ORNL codes calculate the formation, diffusion, and reaction of free radicals and other species along charged-particle tracks in liquid water. As part of this research, these codes are extended to simulate irradiation of pure oxygenated water, oxygenated glycylglycine solutions, and deoxygenated glycylglycine solutions.

Ammonia is released from the reaction between glycylglycine and hydrated electrons within the track. In simulated irradiations of deoxygenated glycylglycine solutions by 250-kVp X-rays, calculated yields of ammonia are in statistically significant agreement with measured yields. In addition, calculated yields of ammonia produced during ^{60}Co gamma irradiation are shown to be greater than calculated yields of ammonia produced during X irradiation. The Monte Carlo code readily shows that this difference is attributable to track-structure effects. This study concludes that Monte Carlo simulations represent a unique and feasible method of understanding indirect radiation damage at the molecular level.

CHAPTER 1

INTRODUCTION

Since the release of the International Commission on Radiological
Protection's Publication 26, recommended limits of exposure to ionizing
radiation have been based upon the risk of stochastic and nonstochastic
effects (ICRP 1977). Central to this system of radiation protection are
risk estimates for human cancer induction and germ cell mutation at low
doses and at low dose rates. Current risk estimates are primarily
obtained through extrapolation of human and animal data at high doses
and dose rates using an assumed shape of the dose-response function at
lower dose levels. Since actual risks of stochastic effects are small
and these effects occur naturally, any epidemiological study seeking to
statistically verify risk estimates at low doses would require a
prohibitive number of subjects. Consequently, efforts to quantify the
dose-response function cannot rely solely upon empirical observation,
but must include research into the mechanisms and supporting theory
behind carcinogenesis and mutagenesis (Upton 1982; Sinclair and Fry
1987).

Deoxyribonucleic acid (DNA) has long been recognized as a critical
molecular target for radiation-induced stochastic effects (Sonntag
1987). The ultimate expression of these effects can be attributed to

1

three fundamental processes: (1) the creation of damage sites in cellular DNA by ionizing radiation; (2) the enzymatic repair of damage sites by the cell; and (3) the propagation of unrepaired damage and its subsequent effects on cellular growth and function. Studies have revealed many details of the latter two processes (Sinclair and Fry 1987). From investigations into the first process, it is known that irradiation of DNA produces strand breaks, base damage, base deletions, DNA-DNA crosslinks, and DNA-protein crosslinks. What is poorly understood, however, are the physical and chemical mechanisms by which radiation produces these types of damage. All three processes, however, must be understood to some degree of detail before a theoretical derivation of the risk of stochastic effects is feasible.

In an attempt to identify the fundamental mechanisms of radiation-induced damage to DNA, a collaborative investigation was initiated between researchers in the Health and Safety Research Division and the Biology Division of the Oak Ridge National Laboratory (ORNL) during the summer of 1986. This effort proposes investigating various molecular systems of increasing complexity. These systems would begin with simple amino acid polymers and would then be extended stepwise through artificially-synthesized DNA subunits of increasing complexity, ultimately to DNA itself.

For each molecular system, two coordinated investigations would be carried out--one experimental and one calculational. In the experimental effort, aqueous solutions of the molecule would be irradiated and the chemical yields of radiation products measured.

In the calculational effort, the radiation experiment would be simulated in complete detail by a Monte Carlo computer model. This computer model would incorporate specific reaction mechanisms that lead to the observable quantitative chemical yields. Comparison of calculated and experimental yields could thus be used to develop a detailed understanding of the mechanisms and pathways by which radiation produces damage at the molecular level. In many instances, this modeling effort would be a first attempt at linking the detailed physics of radiation energy deposition to the detailed chemical damage subsequently produced within biomolecules.

This dissertation presents simulations of the first molecular system to be studied under this new technique. The first system chosen is glycylglycine (a dimer of the amino acid glycine) in aqueous solution. This system has three characteristics which make it a suitable candidate for initial investigation. First, mechanisms of glycylglycine radiolysis have been proposed by past researchers (Makada and Garrison 1972; Garrison *et al*. 1973); thus a framework for model development already exists. Second, the reactions exhibit very little feedback, a fact that, while non-essential, simplifies the simulations. Third, glycylglycine is a relatively small molecule. Consequently, at concentrations ≤ 1.2 M, radiation damage is mostly caused by attack of free radicals produced during irradiation of surrounding water (indirect effects), and not by direct interaction with the incident radiation or its secondary charged particles (direct effects).

Radiolysis of Pure Liquid Water

Radiolysis is defined as chemical decomposition by the action of radiation. By considering a small volume within an irradiated medium, the events which precipitate chemical change can be described in stages. If the volume has dimensions no larger than a few tens of nanometers, these stages begin, at a reference time zero, with the traversal of a charged particle produced directly or indirectly by the radiation source. Only in the case of very high dose rates would this volume be traversed by a second charged particle at a time prior to the completion of these stages. Table 1-1 summarizes the events which characterize these stages and their associated time periods.

Physical Stage

A charged-particle traversing a water volume transfers its energy through inelastic collisions resulting in ionization or excitation of water molecules. Elastic collisions result in a change in trajectory of the primary particle with negligible energy transferred to the water medium. Secondary electrons produced in ionizations may have sufficient energy to ionize and excite water molecules, yet are eventually degraded in energy below the threshold for producing further electronic transitions. The primary particle thus leaves in its wake a track of ionized water molecules (H_2O^+), excited water molecules (H_2O^*), and subexcitation electrons (e_{sub}^-). These events are complete by $\sim 10^{-15}$ s since the passage of the primary particle.

Table 1-1

Stages of Radiolysis for Low-Dose-Rate Irradiations

Stage	Time Period (s)	Events
Physical	$0 - 10^{-15}$	Production of H_2O^*, H_2O^+, and e^-_{sub}
Prechemical	$10^{-15} - 10^{-12}$	Production of H, OH, H_2, H_2O_2, H_3O^+, and e^-_{aq}
Early Chemical	$10^{-12} - 10^{-6}$	Diffusion of track species Chemical reactions within individual charged-particle tracks
Late Chemical	$> 10^{-6}$	Diffusion of track species Chemical reactions between neighboring charged-particle tracks

When the water medium is in the liquid state, the creation of H_2O^+ and H_2O^* are not always localized at the site of initial energy transfer (Heller *et al.* 1974; Ritchie *et al.* 1978). Inelastic collisions in liquid water can result in energy transfers involving $\sim 10^9$ electrons. These collective excitations eventually produce an H_2O^+ or H_2O^* at a site which can be located up to nanometers from the trajectory of the primary particle. This delocalization of energy transfer can play an important role in the subsequent chemistry of the charged-particle track.

The mean rate of energy loss by a charged particle per unit pathlength x in a given medium is called the stopping power of the medium, $(-dE/dx)$. The stopping power of liquid water for electrons, as given by theoretical calculations, is shown in Fig. 1-1. Above 1 MeV, $-dE/dx$ gradually increases due to radiative losses and a relativistic rise in collision losses. The stopping power of liquid water for a charged particle is also referred to as that particle's unrestricted linear energy transfer, or LET.

Prechemical Stage

During the time period from $\sim 10^{-15}$ s to $\sim 10^{-12}$ s, the medium responds to initial changes produced during the physical stage, yet there is not time enough for appreciable diffusion and chemical reaction to take place. An ionized water molecule is thought to react quickly with a neighbor water molecule forming a hydronium ion and a hydroxyl radical:
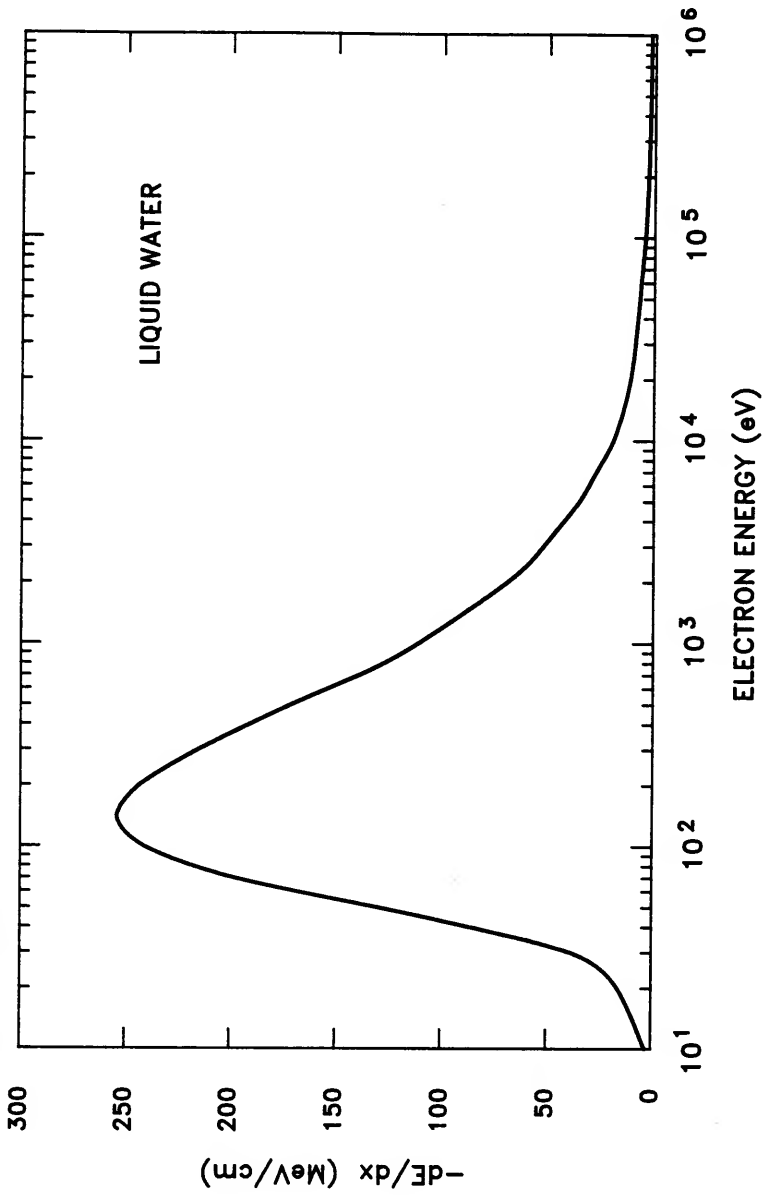
Fig. 1-1. Calculated stopping power of liquid water for electrons (Paretzke *et al.* 1986).

$$H_2O^+ + H_2O \longrightarrow H_3O^+ + OH \ . \qquad (1-1)$$
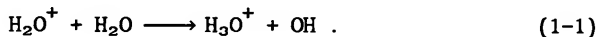
There is experimental evidence (Ogura and Hamill 1973; Hamill 1969) that the H_2O^+ may first migrate (via charge transfer) several tenths of a nanometer before undergoing reaction (1-1). Depending upon the particular molecular transition involved, excitations are thought to either dissociate according to

$$H_2O^* \longrightarrow \begin{cases} H + OH \\ H_2 + O \end{cases} , \qquad (1-2)$$
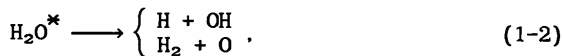
or autoionize with the resulting H_2O^+ undergoing reaction (1-1). The oxygen atom in reaction (1-2) reacts with a neighboring water molecule to form hydrogen peroxide. Also during this time, subexcitation electrons continue to lose energy through vibrational and rotational excitations of the surrounding medium, eventually reaching thermal energies. They become hydrated by $\sim 10^{-12}$ s and are denoted by the symbol e_{aq}^-.

Early Chemical Stage

At $\sim 10^{-12}$ s, a charged-particle track consists of a spatial distribution of OH, H, H_2, H_2O_2, H_3O^+, and e_{aq}^-. These species subsequently undergo diffusion and chemical reaction within the track, resulting in a net decrease of OH, H, e_{aq}^-, and H_3O^+ and a net increase

of H_2, H_2O_2, and OH^-. After $\sim 10^{-6}$ s, the track species have diffused to such an extent that further intratrack reactions are very unlikely and all details of track structure are lost.

Two factors which can provide additional reactions during the early chemical stage are the presence of a radical-scavenging solute and track overlap during irradiations at high dose rates. Radical scavengers compete with intratrack reactions at times dependent upon their concentration. Scavenging reactions are appreciable at $\sim 10^{-7}$ s at one millimolar scavenger concentrations and at $\sim 10^{-10}$ s at one molar scavenger concentrations (Wright *et al.* 1985a). In addition, the degree to which scavenging reactions compete for species within the track lessens with increases in particle LET.

For systems irradiated at very high dose rates, charged-particle tracks can be produced in both temporal and spatial proximity. Under these conditions, intertrack reactions occur at times prior to 10^{-6} s. Examples include systems irradiated by pulses of accelerated electrons, as in pulse radiolysis experiments.

Late Chemistry Stage

With the completion of intratrack reactions, all remaining species continue to diffuse and react with species from neighboring tracks. At high dose rates, this late chemistry stage is characterized primarily by inhomogeneous reactions occurring within track overlap. At lower dose rates, little overlap occurs before the remaining species have diffused far apart and the chemistry of the system quickly becomes one of

homogeneous, steady-state reactions. The time at which the number of intertrack reactions exceeds the number of intratrack reactions is thus dose-rate dependent. At low dose rates, this time is $\sim 10^{-6}$ s.

Research Objective

The objective of this dissertation is to determine the feasibility of studying indirect radiation damage to glycylglycine through detailed Monte Carlo computer simulations. This task is accomplished in three stages. First, a computer model is developed for single-track simulations of glycylglycine radiolysis, through the early chemical stage, in both oxygenated and deoxygenated solutions. Second, this code is used to calculate microsecond yields of various radiation products. Third, these calculated yields are compared to experimental values where available. If reasonable agreement is shown, the calculational approach and its usefulness in investigating more complex molecular systems will be supported.

Table 1-2 summarizes the modeling effort of this and previous studies, along with experimental data currently available with which to make comparisons. The left-hand column lists the four stages of radiolysis, while the remaining columns correspond to three model systems of interest: pure water, deoxygenated glycylglycine solutions, and oxygenated glycylglycine solutions. For the pure water system, a computer model simulating the first three stages was developed at ORNL. Time-dependent yields of OH and e_{aq}^{-} calculated by this code for the

Table 1-2

Summary of Modeling Effort and Experimental Data

Stages of Radiolysis	Systems Modeled		
	Pure Water	Deoxygenated Glycylglycine	Oxygenated Glycylglycine
Physical			
Simulation	Oak Ridge Model	Oak Ridge Model	Oak Ridge Model
Experiment	No Data	No Data	No Data
Prechemical			
Simulation	Oak Ridge Model	Oak Ridge Model	Oak Ridge Model
Experiment	No Data	No Data	No Data
Early Chemical			
Simulation	Oak Ridge Model	This Research	This Research
Experiment	Refs. a,b,c	Refs. g,h	No Data
Late Chemical			
Simulation	Refs. d,e	Future Research	Future Research
Experiment	Ref. f	Refs. g,h	Refs. g,i

References: [a]Jonah et al. (1976)
 [b]Jonah and Miller (1977)
 [c]Sumiyoshi and Katayama (1982)
 [d]Chatterjee et al. (1983)
 [e]Boyd et al. (1980)
 [f]Hochanadel (1952)
 [g]Yoshida et al. (1988)
 [h]Garrison et al. (1973)
 [i]Makada and Garrison (1972)

early chemical stage can be compared to pulse radiolysis measurements in the open literature (Jonah *et al.* 1976; Jonah and Miller 1977; Sumiyoshi and Katayama 1982). In addition, analytical techniques exist for calculating product yields at late times (Chatterjee *et al.* 1983; Boyd *et al.* 1980). Experimental data also exist for this late chemistry stage (Hochanadel 1952).

At glycylglycine concentrations ≤ 1.2 M, indirect radiation effects dominate and the Oak Ridge model can therefore be used, as is, to simulate the physical and prechemical stage of glycylglycine radiolysis (see Table 1-2). Thus, this dissertation primarily involves the development of a simulation code for the early chemical stage of glycylglycine radiolysis in both oxygenated and deoxygenated solutions. Future efforts will include modeling the late chemistry stage of glycylglycine radiolysis by applying the techniques of Chatterjee *et al.* (1983) to the microsecond yields calculated in this dissertation.

Several end products are formed as a result of glycylglycine radiolysis. Experimental efforts at ORNL currently provide yields of both free ammonia and glycylamide as functions of glycylglycine concentration. These yields are determined under irradiation by 250-kVp X-rays for both deoxygenated and oxygenated systems (Yoshida *et al.* 1988). In addition, previous studies provide yields of free ammonia and several other radiolysis products created in both oxygenated and deoxygenated systems under ^{60}Co irradiation (Makada and Garrison 1972; Garrison *et al.* 1973).

Free ammonia in deoxygenated solution is the <u>only</u> radiolysis product whose creation is complete within the early chemical stage. Consequently, experimental support for the simulations performed in this research is limited to comparing calculated and experimental yields of free ammonia in deoxygenated solution. Although no direct comparisons can be made, microsecond yields of additional intermediate products are also calculated for this system.

Product yields are commonly reported as G-values, the number of molecules produced per 100 eV of energy deposited in the system, and are determined as functions of solute concentration. In order to make comparisons with measured G-values of free ammonia produced in photon-irradiated systems, calculated yields are determined as follows. By definition,

$$G(NH_3^f,C) \;\; = \;\; \frac{(100) \; N_t(C)}{E_t},$$ (1-3)

where $G(NH_3^f,C)$ is the G-value of free ammonia at glycylglycine concentration C, $N_t(C)$ is the total number of NH_3 molecules produced at concentration C, and E_t is the total energy deposited in eV. Since a distribution of electron energies is produced during irradiation,

$$G(NH_3^f,C) \ = \ \frac{(100) \int_0^{E_{max}} \bar{N}(NH_3^f,C,E) \ t(E)dE}{\int_0^{E_{max}} E \ t(E)dE} \ , \qquad (1\text{-}4)$$

where $\bar{N}(NH_3^f,C,E)$ is the mean number of NH_3 molecules produced at concentration C by electrons with initial energy E, $t(E)dE$ is the total number of electrons produced with initial energies between E and E + dE, and E_{max} is the maximum initial energy of electrons produced by the incident radiation. Furthermore, $\bar{N}(NH_3^f,C,E)$ can be expressed as

$$\bar{N}(NH_3^f,C,E) \ = \ \frac{\bar{G}(NH_3^f,C,E) \ E}{100} \ , \qquad (1\text{-}5)$$

where $\bar{G}(NH_3^f,C,E)$ is the mean G-value for free ammonia production at glycylglycine concentration C produced by electrons with initial energy E. By substituting Eq. (1-5) into Eq. (1-4),

$$G(NH_3^f,C) \ = \ \frac{\int_0^{E_{max}} \bar{G}(NH_3^f,C,E) \ E \ t(E)dE}{\int_0^{E_{max}} E \ t(E)dE} \qquad (1\text{-}6)$$

or

$$G(NH_3^f,C) \ = \ \int_0^{E_{max}} \bar{G}(NH_3^f,C,E) \ W(E)dE \ , \qquad (1\text{-}7)$$

where $W(E)dE$ represents the fraction of total energy deposition contributed by electrons of initial energy E per energy interval. By this method, G-values calculated for comparison with experiment require separate determinations of $W(E)dE$ and $\bar{G}(NH_3^f,C,E)$. Microsecond yields of additional intermediate products are calculated in a similar manner:

$$G(X,C,\mu s) = \int_0^{E_{max}} \bar{G}(X,C,\mu s,E) \ W(E) \ dE \ , \qquad (1-8)$$

where $\bar{G}(X,C,\mu s,E)$ is the mean microsecond G-value of product X produced by electrons of initial energy E in a solution of glycylglycine at concentration C.

The development of a complete track model for glycylglycine radiolysis is presented in Chapters 2 through 4. Chapter 2 details the existing ORNL model for the physical, prechemical, and early chemical stages of liquid water radiolysis. Chapter 3 describes various modifications and improvements which were made to the ORNL model during this research, yet were still within the context of pure water irradiation. Chapter 4 details the development of a model for the early chemical stage of glycylglycine radiolysis in both oxygenated and deoxygenated systems.

Calculated yields of free ammonia in deoxygenated solution are then presented in Chapters 5 through 7. Chapter 5 gives calculations of

electron spectra for both X-ray and ^{60}Co irradiations, while Chapter 6

presents microsecond yields of free ammonia and additional intermediate

products calculated for monoenergetic electrons. The results of

Chapters 5 and 6 are then used in Chapter 7 to calculate free ammonia

yields in systems irradiated either by both X-rays or by ^{60}Co gamma

rays, followed by comparison with measured values. Conclusions drawn

from this modeling effort and recommendations for future investigations

are presented in Chapter 8.

CHAPTER 2

OAK RIDGE MODEL FOR WATER RADIOLYSIS

The Oak Ridge model for water radiolysis was developed at the
Health and Safety Research Division (formerly the Health Physics
Division) of the Oak Ridge National Laboratory (Hamm *et al.* 1976;
Ritchie *et al.* 1978; Turner *et al.* 1981; Wright *et al.* 1983; Turner *et
al.* 1983; Hamm *et al.* 1985; Wright *et al.* 1985a; Wright *et al.* 1985b;
Turner *et al.* 1988a; Turner *et al.* 1988b). The model is incorporated
into three Monte Carlo computer codes, OREC, SPCS, and RADLYS. These
codes correspondingly simulate the physical, prechemical, and early
chemical stages of charged-particle track development in liquid water.
The late chemistry stage, if needed, can be treated in a separate set of
calculations.

Furthermore, two versions of OREC exist--one for transporting
electrons and one for transporting protons or alpha particles. Since
all experiments in the ORNL project have been limited thus far to photon
irradiations, only the electron transport version of OREC will be
discussed in this and in other chapters. It is important to note,
however, that simulation codes for the other stages of radiolysis are
applicable for any charged-particle track. This is true for both the

pure water codes presented in this chapter and also the simulation code
for glycylglycine radiolysis presented in Chapter 4.

Physical Stage

The Oak Ridge model for the physical stage was formulated in two
phases. First, inverse mean free paths (macroscopic cross sections) for
inelastic and elastic electron-liquid water interactions were compiled
from experimental data in all three phases and from theoretical
calculations. Second, an electron transport code based upon these cross
sections was developed; the code follows a primary electron and all of
its secondary electrons through liquid water until their energies fall
below the threshold for further electronic excitation. The transport
code records the spatial location of all inelastic events and
subexcitation electrons for subsequent development of the track during
the prechemical stage.

Inverse Mean Free Paths for Inelastic Scattering

The cross sections for inelastic scattering are obtained from
dielectric theory in which liquid water is assumed to respond to the
passage of charged particles as any dielectric medium responds to an
electromagnetic disturbance (Heller *et al*. 1974; Ritchie *et al*. 1978).
This response is quantitatively characterized by the medium's complex
dielectric function $\epsilon(\omega,q)$, where ω and q are, respectively, the energy

and magnitude of the momentum transferred to the medium by the disturbance. Cross sections derived from $\epsilon(\omega,q)$ include the *a priori* collective effects characteristic of the condensed phase.

The principal cross section derived from dielectric theory is the total differential inverse mean free path (total DIMFP), $d\mu/d\omega$, and is the probability an electron of energy E will have an energy loss between ω and $\omega + d\omega$ per unit length traveled per unit energy lost. The total macroscopic cross section of the medium at energy E is obtained by integrating $d\mu/d\omega$ over all possible energy losses. For non-relativistic electrons, the total DIMFP is given by

$$\frac{d\mu}{d\omega} = \frac{1}{\pi E} \int_{q^-}^{q^+} \frac{\epsilon_2(\omega,q)}{\epsilon_1^{\,2}(\omega,q) + \epsilon_2^{\,2}(\omega,q)} \; \frac{dq}{q} \quad , \qquad (2\text{-}1)$$

where E is the electron energy, ϵ_1 and ϵ_2 are the real and imaginary parts of the dielectric function, and $q^{\pm}$ are the kinematic limits of momentum transfer. All quantities are in atomic units such that energies are given in multiples of 27.2 eV and lengths are given in multiples of 0.0529 nm. Modifications to Eq. (2-1) are used for electrons of relativistic energies. The fraction involving ϵ_1 and ϵ_2 in the integrand is the energy-loss function $Im(-1/\epsilon)$, the imaginary part of the complex function $(-1/\epsilon)$. A plot of this quantity for liquid water, which forms a three-dimensional surface as a function of ω and q, is shown in Fig. 2-1. The regions corresponding to excitation and
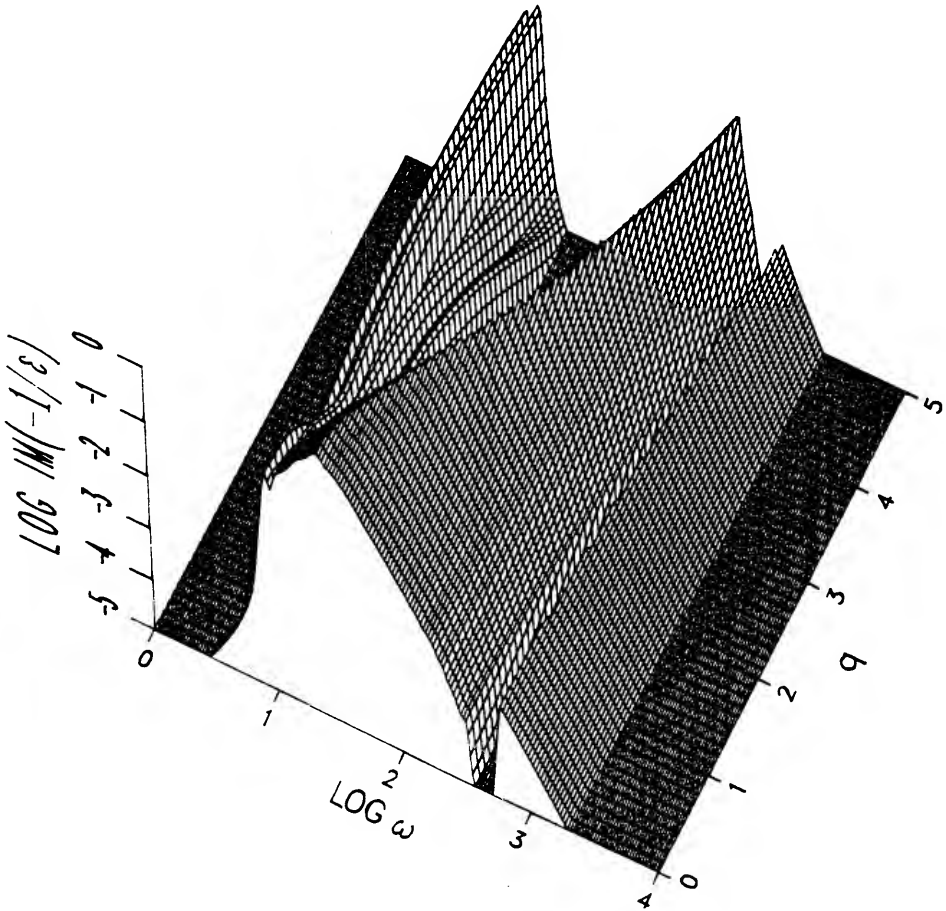
Fig. 2-1. Energy-loss function $\text{Im}[-1/\epsilon(\omega,q)]$ for liquid water above the plane $\text{Im}(-1/\epsilon) = 10^{-15}$, with ω in eV and q in atomic units (Turner *et al.* 1988b).

ionization, which merge in the q = 0 plane, separate at higher values of q. The ridge on the right at relatively large ω is due to K-shell ionization of oxygen, which has a threshold of 540 eV.

The energy-loss function in Fig. 2-1 is based on experimental data for water in all three phases and on theoretical principles. At values of q much larger than the mean momentum of electrons in the ground state of the medium, it is expected that target electrons will respond as if free and initially at rest. Values of ω and q thus become uniquely related and the energy-loss function corresponding to ionization approaches a sharp structure referred to as the Bethe ridge.

Values for the energy-loss function in the q = 0 plane are obtained directly from the optical data for liquid water. In this system, photons transfer energy but not momentum to the media surface, and $\epsilon_1(\omega,0)$ and $\epsilon_2(\omega,0)$ are inferred from measured values of surface reflectance at photon energy $E = \omega$ (Heller *et al.* 1974). The values of $\epsilon_2(\omega,0)$ and $\epsilon_1(\omega,0)$ are then fit using the functional forms

$$\epsilon_2(\omega,0) \;=\; \omega_p^2 \; \sum_n \; \frac{2\, f_n \gamma_n^3 \omega^3}{[(E_n^2 - \omega^2)^2 + \gamma_n^2 \omega^2]^2} \qquad (2\text{-}2)$$

$$\epsilon_1(\omega,0) \;=\; 1 + \omega_p^2 \; \sum_n \; f_n \; \frac{(E_n^2 - \omega^2)\,[(E_n^2 - \omega^2)^2 + 3\gamma_n^2 \omega^2]}{[(E_n^2 - \omega^2)^2 + \gamma_n^2 \omega^2]^2}, \quad (2\text{-}3)$$

where $\omega_p^2 = 4\pi N_m$, N_m is the density of water molecules, E_n are resonance energies, γ_n are damping constants, and f_n are oscillator strengths, all taken to be fitting parameters.

Values of the energy-loss function in the $q \neq 0$ portion of the $q-\omega$ plane are extrapolated by allowing the fitting parameters E_n and γ_n to become q-dependent. Constraints on fitting parameters are dictated by certain quantum-mechanical sum rules such as

$$\int_0^\infty \omega \; \epsilon_2(\omega,q) \; d\omega \;\; = \;\; \frac{\pi}{2} \; Z \; \omega_p^2 \qquad\qquad (2\text{-}4)$$

and

$$\int_0^\infty \omega \; Im\left[\; \frac{-1}{\epsilon(\omega,q)} \; \right] \; d\omega \;\; = \;\; \frac{\pi}{2} \; Z \; \omega_p^2 \; , \qquad (2\text{-}5)$$

where Z is the number of electrons per water molecule.

To account for different modes of energy absorption in liquid water, the total DIMFP is partitioned into 11 partial DIMFP's, each associated with a particular excitation or ionization transition of the water molecule. These transitions are listed in Table 2-1 along with their classification type used in the transport code. The partitioning of cross sections is accomplished by associating $\epsilon_2^{(j)}(\omega,q)$ with the jth mode of energy absorption such that $\epsilon_2(\omega,q) = \Sigma_j \; \epsilon_2^{(j)}(\omega,q)$. The partial DIMFP for the jth mode of energy absorption, $d\mu^{(j)}/d\omega$, is then

Table 2-1

Modes of Electronic Energy Absorption

	Interaction Type	Presumed Transition
Excitations:	1	$\tilde{A}^1B_1$
	2	$\tilde{B}^1A_1$
	3	Rydberg A+B
	4	Rydberg C+D
	5	Diffuse Band
	6	Dissociative Excitation
Ionizations:	7	K-Shell
	8	$1b_1$
	9	$3a_1$
	10	$1b_2$
	11	$2a_1$

Note: Notation for excitations from Green and Rio (1982) and ionizations from Tan *et al.* (1978).

defined by replacing $\epsilon_2(\omega,q)$ in the numerator of the integrand of Eq. (2-1) by $\epsilon_2{}^{(j)}(\omega,q)$.

Inverse Mean Free Paths for Elastic Scattering

Data on the elastic scattering of electrons in liquid water do not exist. Therefore, total and differential scattering cross sections for atomic hydrogen and oxygen are used under the assumption that electrons scatter incoherently in liquid water. For electron energies up to 1000 eV, scattering probabilities are obtained from phase shift calculations. Cross sections at higher energies are obtained by using the Thomas-Fermi model in the first Born approximation. In this model, the total elastic cross section as a function of velocity v and atomic number Z is approximated by

$$\sigma = \frac{\pi Z^2}{v^4} \frac{1}{a^2(1 + a^2)} , \qquad (2\text{-}6)$$

where

$$a = \frac{0.565\ Z^{1/3}s}{v} \qquad (2\text{-}7)$$

and s is an adjustable parameter of the order of 0.66. The angular distribution is approximated by

$$\frac{d\sigma}{d\theta} = \frac{z^2}{4v^4(a^2 + \sin^2 \frac{\theta}{2})^2} \cdot \qquad (2\text{-}8)$$

where θ is the polar angle of scatter.

Electron Transport

The electron transport code OREC models the physical process of energy deposition by electrons in liquid water. The code begins by considering a primary electron in a liquid-water medium with a given initial energy and trajectory. A flight distance is selected for the primary electron based upon the total inverse mean free path for all elastic and inelastic collisions at that electron energy. The electron is then moved to this collision site. Next, a type of interaction is selected based on the partial IMFP's at that same energy.

If a collision is elastic, an angle of scatter is selected from Eq. (2-8) and the flight distance to the next interaction is chosen. If a collision is inelastic, an energy loss is selected based upon the partial DIMFP for that event type and at that electron energy. If the energy loss is less than 50 eV, a delocalization of the energy transfer is allowed to occur. This delocalization is a consequence of collective effects in the condensed phase and is modeled by displacing the interaction site through a lateral distance r in a random direction azimuthal to the incident particle's path. The distance r is chosen from the distribution

$$P(r)dr = \frac{e^{-\omega r/v\gamma} r dr}{r^2 + b^2} , \qquad (2\text{-}8)$$

where ω is the energy loss, v is the particle's velocity, and b and γ are constants (taken to be 0.2 nm and 5, respectively, for liquid water).

If an inelastic collision is an excitation, the electron's energy is reduced by the energy loss selected and the electron is allowed to continue in its precollision direction. If an inelastic collision is an ionization, the electron's energy is also reduced by the energy loss selected, but is allowed to scatter as though it collided with a free electron. The secondary electron produced is scattered as though initially free and is given an energy equal to the energy lost by the primary electron minus the binding energy of the target electron.

Each time a secondary electron is produced, the code continues by transporting the electron with the lowest kinetic energy. When that electron's energy falls below 7.4 eV, the assumed threshold for further electronic excitation of liquid water, the code proceeds by transporting the higher-energy electron. This process is continued until all of the original electron's energy is expended in the creation of H_2O^*, H_2O^+, and subexcitation electrons. The output of OREC is then the spatial location of these three species.

As an example of these calculations, Fig. 2-2 shows the complete tracks of six 800-keV electrons all starting at the same location and traveling horizontally to the right. The plots were made by marking a
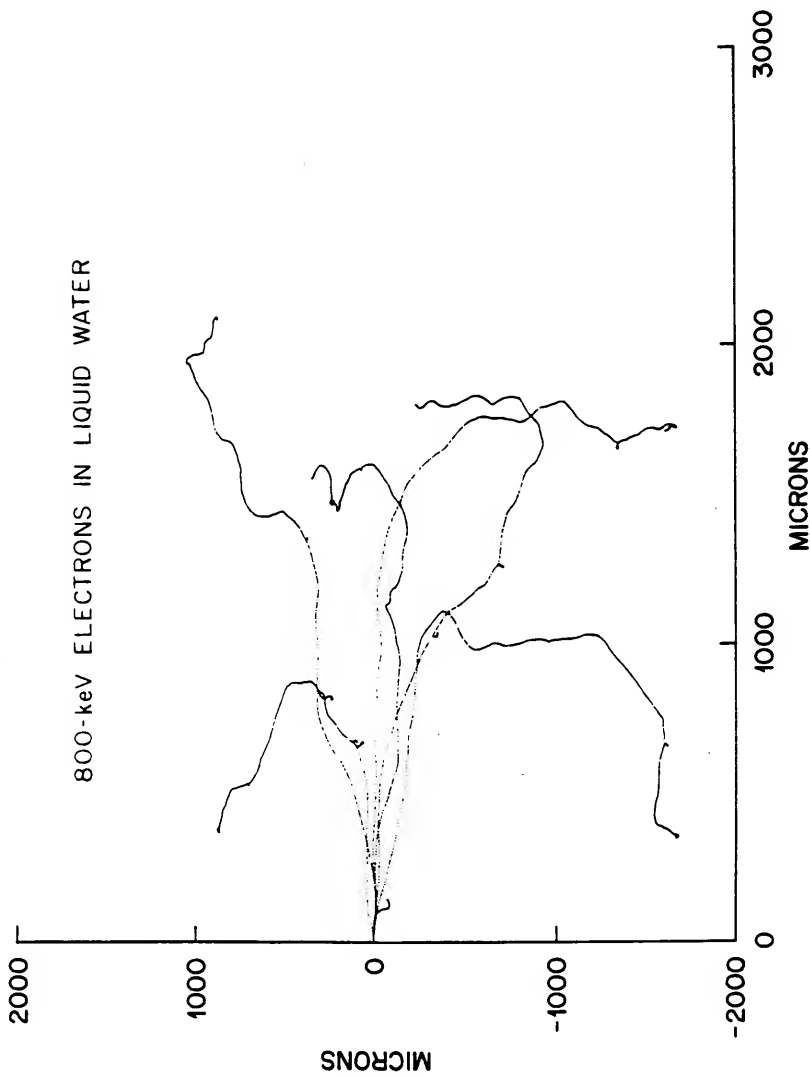
ORNL-DWG 86-10232**R**

Fig. 2-2. Two-dimensional projection of six 800-keV electron tracks in liquid water. All electrons were started at the origin traveling horizontally to the right. Each dot marks the projected location of every fifth inelastic event (Turner et al. 1988a).

dot at the projected location of every fifth inelastic event experienced by the primary electron or one of its secondaries. Several physical aspects of electron tracks are evident. Elastic scattering becomes more pronounced as the electron losses energy, resulting in an increasingly wandering track. Delta rays produced at sites of high energy loss are also shown. Finally, the increase in stopping power at lower electron energies (Fig. 1-1, p. 7) is evident as each track plot becomes increasingly darker along its length.

Prechemical Stage

This stage of track development is characterized by the conversion of the species H_2O^*, H_2O^+, and e^-_{sub} into chemical reactants. In the simulations, this process is associated with the time period 10^{-15} s to 10^{-12} s with respect to local regions of a charged-particle track. The prechemical stage is modeled by the code SPCS whose input is the spatial location of all H_2O^*, H_2O^+, and e^-_{sub}'s computed by the transport code OREC.

When an H_2O^+ is formed, it is first allowed to migrate in a random direction through a distance selected from a Gaussian distribution with a mean displacement 0.75 nm. It then reacts with a neighboring water molecule according to

$$H_2O^+ + H_2O \longrightarrow H_3O^+ + OH. \qquad (2\text{-}9)$$
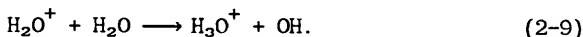
At 10^{-12} s, the products on the right replace the original H_2O^+ and are separated by a distance chosen from a Gaussian distribution with a mean value of 0.29 nm, the diameter of a water molecule. Since it is not known in which direction the hydrogen atom transfer occurs, the position of the H_3O^+ is taken to be that of the original H_2O^+ in 50% of the reactions, with the OH radical placed about it in a randomly selected direction. The positions of the two species are reversed in the other 50% of the reactions.

When an H_2O^* is formed, one of several subsequent pathways is chosen, depending on which of the six specific excited states is involved (see Table 2-1, p. 23). The $\tilde{A}^1B_1$ and $\tilde{B}^1A_1$ transitions (event types 1 and 2) result, respectively, in the following two dissociations:

$$H_2O^* \longrightarrow \left\{ \begin{array}{l} H + OH \\ H_2 + O \end{array} \right. . \qquad (2\text{-}10)$$
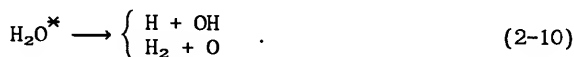
The oxygen radical produced in the second dissociation is assumed to react quickly with a neighboring water molecule to form H_2O_2. In the other excitations (event types 3 through 6), which include high Rydberg states seen in water vapor, it is assumed that an electron can be lost

to surrounding water molecules, leading to the formation of H_2O^+ and reaction (2-9).

The subexcitation electrons formed in the physical stage thermalize and become hydrated by 10^{-12} s. A hydration distance is randomly selected for each subexcitation electron from a Gaussian distribution with a mean displacement of 3 nm. Each subexcitation electron is thus displaced by this distance in a random direction after which it is designated a hydrated electron, e_{aq}^-. A mean hydration distance of 3 nm is used so as to obtain agreement between calculated and measured yields of OH and e_{aq}^- during the early chemical stage.

As an example of the calculations made at this stage of electron track development, Fig. 2-3 shows the spatial location of reactive species produced in the first 32 nm of a 4-keV electron track. The electron was started at the origin in an initial trajectory along the horizontal axis. A clustering of species is evident with hydrated electrons spread over a somewhat greater volume than the other reactants.

Early Chemical Stage

The early chemical stage of track development is modeled by the computer code RADLYS and is associated with the time period 10^{-12} s to 10^{-6} s with respect to local regions of the track. During this interval, reactive species produced within the track undergo diffusion
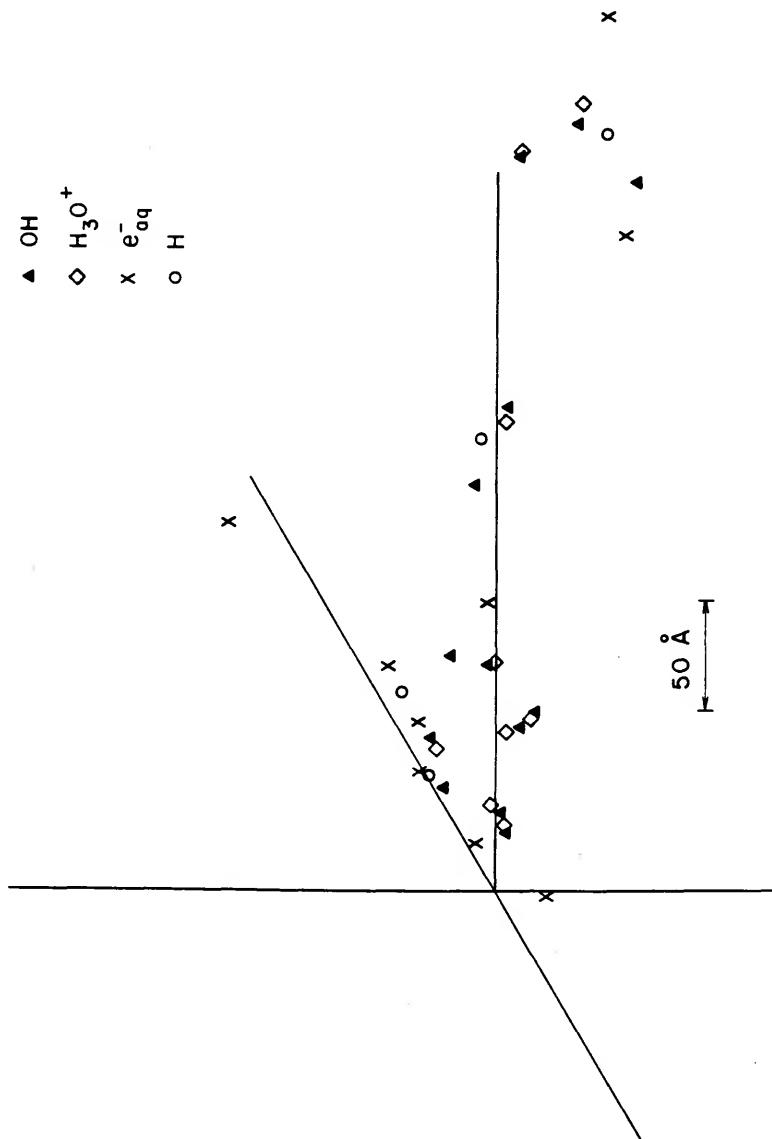
Fig. 2-3. Positions and identities of reactive species in the first 32 nm of a 4-keV electron track in liquid water (Turner et al. 1988b).

and chemical reaction. These processes are simulated using relationships drawn from diffusion and collision theory.

Theory of partially diffusion-controlled reactions

The thermal motion of chemical reactants can be viewed on a molecular level as discrete displacements, or "jumps," between molecules of the surrounding medium. Starting with Fick's first law of diffusion, one can ascribe a root-mean-square jump distance λ traveled by a reactant during a jump time τ according to the relation

$$D = \frac{\lambda^2}{6\tau} , \qquad (2\text{-}11)$$

where D is the experimentally determined diffusion coefficient for that reactant (Chang 1981). By assuming that diffusive jumps are on the order of 0.29 nm, the diameter of a water molecule, experimental diffusion coefficients for radiogenic free radicals correspond to jump times on the order of 3×10^{-12} s. Table 2-2 gives diffusion coefficients and root-mean-square jump distances for various species during a 3×10^{-12} s jump time.

The contribution of diffusion to the rate of a chemical reaction was originally worked out by Smoluchowski (Smoluchowski 1916; Mozumder 1978). In his model, a reactant A was considered a sink towards which another reactant B diffuses. Solving Fick's law of diffusion and using

Table 2-2

Reactant Species, Diffusion Coefficients D,
and RMS Jump Distances λ

Species	D (10^{-5} cm^{2}s^{-1})	λ (nm)
OH	2.5	0.21
H_3O^+	9.5	0.41
e^-_{aq}	5.0	0.30
H	8.0	0.38
OH^-	5.3	0.31
H_2O_2	1.4	0.16

Source: Wright *et al.* (1985b).

the boundary condition that the concentration of reactant B is zero at a distance R from reactant A, he showed that

$$k_d = 4\pi DR , \qquad\qquad (2\text{-}12)$$

where k_d is the reaction rate constant assuming the reaction is completely diffusion-controlled, D is the sum of the diffusion constants for reactants A and B, and R is the reaction radius. Mozumder (1978) used this model to show that the probability of two species reacting in time t, that were originally separated by distance B, is given by

$$P(t) = \frac{R}{B}\ \text{erfc}\left[\ \frac{(B - R)}{\sqrt{4Dt}}\ \right] , \qquad\qquad (2\text{-}13)$$

where erfc is the error function complement.

The boundary condition proposed by Smoluchowski is no longer valid, however, when the mean jump distance of a reactant is comparable to the reaction radius or there exist energetic or geometric restrictions which must be met before a reaction can proceed. Noyes solved Fick's diffusion equation by using instead a radiative boundary condition (Noyes 1961; Mozumder 1978), and obtained the expression

$$k_{obs} = \frac{k_d \, k_a}{k_d + k_a} \, , \tag{2-14}$$

where k_{obs} is the reaction rate constant expected to be observed, k_d is the rate constant if the reaction were diffusion-controlled, and k_a is the rate constant if the reaction were not diffusion-controlled. The activation-controlled rate constant k_a is given by $k_a = \sigma v P$, where σ is the collision cross section of the reaction, v is the approach velocity of reactant B relative to A, and P is the probability of reaction during a single collision (Wright et al. 1988). Thus

$$k_a = \pi R^2 \, \frac{\bar{\lambda}}{\tau} \, P \, , \tag{2-15}$$

where $\bar{\lambda}$, the mean jump distance, is given by

$$\bar{\lambda}^2 = \overline{\lambda^2} \left[\frac{8}{3\pi} \right] \, . \tag{2-16}$$

The mean square jump distance, $\overline{\lambda^2}$, is given as the sum of the squares of the jump distances for reactants A and B:

$$\overline{\lambda^2} = \lambda_A^{\,2} + \lambda_B^{\,2} \, . \tag{2-17}$$

Using Eqs. (2-11) and (2-15) in Eq. (2-14), one obtains

$$k_{obs} = 4\pi DR \left[\frac{3RP\bar{\lambda}}{3RP\bar{\lambda} + 2\overline{\lambda^2}} \right] . \tag{2-18}$$

The solution to Fick's diffusion equation under a radiative boundary condition yields a zero concentration of reactant B, not at the reaction radius R, but at a reduced radius a given by

$$a = R \left[\frac{3RP\bar{\lambda}}{3RP\bar{\lambda} + 2\overline{\lambda^2}} \right] . \tag{2-19}$$

The reduced radius is related to the observed reaction rate constant by $k_{obs} = 4\pi Da$. Mozumder's expression for the probability of reaction in time t then becomes

$$P(t) = \frac{a}{B} \, erfc \left[\frac{(B - a)}{\sqrt{4Dt}} \right] . \tag{2-20}$$

Table 2-3 lists the primary reactions occurring in the water radiolysis along with their observed rate constants, reaction radii, and reduced radii. Two of the reactions occur with a collision probability of 1/7 and 1/3, respectively.

Table 2-3

Chemical Reactions, Rate Constants k, Reaction Radii R, Reduced Radii a

Reaction		$k \ (10^{10} \ M^{-1} \ s^{-1})$	R (nm)	a (nm)
$H + OH$	$\longrightarrow H_2O$	3.2	0.61	0.40
$e_{aq}^- + OH$	$\longrightarrow OH^-$	3.0	0.73	0.53
$e_{aq}^- + H + H_2O$	$\longrightarrow H_2 + OH^-$	2.4	0.43	0.25
$e_{aq}^- + H_3O^+$	$\longrightarrow H + H_2O$	2.3	0.40	0.21
$H + H$	$\longrightarrow H_2$	2.1	0.25	0.10
$OH + OH$	$\longrightarrow H_2O_2$ (P=1/7)	0.6	0.60	0.16
$2e_{aq}^- + 2H_2O$	$\longrightarrow H_2 + 2OH^-$	0.6	0.20	0.08
$H_3O^+ + OH^-$	$\longrightarrow 2H_2O$	12.0	1.08	1.08
$e_{aq}^- + H_2O_2$	$\longrightarrow OH^- + OH$ (P=1/3)	1.2	0.60	0.25

Source: Wright *et al.* (1985b).

Simulation of Track Chemistry

As an example of the calculations performed during the chemical
stage, the upper left panel of Fig. 2-4 shows the entire track of the
4-keV electron shown previously in Fig. 2-3, each dot representing a
reactive species at 10^{-12} s. The calculations of the chemical stage
begin with such a track. The code RADLYS checks pairs of species to see
if they are able to react with one another according to Table 2-3, and
if they are within the required reaction radius R. The order in which
the species are checked follows the same order in which their precursor
species at 10^{-15} s were formed. If a pair does react with collision
probability P, the reactants are removed from further consideration and
their products are created at the reaction site separated by a
root-mean-square distance of two molecular diameters. If the pair does
not react, a new pair is considered, one member taken from the previous
pair, and this checking continues throughout the track.

After permitting all possible reactions to proceed, the code allows
all unreacted species to undergo an elementary diffusive jump
corresponding to a time interval of 3×10^{-12} s. Specifically, each
species is moved in a random direction through a distance selected from
a Gaussian distribution with a mean displacement λ calculated by Eq.
(2-11) (p. 32). After all species are jumped, the pairwise checking is
repeated. The chemical development of the track proceeds by alternating
simulations of chemical reaction and diffusion.

The above process, referred to as Reaction Scheme I, becomes
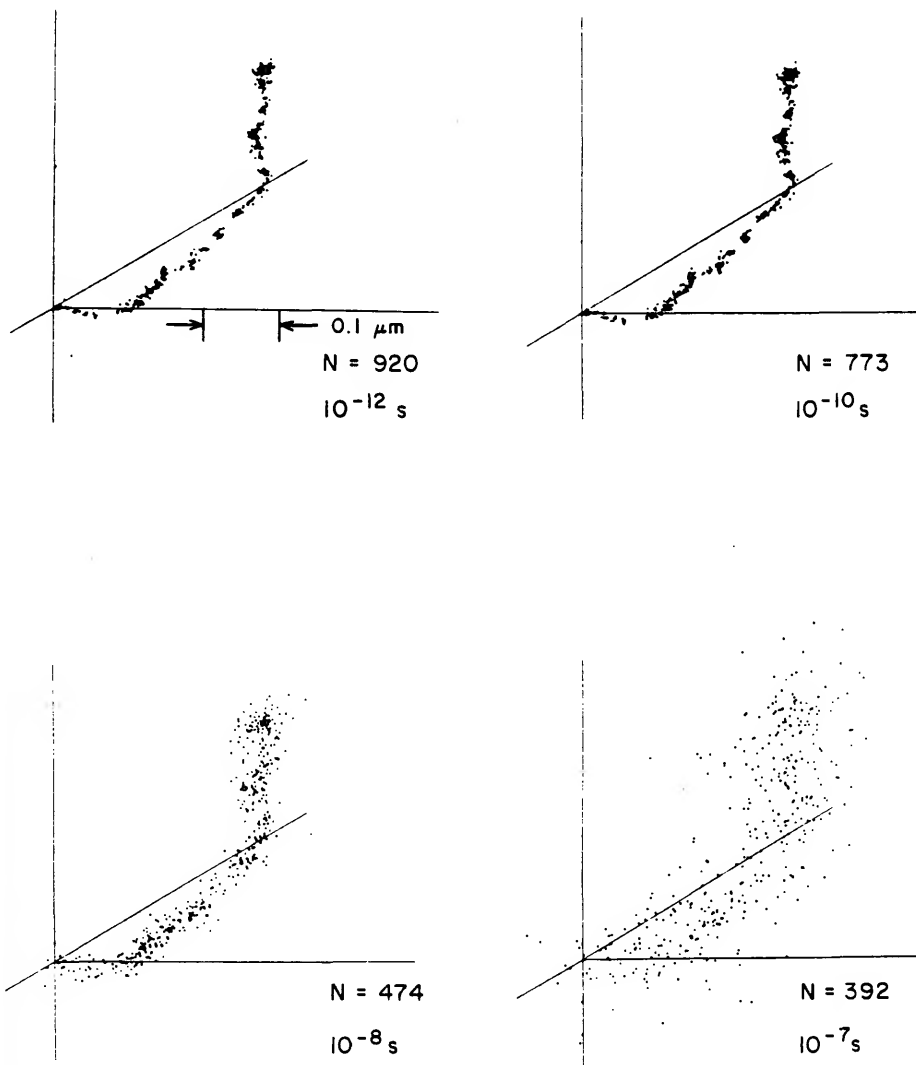increasingly inefficient after 30 elementary jumps such that very few

ORNL-DWG 87-13030

Fig. 2-4. Chemical evolution of a 4-keV electron track in liquid water from 10^{-12} s to 10^{-7} s. Each dot marks the location of a reactive chemical species (Turner *et al.* 1988b).

additional reactions occur between jumps. During the time 10^{-10} s to 10^{-6} s, Reaction Scheme II is implemented in which jump intervals larger than three picoseconds are considered. During jump intervals in Scheme II, pairs of species are allowed to react with a probability given by Eq. (2-20) (p. 36). For each reaction, the products are placed at a reaction site midway between the positions of the reactants at the beginning of the jump interval. Unreacted species are allowed to diffuse over this jump interval to the next time point.

The remaining panels of Fig. 2-4 show the result of these calculations. Of the 920 reactive species originally present at 10^{-12} s, only 392 remain at 10^{-7} s. This decrease is expected since the primary result of the reactions in Table 2-3 is the conversion of reactive free radicals (H, OH, e_{aq}^-) to unreactive molecular products (H_2, H_2O_2, H_2O). By 10^{-6} s, the remaining species have diffused to the extent that most evidence of track structure is gone and few remaining intratrack reactions are possible. After a microsecond, the remaining species continue to diffuse away from the track center and will begin to react with species produced from neighboring tracks.

CHAPTER 3

MODIFICATIONS TO THE OAK RIDGE MODEL

Prior to development of a simulation code for the early chemical stage of glycylglycine radiolysis, several modifications were made to the Oak Ridge model for pure water radiolysis. Thermalization of subexcitation electrons was made an explicit function of electron energy. Agreement was reached between calculated and experimental yields of OH and e_{aq}^- as a function of time by making assumptions as to the fate of H_2O^* and H_2O^+ during the prechemical stage. Other changes included incorporating reactions with dissolved oxygen, improving the scheme for locating reaction sites during the early chemical stage, and adding calculations of standard deviations for all product yields. At the close of this chapter, a critique of the modified codes is given.

Thermalization of Subexcitation Electrons

In the transport code OREC, the threshold for electronic excitation of liquid water is 7.4 eV. Electrons which fall below that threshold after an energy loss event are designated subexcitation electrons and are not transported further. Subsequently, the code SPCS simulates

41

their thermalization by assuming each undergoes hydration during a root-mean-square displacement of 3 nm.

A more realistic treatment would allow electrons to thermalize through a distance dependent upon their subexcitation energy. From Fermi age theory (Bethe *et al*. 1938, Fermi 1949, Weinberg and Wigner 1958), the root-mean-square distance traveled by an electron that is liberated into a medium at velocity v_o and slows down to thermal velocity v_{th} is given as

$$r(v_o) = \left[2 \int_{v_{th}}^{v_o} \frac{v \, dv}{\Sigma_{et}(v) \, S(v)} \right]^{\frac{1}{2}}, \qquad (3-1)$$

where $\Sigma_{et}(v)$ is the elastic transport inverse mean free path, $S(v)$ is the stopping power of the medium, and atomic units are used throughout. Both these quantities and the subsequent evaluation of Eq. (3-1) are discussed separately.

Stopping Power for Low-Energy Electrons

From dielectric theory (Ritchie 1959, Ritchie *et al*. 1975), one can formulate the stopping power for low-energy electrons of velocity v as

$$S(v) \; = \; \frac{2}{\pi v^2} \int_0^{\frac{v^2}{2}} \omega \; \ln\left[\frac{v}{D\omega}\right] \frac{\epsilon_2(\omega,0) \; d\omega}{\epsilon_1^2(\omega,0) + \epsilon_2^2(\omega,0)} \; , \quad (3\text{-}2)$$

where ω is the energy lost to vibrational and rotational excitations and D is the intermolecular distance of the medium, taken to be 0.3 nm for water. In addition, $\epsilon_1(\omega,0)$ and $\epsilon_2(\omega,0)$ are the real and imaginary parts of the dielectric constant at zero momentum transfer. Values of ω are restricted so that only positive values of the logarithm term of the integrand are used. Since there is negligible momentum transfer accompanying energy losses by electrons at low velocities, the water responds as if a photon of energy ω is absorbed. Therefore, ϵ_1 and ϵ_2 can be obtained from optical properties of liquid water. Specifically,

$$\epsilon_1(\omega,0) \; = \; n_r^2 - n_i^2 \qquad (3\text{-}3)$$

and

$$\epsilon_2(\omega,0) \; = \; 2n_r n_i \; . \qquad (3\text{-}4)$$

where n_r and n_i are the real and imaginary parts of the index of refraction and are obtained from surface reflectance measurements at photon energy ω (Heller et al. 1974). Tabulated values of n_r and n_i exist for photons in the energy ranges 0.00002 to 0.62 eV (Zoloratev and

Demin 1977), 0.47 to 3.44 eV (Palmer and Williams 1974), and 2.0 to 25.6 eV (Heller *et al.* 1974). By using Eqs. (3-3) and (3-4), the energy-loss function $Im(-1/\epsilon)$ is computed and is shown in Fig. 3-1. Equation (3-2) is then evaluated to give the stopping power for low-energy electrons shown in Fig. 3-2.

Elastic Transport IMFP for Low-Energy Electrons

For an electron of velocity v, the elastic scattering inverse mean free path, $\Sigma_e(v)$, is defined by the expression

$$\Sigma_e(v) = \frac{2\pi N_a \rho}{A} \int_0^\pi \sigma(v,\theta) \sin\theta \, d\theta , \qquad (3-5)$$

where N_a is Avogadro's number, ρ and A are the density and atomic number of the medium, θ is the polar angle of scatter, and σ is the elastic scattering cross section, differential in angle θ. To measure the importance of elastic scattering on electron transport, σ is weighted by the factor $(1-\cos\theta)$ to obtain the elastic transport inverse mean free path, $\Sigma_{et}(v)$. Thus,

$$\Sigma_{et}(v) = \frac{2\pi N_a \rho}{A} \int_0^\pi \sigma(v,\theta) (1-\cos\theta) \sin\theta \, d\theta . \qquad (3-6)$$

Experimental values of σ are reported for electrons in water vapor at energies of 0.01 to 10 eV (Itikawa 1978) and 4 to 10 eV (Danjo and
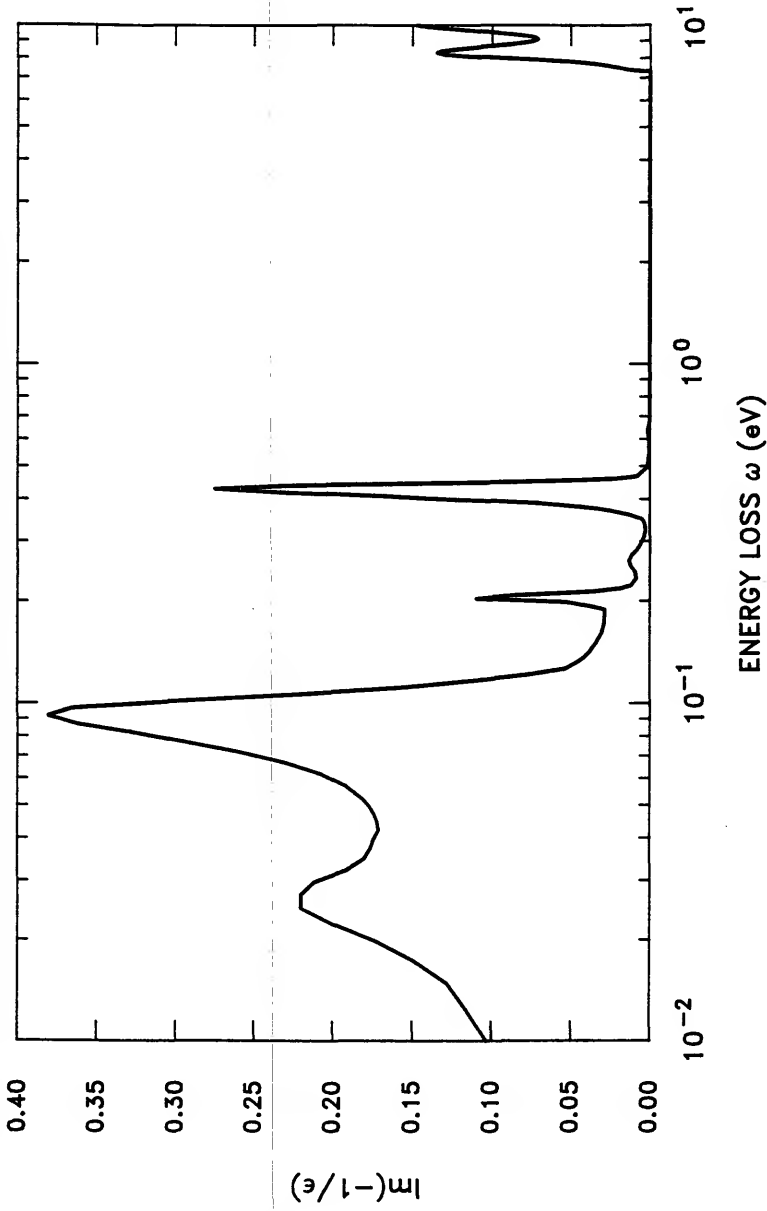
Fig. 3-1. Energy-loss function Im[−1/ε(ω,0)] for liquid water at values of energy-loss ω less than 10 eV and momentum transfer q = 0.
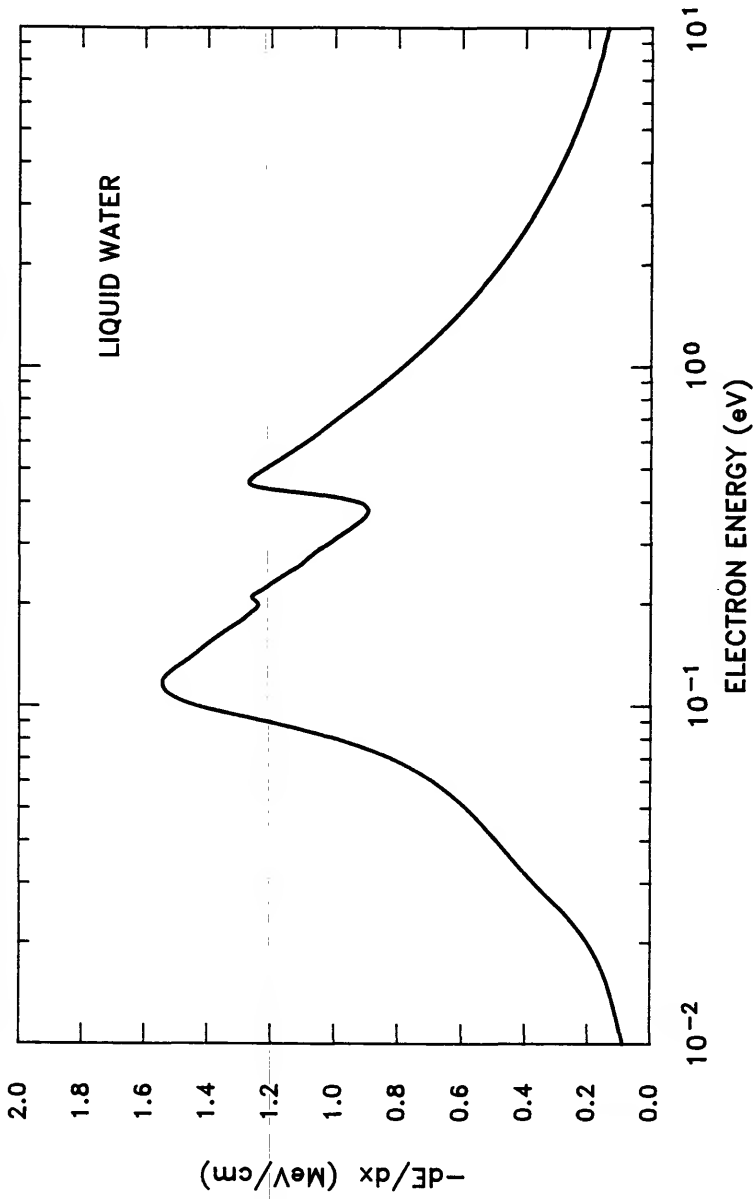
Fig. 3-2. Calculated stopping power of liquid water for low-energy electrons.

Nishimura 1985). A recent study has suggested that elastic cross sections may be an order of magnitude smaller in solid media (Bader *et al*. 1988). A comparison of calculated and measured time decay of e_{aq}^- (discussed in the following section) suggest a scaling of vapor elastic cross sections by 0.6 to obtain values for liquid water. Values of σ for water vapor are thus scaled by 0.6 and Eq. (3-6) is evaluated to give Σ_{et} as a function of electron energy as shown in Fig. 3-3.

Thermalization Distances for Low-Energy Electrons

Using $S(v)$ and $\Sigma_{et}(v)$ for electrons in the energy range 0.01 to 10.0 eV, Eq. (3-1) is evaluated to give the rms thermalization distance $r(E)$ for low-energy electrons shown in Fig. 3-4. A modified version of the code SPCS includes the function $r(E)$ in its treatment of electron thermalization and hydration during the prechemical stage of radiolysis. Specifically, the energy E of each subexcitation electron followed in OREC is passed to the code SPCS. SPCS then creates a hydrated electron in a random direction at an rms distance $r(E)$ from its prethermalized position. Electrons produced through autoionization of type 3-6 excitations are also thermalized through an rms distance $r(E)$, where their energy E is assumed to equal the energy of their parent excited state minus an average binding energy of 8 eV.
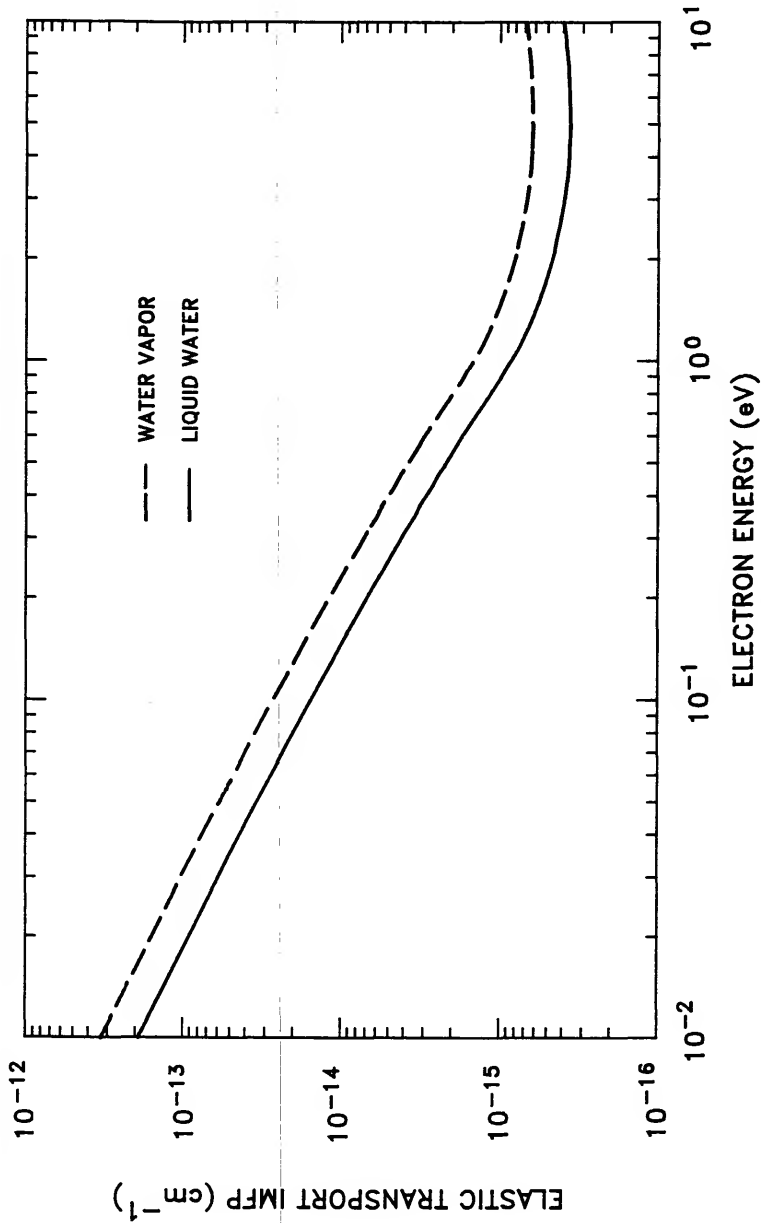
Fig. 3-3. Elastic transport inverse mean free paths for low-energy electrons in water. Values for water vapor are from Itikawa (1978) and Danjo and Nishimura (1985), and were scaled by 0.6 to obtain those for liquid water.
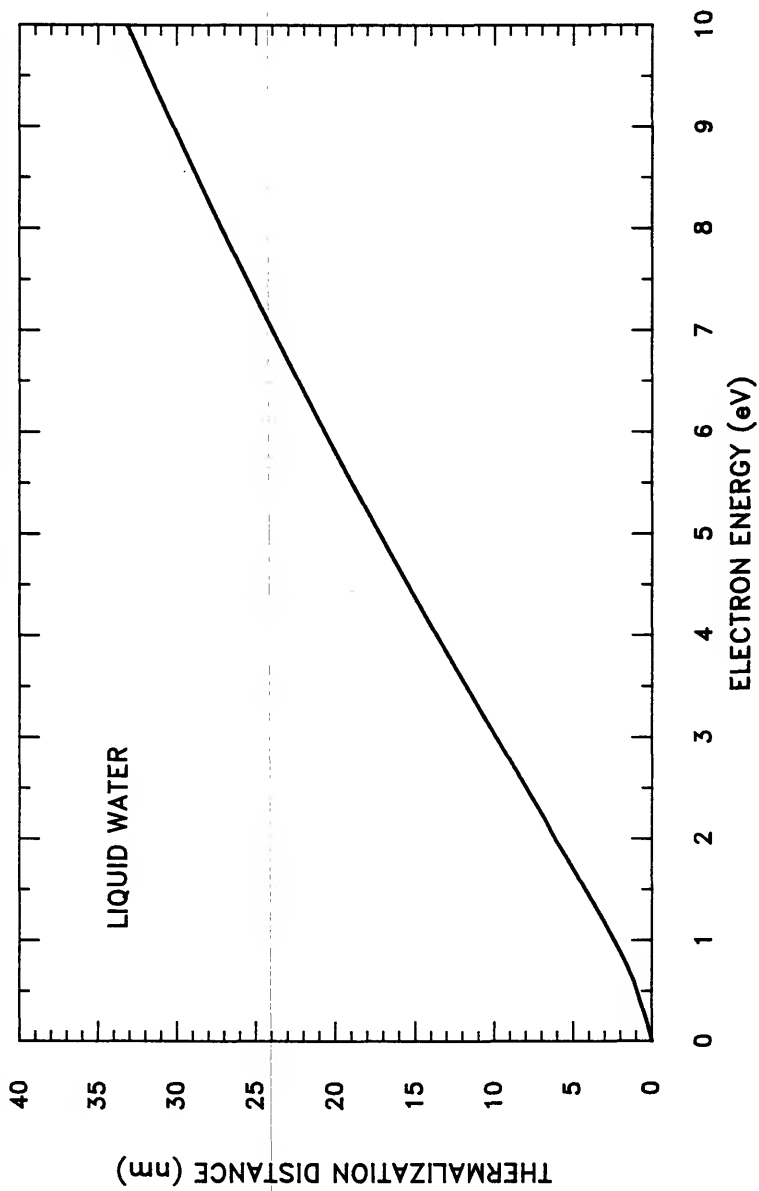
Fig. 3-4. Calculated thermalization distance for low-energy electrons in liquid water.

Time Decay of Hydrated Electrons and OH Radicals

There is limited experimental data on yields of radiolytic products in pure water for times earlier than 10^{-6} s. Such data provide a means of supporting the calculated yields given by the Oak Ridge model. Three studies exist which report the G-value for hydrated electrons from 100 ps to 3 ns (Jonah et al. 1976), the G-value for hydrated electrons at 30 ps (Sumiyoshi and Katayama 1982), and the G-value for the OH radicals from 200 ps to 3 ns (Jonah and Miller 1977). In these studies, sample cells are irradiated by a pulse of high-energy electrons. At the same time, a portion of the electron beam is intercepted by a cell containing 1 atm of xenon in which Cerenkov radiation is generated for use as an analyzing light. By delaying the Cerenkov light, absorbance by e_{aq}^- or OH radicals is measured as a function of time relative to the arrival of the electron pulse.

In the Jonah studies, 20- to 22-MeV electrons were used, while in the Sumiyoshi and Katayama study, 45-MeV electrons were used. Both secondary-electron spectra and collision stopping powers are fairly energy independent for electrons in the energy range 1 MeV to 50 MeV; therefore, chemical yields within track segments of electrons at these energies are not expected to differ greatly.

Figure 3-5 shows time-dependent yields of OH radicals and e_{aq}^- for 1-MeV electron track segments as calculated by the unmodified ORNL model described in Chapter 2. Experimental data is also shown. The initial yield and decay rate of hydrated electrons is not in accordance with
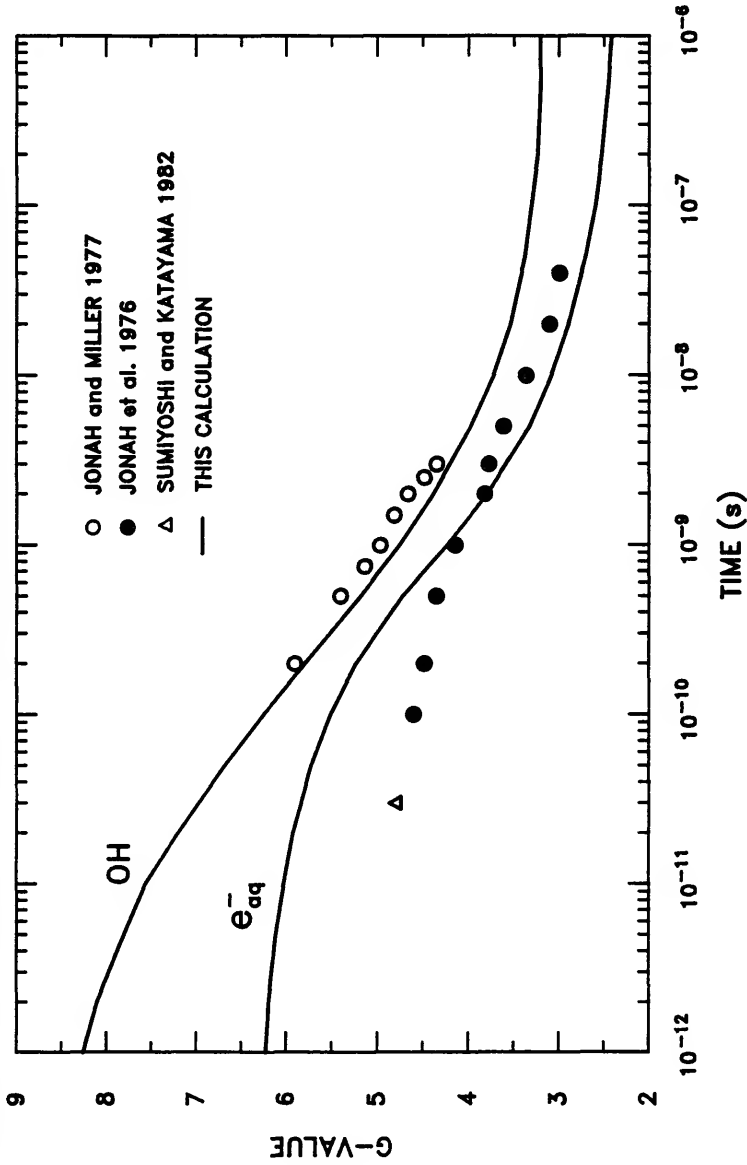
Fig. 3-5. Time-dependent yields of OH radicals and hydrated electrons in liquid water. Solid curves were calculated for 1-MeV electron track segments by the code described in Chapter 2.

experiment. So as to achieve better agreement, modifications are made to the code SPCS.

The decay rates of hydrated electrons and OH radicals within a track are greatly dependent upon their spatial distribution at 10^{-12} s. In addition, these decay rates are not independent due to reactions such as $e_{aq}^- + OH \longrightarrow OH^-$. Using the thermalization scheme described in the previous section and by increasing the migration distance of H_2O^+ from 0.75 nm to 1.25 nm, the calculated decay rate of hydrated electrons is brought into agreement with experiment.

To match the experimentally suggested initial yield of e_{aq}^-, the scheme shown in Table 3-1 for partitioning of H_2O^* into dissociations and autoionizations is adopted. In this scheme, 25% of type 1 excitations and 23% of type 3-6 excitations are allowed to relax, where ΔE represents thermal energy transferred locally to the medium. The results of revised calculations of OH and e_{aq}^- yields as functions of time are shown in Fig. 3-6. By making these modifications to the Oak Ridge model, excellent agreement between calculated and measured values is achieved.

Additional Chemical Reactions

The reactions listed in Table 2-3 (p. 37) represent the primary ones occurring within charged-particle tracks in liquid water. These reactions are virtually diffusion controlled with rate constants on the

Table 3-1

Assumed Partitioning of Excitations

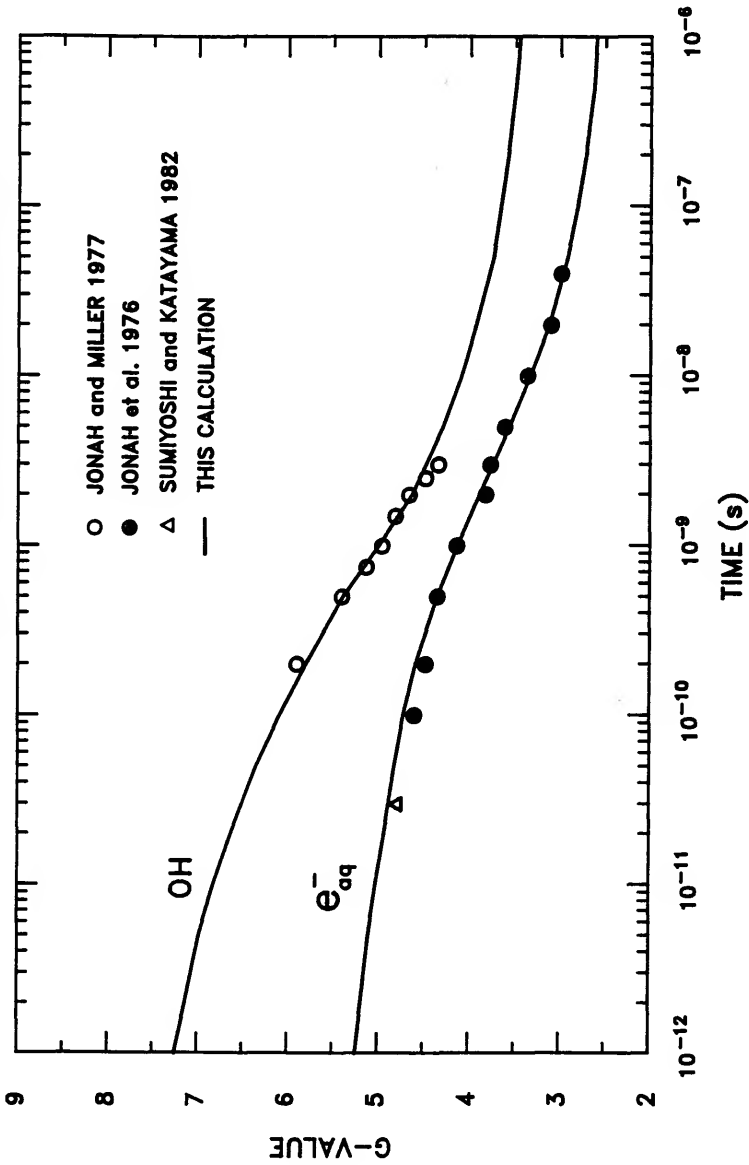| TYPE 1 | H_2O^* $\longrightarrow$ H + OH | 75% |
	$H_2O + \Delta E$	25%
TYPE 2	H_2O^* $\longrightarrow$ H_2 + O	100%
TYPE 3-6	H_2O^* $\longrightarrow$ $H_2O^+ + e^-_{sub}$	57%
	H + OH	20%
	$H_2O + \Delta E$	23%

Fig. 3-6. Time-dependent yields of OH radicals and hydrated electrons in liquid water. Solid curves were calculated for 1-MeV electron track segments using the electron thermalization scheme of Chapter 3 and the partitioning scheme for excitations shown in Table 3-1.

order of 10^{10} $M^{-1}s^{-1}$. Reactions between free radicals and molecules of biological interest occur with rate constants in the range 10^5 $M^{-1}s^{-1}$ to 10^9 $M^{-1}s^{-1}$. Therefore, pure water reactions which occur at comparable rates must also be considered in a complete simulation of the chemical stage. In addition, molecular oxygen reacts with e_{aq}^- to form the superoxide radical (O_2^-), while reaction with H radicals form its conjugate acid, the hydroperoxyl radical (HO_2). Subsequent reactions between O_2^-, HO_2, and the pure water species virtually double the number of reactions possible during the chemical stage.

Additional reactions are thus incorporated into RADLYS, five occuring in pure water radiolysis and fifteen occurring in the presence of molecular oxygen. Four of the oxygen reactions are considered to follow pseudo-first-order kinetics and are treated separately from the remaining second-order reactions.

Second-Order Reactions

An extensive list of reactions occurring in pure water and in the presence of dissolved oxygen was compiled as part of the computer program MACKSIM developed at Canada's Chalk River Nuclear Laboratories (Boyd *et al.* 1980). MACKSIM calculates steady-state concentrations of species produced during continuous low-dose-rate irradiation of water systems, thus simulating the late chemistry stage of radiolysis. These reactions are incorporated into RADLYS and are listed in Table 3-2. Rate constants for the first ten reactions are fairly consistent with ones previously used in RADLYS since they were both taken from the same

Table 3-2

Revised Reactions, Rate Constants k, Reaction Radii R, Reduced Radii a

Reaction		$k\ (10^{10}\ M^{-1}\ s^{-1})^a$	R (nm)	a (nm)
$H + OH$	$\longrightarrow H_2O$	2.0	0.43	0.25
$e_{aq}^- + OH$	$\longrightarrow OH^-$	3.0	0.72	0.53
$e_{aq}^- + H + H_2O$	$\longrightarrow H_2 + OH^-$	2.5	0.45	0.25
$e_{aq}^- + H_3O^+$	$\longrightarrow H + H_2O$	2.2	0.39	0.20
$H + H$	$\longrightarrow H_2$	1.0	0.23	0.083
$OH + OH$	$\longrightarrow H_2O_2\ \ (P=1/7)$	0.55	0.55	0.15
$2e_{aq}^- + 2H_2O$	$\longrightarrow H_2 + 2OH^-$	0.50	0.18	0.066
$H_3O^+ + OH^-$	$\longrightarrow 2H_2O$	14.3	1.58	1.28
$e_{aq}^- + H_2O_2$	$\longrightarrow OH^- + OH\ \ (P=1/3)$	1.2	0.57	0.25
$OH + OH^-$	$\longrightarrow H_2O + O^-$	1.2	0.36	0.20
$OH + H_2O_2$	$\longrightarrow H_2O + HO_2$	0.0033	0.015	0.0011
$H + H_2O_2$	$\longrightarrow H_2O + OH$	0.0090	0.020	0.0013
$OH + H_2$	$\longrightarrow H_2O + H$	0.0036	0.013	0.00063
$H + OH^-$	$\longrightarrow H_2O + e_{aq}^-$	0.0021	0.0087	0.00021

[a]Rate constants from Boyd *et al.* (1980).

National Bureau of Standards compilations (Anbar *et al.* 1973, Ross 1975, Anbar *et al.* 1975, Farhataziz and Ross 1977). The last four reactions listed are secondary reactions with rate constants on the order of 10^7 $M^{-1}s^{-1}$. Table 3-3 lists reactions in the presence of molecular oxygen. A revised list of diffusion constants for all chemical species is given in Table 3-4.

Pseudo-First-Order Reactions

Bimolecular reactions in which there is negligible consumption of one reactant demonstrate first-order kinetics and are referred to as pseudo-first-order reactions. The last two reactions listed in Table 3-3 are good examples, since one of the reactants is the aqueous solvent. The first two reactions in that table, ones representing scavenging by molecular oxygen, approach the pseudo-first-order limit under two conditions. First, only a small fraction of the total oxygen supply should be consumed during the irradiation, thus implying limits on total absorbed dose for closed systems. Second, the concentration of dissolved oxygen must be large relative to concentrations of e_{aq}^- and H radicals within individual electron tracks. These radicals are initially produced in local concentrations of ~10 mM, yet are diluted several orders of magnitude as the track diffuses outward within one microsecond. Concentrations of dissolved oxygen appear large in comparison, even for air-saturated systems.

The four pseudo-first-order reactions listed in Table 3-3 are simulated in the code RADLYS as follows. Each species (e_{aq}^-, H, HO_2, or

Table 3-3

Oxygen Reactions, Rate Constants k, Reaction Radii R, Reduced Radii a

Reaction		k $(10^{10}$ M^{-1} $s^{-1})^a$	R (nm)	a (nm)
$e_{aq}^- + O_2$	$\longrightarrow O_2^-$	1.9^b		
$H + O_2$	$\longrightarrow HO_2$	1.8^b		
$H_3O^+ + O_2^-$	$\longrightarrow HO_2 + H_2O$	4.5	0.74	0.51
$H + HO_2$	$\longrightarrow H_2O_2$	2.0	0.45	0.26
$OH + O_2^-$	$\longrightarrow OH^- + O_2$	0.90	0.39	0.26
$HO_2 + OH$	$\longrightarrow H_2O + O_2$	1.2	0.50	0.35
$H + O_2^-$	$\longrightarrow HO_2^-$	2.0	0.44	0.26
$e_{aq}^- + O_2^- + H_2O$	$\longrightarrow HO_2^- + OH^-$	1.3	0.40	0.24
$e_{aq}^- + HO_2^-$	$\longrightarrow O^- + OH^-$	0.35	0.17	0.066
$H_3O^+ + HO_2^-$	$\longrightarrow H_2O + H_2O_2$	2.0	0.41	0.23
$HO_2 + HO_2$	$\longrightarrow H_2O_2 + O_2$	0.00020	0.0036	0.000066
$HO_2 + O_2^-$	$\longrightarrow HO_2^- + O_2$	0.0089	0.025	0.0029
$HO_2 + H_2O$	$\longrightarrow H_3O^+ + O_2^-$	0.000080^b		
$O^- + H_2O$	$\longrightarrow OH + OH^-$	0.00017^b		

[a]Rate constants from Boyd *et al.* (1980).

[b]Modeled as pseudo-first-order reactions.

Table 3-4

Reactant Species and Diffusion Coefficients D

Species	$D \ (10^{-5} \ cm^2 s^{-1})$	Reference
OH	2.5	Wright *et al.* (1985b)
H_3O^+	9.5	"
e_{aq}^-	5.0	"
H	8.0	"
OH^-	5.3	"
H_2O_2	1.4	"
H_2	5.0	Burns *et al.* (1981)
O_2	2.1	"
HO_2	2.0	"
O_2^-	2.1	"
HO_2^-	2.0	Estimated
O^-	2.0	"

O^-) is allowed to react with probability P_1 over a time interval Δt according to

$$P_1 = 1 - e^{-kC\Delta t} \quad , \tag{3-7}$$

where k is the reaction's second-order rate constant and C is the concentration of either O_2 or H_2O, the latter assumed to be 55.5 M. If a reaction did not occur, the species is allowed to diffuse over the full Δt. If a reaction did occur, the species is first allowed to diffuse over the time interval $f\Delta t$, followed by diffusion of the products over the the remaining interval $(1-f)\Delta t$, where $0 \leq f \leq 1$. The fraction f is determined with probability P_2 according to

$$P_2 = \frac{1 - e^{-kCf\Delta t}}{1 - e^{-kC\Delta t}} \quad . \tag{3-8}$$

The scavenging capability of O_2 is demonstrated in Fig. 3-7 and 3-8. Yields of e_{aq}^- as functions of time for 500-eV electrons at several values of the oxygen pressure are shown in Fig. 3-7. Oxygen gas above the water and at these pressures is assumed to be in equilibrium with dissolved oxygen. The pressure of 0.209 atm corresponds to that of oxygen in atmospheric air. Figure 3-8 gives yields at 10^{-7}s for OH, e_{aq}^-, and H as functions of oxygen pressure.
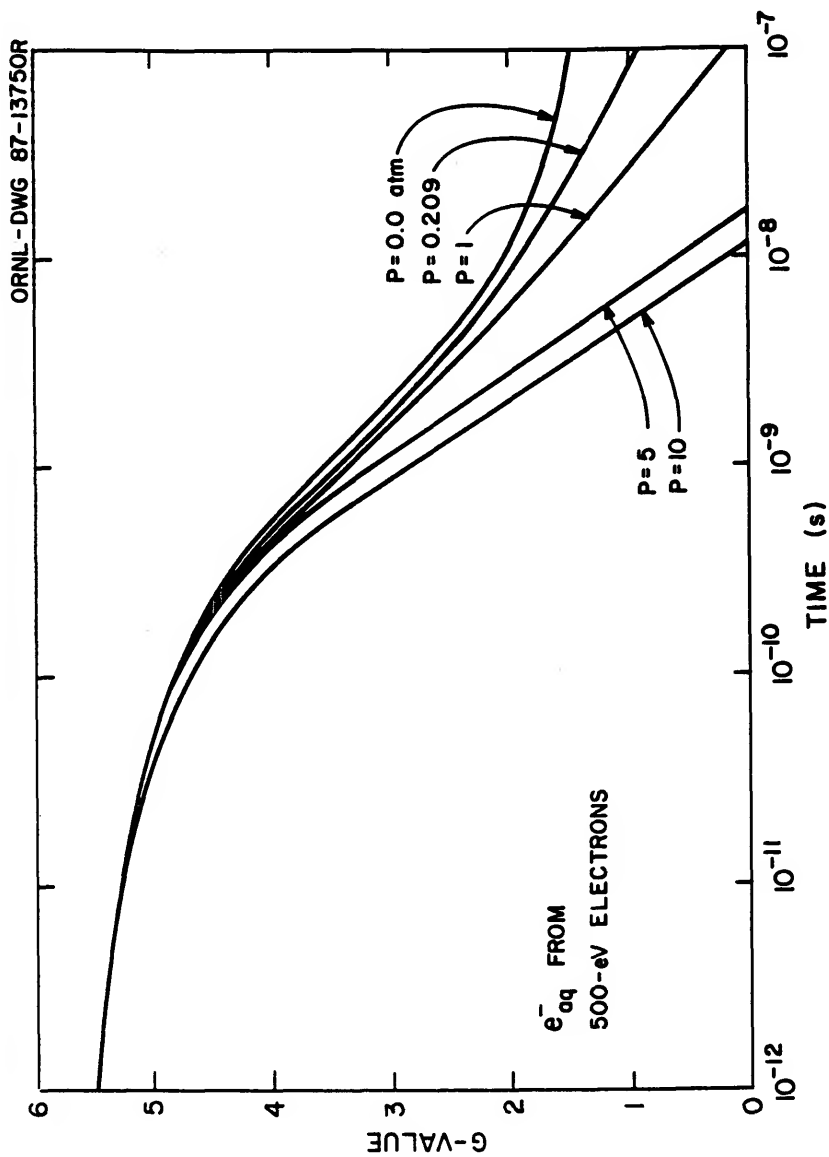
Fig. 3-7. Calculated time-dependent yield of hydrated electrons as a function of oxygen partial pressure (Turner et al. 1988b).
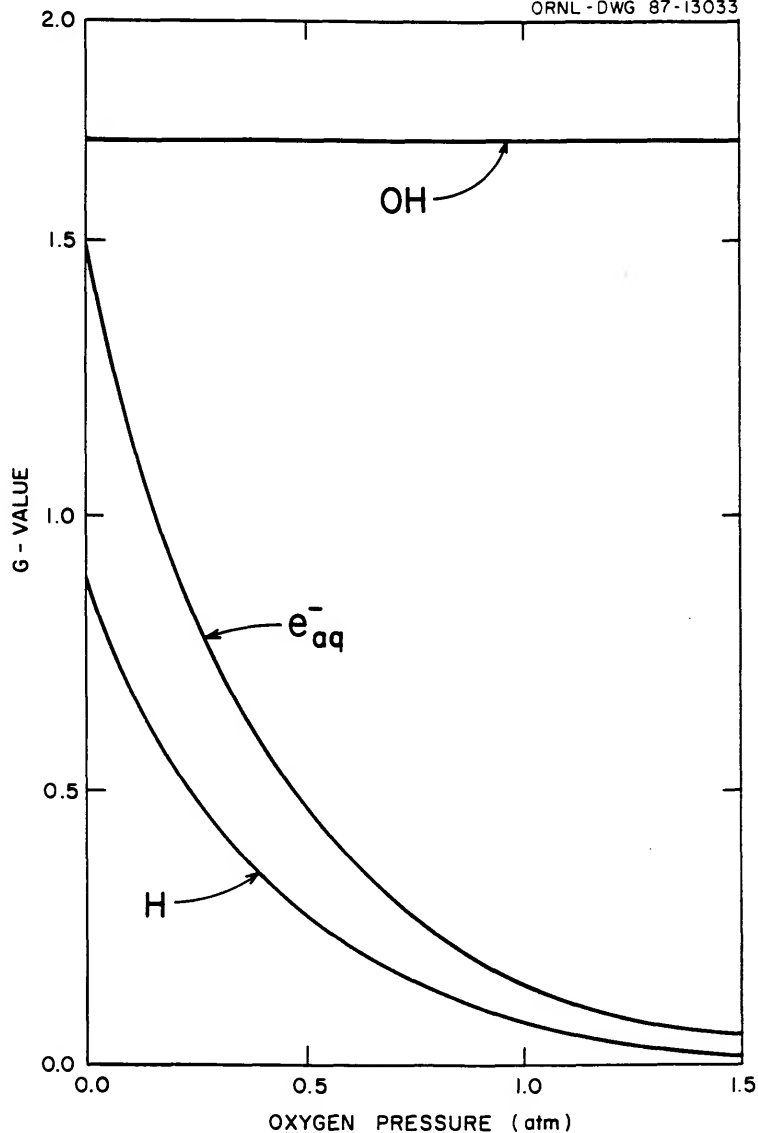
Fig. 3-8.   Yields of OH, H, and hydrated electrons at 10^{-7} s calculated for 500-eV electrons as functions of oxygen partial pressure (Turner *et al.* 1988b).

Location of Reaction Sites

When a second-order reaction occurs between a pair of species located at positions (x_1, y_1, z_1) and (x_2, y_2, z_2), the reaction site is placed midway along the line segment connecting their positions. This is a reasonable assumption when elementary diffusive jumps are employed during Reaction Scheme I, yet becomes less realistic when longer time intervals are simulated during Reaction Scheme II. A location scheme is thus implemented which takes into account the relative diffusion of the two species. Specifically, the coordinates of the reactants are weighted inversely by their diffusion distances λ. The x-coordinate of the reaction site, for example, is given by

$$x_r = \frac{(x_1/\lambda_1) + (x_2/\lambda_2)}{(1/\lambda_1) + (1/\lambda_2)} \ , \tag{3-9}$$

which reduces to

$$x_r = x_1\left[\frac{\lambda_2}{\lambda_1 + \lambda_2}\right] + x_2\left[\frac{\lambda_1}{\lambda_1 + \lambda_2}\right] . \tag{3-10}$$

Since $\lambda = \sqrt{6D\tau}$,

$$x_r = x_1\left[\frac{\sqrt{D_2}}{\sqrt{D_1} + \sqrt{D_2}}\right] + x_2\left[\frac{\sqrt{D_1}}{\sqrt{D_1} + \sqrt{D_2}}\right] . \tag{3-11}$$

These same weighting factors are also used to determine the y- and z-coordinates of the reaction site. This method still assumes that the most probable location for the reaction is along the line segment connecting the species at the beginning of the time interval. More sophisticated methods would select a reaction site according to a predetermined spatial probability distribution.

Precision of Reported Product Yields

Product yields are reported by the code RADLYS as G-values, the total number of molecules produced per 100 eV of energy deposition. Thus for a series of simulated electron tracks,

$$G \ = \ \frac{(100)N_t}{E_t} \ = \ \frac{(100)\bar{N}}{\bar{E}} \qquad (3\text{-}12)$$

where N_t is the total number of molecules produced, E_t is the total energy deposited in eV, $\bar{N}$ is the average number of molecules produced per track, and $\bar{E}$ is the average energy deposited per track. It is instructive to know the precision of reported yields and therefore calculations giving the variance of product yields are added to the code RADLYS. Since $\bar{N}$ and $\bar{E}$ are highly correlated,

$$\left[\frac{\sigma_G}{G}\right]^2 \;=\; \left[\frac{\sigma_{\bar{N}}}{\bar{N}}\right]^2 \;+\; \left[\frac{\sigma_{\bar{E}}}{\bar{E}}\right]^2 \;-\; 2\,\frac{\sigma_{\overline{NE}}^2}{\bar{N}\,\bar{E}} \;, \qquad (3\text{-}13)$$

where $\sigma_{\overline{NE}}^2$ is the covariance between $\bar{N}$ and $\bar{E}$ (Bevington 1969). For a series of monoenergetic electrons of energy E, both $\sigma_{\overline{NE}}$ and $\sigma_{\bar{E}}$ are zero and Eq. (3-13) reduces to

$$\sigma_G \;=\; \frac{100\,\sigma_{\bar{N}}}{E} \;. \qquad (3\text{-}14)$$

Critique of Model

In attempting to formulate a model linking the physics and chemistry of irradiated water, many uncertainties necessarily exist. It is instructive to review these limitations for each stage in the simulation.

Physical Stage

Cross sections used by the transport code OREC are derived from a theory in which compliance with quantum-mechanical restrictions is met, collective effects of the liquid state are included, and experimental data in all three phases are incorporated. Thus, the program is

believed to provide a representative simulation of electron transport in liquid water.

In a recent study (Turner *et al.* 1988a), OREC's liquid-water cross sections were scaled for plastic media. Subsequently, a version of OREC using these modified cross sections was used to simulate the beta response of a scintillator probe to both point and plaque sources. Calculated depth-dose curves were in good agreement with measured pulse-height spectra, thus providing an indirect check with experiment.

Since Monte Carlo techniques are used in the simulation code, new experimental and theoretical data can be readily incorporated into the program. Currently, a reassessment of the code's cross sections for elastic scattering is planned in light of recent experiments in water vapor (Danjo and Nishimura 1985).

Prechemical Stage

Of the three stages of the radiolysis simulated in the Oak Ridge model, the prechemical stage is based least upon experimental data. Physical limitations of pulse radiolysis techniques prohibit investigating events occurring prior to 10^{-12} s (Spinks and Woods 1976). Subsequently, various assumptions are made in the model as to the mechanisms linking the physical and chemical stages.

A much needed improvement to the model is the prescription of electron thermalization presented in this chapter. It is not complete, however, since the scaling of elastic scattering cross sections from the vapor to the liquid was somewhat arbitrary. A method which will be

implemented in the near future proposes to use both optical data and dielectric theory in an independent derivation of these cross sections for liquid water. This would leave the migration distance of H_2O^+ and the partitioning of excitations as the only adjustable parameters available to fit the pulse radiolysis data shown in Figure 3-6. It is hoped that all parameters used would eventually be firmly based upon theory, experiment, or both.

An additional phenomenon not considered at present is that of geminate recombination. Geminate pairs of radicals (i.e., produced from the same H_2O^*) are currently allowed to recombine as early as 10^{-12} s, the beginning of the early chemical stage. However, during an ionization produced by the primary electron or an autoionization of an H_2O^*, the subexcitation electron is always thermalized and hydrated. It is conceivable that a fraction of these electrons are recaptured by their parent H_2O^+ forming a H_2O^*. If recapture is possible, it remains to be seen whether these electrons would produce further ionization or excitation in the medium prior to recombination. As an alternative to the partitioning of H_2O^*, geminate recombination could be an explanation for the high initial yields e_{aq}^- shown in Fig. 3-5 (p. 51).

Early Chemical Stage

Parameters used in simulating the early chemical stage are almost exclusively taken from experimental data. However, limitations on computer run-time permit only an approximate treatment of diffusion and chemical reaction. If calculational limitations did not exist,

diffusive jump distances would be limited to molecular diameters throughout track development. Between jumps, the total number of reactant pairs whose separation is within their reaction radii would be tabulated. If a species is capable of undergoing more than one reaction, the reaction allowed to proceed would be selected at random.

To understand the number of calculations required in this more realistic approach, consider the calculation of G-values for 100-keV electrons. Each track might contain ~23,000 species at 10^{-12} s. For diffusive jumps corresponding to 3 ps, some 333,333 time points would be needed in order to simulate track development out to a microsecond. At early time points, ~260,000,000 reactant pairs would be checked for possible reactions and at latter times, assuming half the number of reactants remain in the track, ~66,000,000 pairs would be checked. These calculations would then be performed for ~100 tracks to achieve good statistics on product yields.

The number of required calculations is reduced in RADLYS by allowing reactions to proceed as soon as they are found, thus avoiding having to choose among several possible reactions for each species at any given time. In addition, longer jump times are simulated during the time interval 10^{-10} s to 10^{-6} s and Eq. (2-20) (p. 36) is used to determine reaction probabilities for reactant pairs within the track. This equation, however, is only strictly valid for isolated reactant pairs and is thus applicable only as the track becomes very diffuse.

Regardless of its uncertainties, the modified Oak Ridge model demonstrates excellent agreement with experimental data on

time-dependent yields for e_{aq}^- and OH radicals, the primary initiators of biological damage. Its extension to systems such as aqueous solutions of glycylglycine is therefore made with some degree of confidence.

CHAPTER 4

MODEL FOR THE EARLY CHEMICAL STAGE
OF GLYCYLGLYCINE RADIOLYSIS

In the late 1960's and early 1970's, the radiation chemistry of glycylglycine in aqueous solution was investigated at the Lawrence Berkeley Laboratory as part of a continuing effort to understand radiation effects on amino acids, peptides, and proteins. Under the direction of Warren M. Garrison, several investigations sought to measure yields of radiolytic chemical products. Reaction schemes were proposed to account stoichiometrically for all products analyzed. Studies were made in both oxygenated systems (Makada and Garrison 1972) and deoxygenated systems (Garrison *et al.* 1973); measured product yields from these studies are shown in Tables 4-1 and 4-2. Many of the reactions outlined in these two investigations were confirmed during the late 1970's and early 1980's through experimental techniques of spin trapping, pulse radiolysis, and electron spin resonance (ESR) spectroscopy (Garrison 1987).

This chapter presents a model for the early chemical stage of glycylglycine radiolysis. Its foundation is the Oak Ridge model for deoxygenated and oxygenated water radiolysis presented in Chapters 2 and 3. The reactions proposed in Garrison *et al.* (1973) for deoxygenated

Table 4-1

Product G-Values in the ^{60}Co Irradiation of Glycylglycine
in Deoxygenated Aqueous Solution

Product	0.05 M	1.0 M	Solid
Total Ammonia	3.3	5.2	5.4
Free Ammonia	2.8	3.8	3.5
Acetylglycine	0.9	2.9	3.3
Glyoxylic Acid	0.52	0.76	1.0
Formaldehyde	<0.10	0.22	0.30
Aspartic Acid	1.1	0.30	0.1
Diaminosuccinic Acid	0.8	1.7	Present
Succinic Acid	< 0.1	< 0.1	< 0.1

Source: Table I of Garrison *et al.* (1973).

Table 4-2

Product G-Values in the ^{60}Co Irradiation of 0.05 M Glycylglycine
in Oxygenated Aqueous Solution

Product	0.05 M
Total Ammonia	4.8
Free Ammonia	~2
Formaldehyde	0.1
Glyoxylic Acid	1.9
Formic Acid	1.6
Hydrogen Peroxide	2.1

Source: Table II of Makada and Garrison (1972).

solutions of glycylglycine and the reactions proposed in Makada and Garrison (1972) for oxygenated solutions of glycylglycine are thus added to the existing pure water reactions in the code. All second-order reactions added to the code are modeled according to the techniques presented in Early Chemical Stage of Chapter 2; all pseudo-first-order reactions added are modeled according to the techniques presented in Additional Chemical Reactions of Chapter 3.

There are seventeen reactions describing glycylglycine radiolysis in oxygenated and deoxygenated solutions. However, the rate constant for only one of these reactions is given in the two Garrison references. Consequently, an extensive literature search was made for all values. In cases where rate constants are unavailable, estimates are made from analogous reactions or they are inferred from measured yields of final products.

After a brief review of glycylglycine structure and notation, the model is presented in three sections: (1) the initiating reactions between glycylglycine and radiogenic free radicals; (2) the subsequent reactions in deoxygenated systems; and (3) the subsequent reactions in oxygenated systems. For each section, the reactions as proposed in Garrison et al. (1973) or Makada and Garrison (1972) are presented, followed by estimates of rate constants and schemes for reaction modeling. Makada and Garrison (1972) studied only the chemistry of 0.05 M glycylglycine; thus, the reactions proposed here for oxygenated systems may not be valid for concentrated solutions of glycylglycine.

Glycylglycine Structure

The amino acid glycine, $NH_3^+CH_2COO^-$, has the structure

,
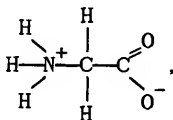
where NH_3^+- is the amino group, $-COO^-$ is the carboxyl group, and the central carbon atom is referred to as the α-carbon. Glycylglycine is formed when the amino group of one glycine reacts with the carboxyl group of another:
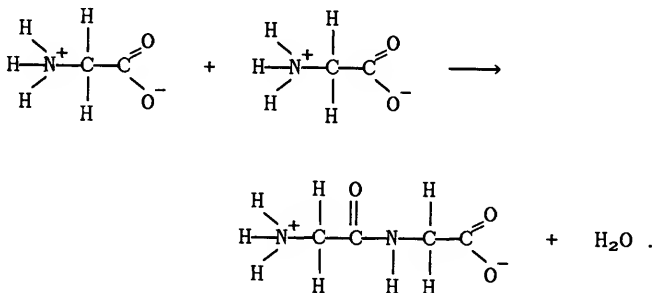
The resulting bond between the two glycine α-carbons, $-\overset{O}{\overset{\|}{C}}-\overset{H}{\overset{|}{N}}-$, is called the peptide bond and thus glycylglycine is termed a dipeptide. The two α-carbons of the glycylglycine molecule are notationally

distinguished by their adjacent functional groups; thus the two carbons are respectively the N-terminal (amino end) and C-terminal (carboxyl end) α-carbon. When catalyzed by the addition of a strong acid or base, a hydrolysis reaction splits the peptide bond through the addition of the elements of water, thus reversing the above reaction. The glycylglycine molecule is denoted in this chapter using the conventional notation $NH_3^+CH_2CONHCH_2COO^-$.

Glycylglycine can exist in three protonated forms,

$$NH_3^+CH_2CONHCH_2COOH \overset{pK \simeq 3.1}{\rightleftharpoons} \underset{\text{(zwitterion)}}{NH_3^+CH_2CONHCH_2COO^-} \overset{pK \simeq 8.1}{\rightleftharpoons} NH_2CH_2CONHCH_2COO^- ,$$
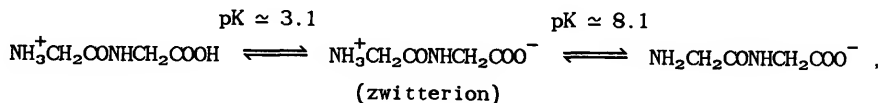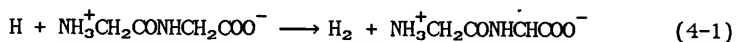
where the pK values correspond to the pH at which two of the forms exist in equal concentrations. The radiation chemistry of glycylglycine depends greatly upon the protonated form of the molecule. For simplicity, all experimental and calculational investigations of glycylglycine are limited to a pH of ~5.9, where the molecule is predominantly in the zwitterion form.
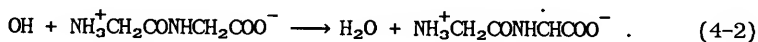
Initiating Reactions

Reactions During Irradiation

The radiolysis of glycylglycine begins with three reactions between the solute and radicals produced within charged-particle tracks. Two reactions involve abstraction of a hydrogen atom from the C-terminal α-carbon:

$$H + NH_3^+CH_2CONHCH_2COO^- \longrightarrow H_2 + NH_3^+CH_2CONH\overset{\bullet}{C}HCOO^- \qquad (4\text{-}1)$$

and

$$OH + NH_3^+CH_2CONHCH_2COO^- \longrightarrow H_2O + NH_3^+CH_2CONH\overset{\bullet}{C}HCOO^- \ . \qquad (4\text{-}2)$$

Hydrogen abstraction is not energetically favorable at other locations along the molecule as long as it is in its zwitterion form (Simic 1983). The dot shown above the C-terminal α-carbon indicates the presence of an unpaired electron and the resulting secondary free radical is hereafter referred to as the H-abstraction radical.

The third initiating reaction involves interaction of a hydrated electron with the carbonyl group ($-\overset{\overset{\displaystyle O}{\displaystyle \|}}{C}-$) of the peptide bond forming an electron adduct:

$$e^-_{aq} + NH_3^+CH_2CONHCH_2COO^- \longrightarrow NH_3^+CH_2\overset{O^-}{\underset{\cdot}{\underset{|}{C}}}\overset{H}{\underset{|}{N}}CH_2COO^- . \qquad (4-3)$$
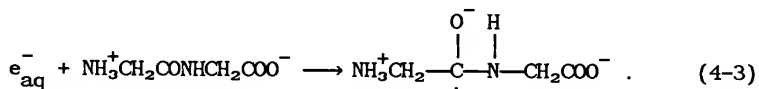
The double bond character of the $C = O$ within the carboxylic group is considerably less than that of the $C = O$ within the peptide bond; thus electron attachment to the former is negligible (Willix and Garrison 1967). Following reaction (4-3), the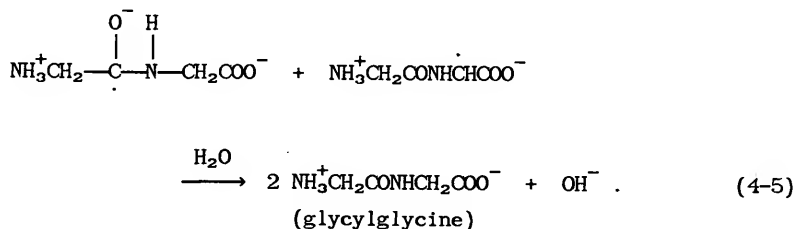 electron is transferred intramolecularly toward the positive amino group, resulting in reductive deamination of the molecule:

$$NH_3^+CH_2\overset{O^-}{\underset{\cdot}{\underset{|}{C}}}\overset{H}{\underset{|}{N}}CH_2COO^- \xrightarrow{\;H^+\;} NH_4^+ + \overset{\cdot}{C}H_2CONHCH_2COO^- . \qquad (4-4)$$
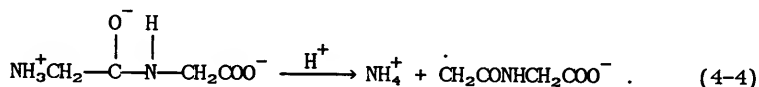
In order to be consistent with the terminology of Garrison et al. (1973), the ammonium ion produced in reaction (4-4) will be referred to as free ammonia, thus distinguishing it from other bound sources of ammonia. At a pH of 5.9, ammonia remains in solution predominantly as NH_4^+. In this dissertation, the second product of reaction (4-4) will be referred to as the deamination radical.

Reductive deamination of glycylglycine in reaction (4-4) is not always 100% efficient (Simic et al. 1970). If the electron adduct encounters an H-abstraction radical before it completes the electron transfer, a reconstitution reaction may follow via

$$NH_3^+CH_2 \overset{\overset{O^-}{|}}{\underset{\cdot}{C}} \overset{\overset{H}{|}}{N} CH_2COO^- \quad + \quad NH_3^+CH_2CONH\overset{\cdot}{C}HCOO^-$$

$$\xrightarrow{\text{H}_2\text{O}} \quad 2 \ NH_3^+CH_2CONHCH_2COO^- \quad + \quad OH^- \ . \tag{4-5}$$
$$\text{(glycylglycine)}$$

Such a reaction is thought to be important only in systems irradiated at high dose rates, such as during pulse radiolysis, or possibly within individual high-LET tracks.

Rate Constants and Modeling Scheme

Since the protonation state of glycylglycine changes with pH, rate constants for the initiating reactions (4-1), (4-2), and (4-3) are pH dependent. A list of experimentally determined rate constants for these reactions is given in Table 4-3. Since both the experiments and calculations of this research were performed at a pH of 5.9, the rate constants selected from Table 4-3 are $k_{4-1} = 5.2 \times 10^6 \ M^{-1}s^{-1}$ for reaction (4-1) (Neta and Schuler 1971), $k_{4-2} = 2.2 \times 10^8 \ M^{-1}s^{-1}$ for reaction (4-2) (Scholes $et \ al.$ 1965), and $k_{4-3} = 2.2 \times 10^8 \ M^{-1}s^{-1}$ for reaction (4-3) (Tal and Faraggi 1975).

These three initiating reactions are modeled as pseudo-first-order reactions such that each H, OH, and e_{aq}^- is allowed to react with the solute with a probability $P = 1 - e^{-kC\Delta t}$, where k is the second-order rate constants listed above, C is the concentration of glycylglycine,

Table 4-3

Rate Constants for Initiating Reactions

Reaction	k ($M^{-1}s^{-1}$)	pH	Reference[a]
H + glygly	2.6×10^6	1	Neta and Schuler (1971)
	5.2×10^6	~7	Neta and Schuler (1971)[b]
OH + glygly	2.6×10^8	6 – 7	Adams $et\ al.$ (1965)
	2.2×10^8	5.5 – 6	Scholes $et\ al.$ (1965)
	4.4×10^8	4.2	Simic $et\ al.$ (1970)
	2.4×10^8	6.2	Masuda $et\ al.$ (1976)
e_{aq}^- + glygly	3.4×10^8	–	Davies $et\ al.$ (1965)
	2.5×10^8	6.38	Braams (1967)
	3.7×10^8	6.4	Simic and Hayon (1971)
	2.2×10^8	5.9	Tal and Faraggi (1975)

[a]Most references obtained from Dr. Alberta B. Ross, Radiation Chemistry Data Center, Radiation Laboratory, University of Notre Dame.
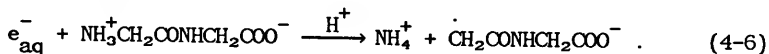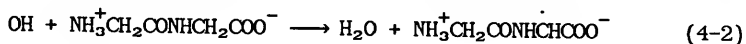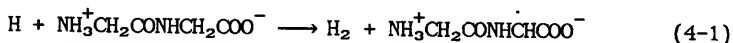
[b]Value at neutral pH was estimated from measured value at pH 1.

and Δt is the time interval modeled. This assumption is thought to be reasonable even at times of $\sim 10^{-12}$ s (before the track species have diffused appreciably), and at glycylglycine concentrations as low as 0.025 M.

Chemistry in Deoxygenated Solution

Reactions During Irradiation

During the irradiation of deoxygenated solutions of glycylglycine, the initiating reactions with radiogenic free radicals can be summarized as follows:

$$H + NH_3^+CH_2CONHCH_2COO^- \longrightarrow H_2 + NH_3^+CH_2CONH\overset{.}{C}HCOO^- \tag{4-1}$$

$$OH + NH_3^+CH_2CONHCH_2COO^- \longrightarrow H_2O + NH_3^+CH_2CONH\overset{.}{C}HCOO^- \tag{4-2}$$

$$e_{aq}^- + NH_3^+CH_2CONHCH_2COO^- \xrightarrow{\ H^+\ } NH_4^+ + \overset{.}{C}H_2CONHCH_2COO^- \ . \tag{4-6}$$
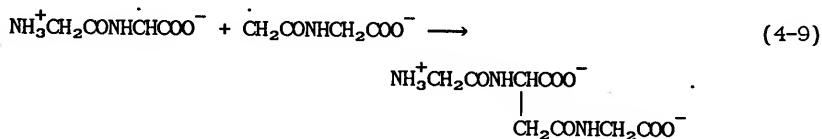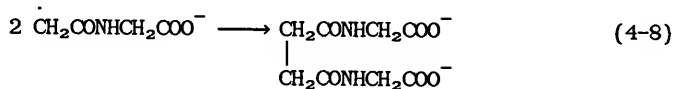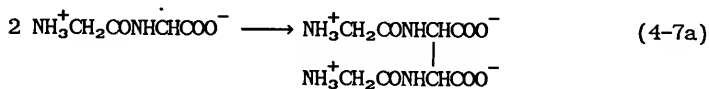
In presenting the result of hydrated electron attack as that shown in reaction (4-6), two assumptions are made: first, the electron adduct intermediate of reactions (4-3) and (4-4) is very short-lived and need not be modeled explicitly; and second, the yield of the reconstitution reaction (4-5) is negligible. The latter assumption is generally a
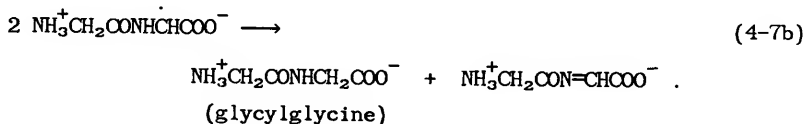
valid one, especially during low-dose-rate photon irradiations. In
addition, it is implied that k_{4-6} equals k_{4-3} given earlier.

The secondary free radicals formed in reactions (4-1), (4-2), and
(4-6) are removed through the following interradical reactions:

$$2 \ \overset{\cdot}{NH_3^+CH_2CONHCHCOO^-} \longrightarrow \begin{array}{c} NH_3^+CH_2CONHCHCOO^- \\ | \\ NH_3^+CH_2CONHCHCOO^- \end{array} \qquad (4\text{-}7a)$$

$$2 \ \overset{\cdot}{CH_2CONHCH_2COO^-} \longrightarrow \begin{array}{c} CH_2CONHCH_2COO^- \\ | \\ CH_2CONHCH_2COO^- \end{array} \qquad (4\text{-}8)$$

$$\overset{\cdot}{NH_3^+CH_2CONHCHCOO^-} + \overset{\cdot}{CH_2CONHCH_2COO^-} \longrightarrow \qquad (4\text{-}9)$$
$$\begin{array}{c} NH_3^+CH_2CONHCHCOO^- \\ | \\ \overset{\cdot}{CH_2CONHCH_2COO^-} \end{array}$$
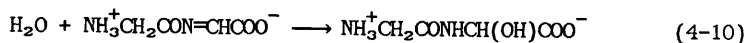
In these reactions, a covalent bond is formed between two species at the
site of their original unpaired electron. The products of reactions
(4-7a), (4-8), and (4-9) are precursors to diaminosuccinic acid,
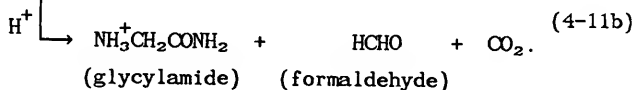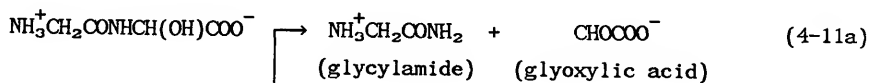succinic acid, and aspartic acid, respectively.

An alternative pathway for reaction (4-7a) during irradiation is
the disproportionation reaction

$$2 \ NH_3^+CH_2CONH\overset{\cdot}{CH}COO^- \longrightarrow \qquad\qquad (4\text{-}7b)$$

$$NH_3^+CH_2CONHCH_2COO^- \ + \ NH_3^+CH_2CON=CHCOO^- \ .$$
$$\text{(glycylglycine)}$$

The subsequent chemistry of the latter product, a dehydropeptide, yields glycylamide, glyoxylic acid, and formaldehyde via

$$H_2O \ + \ NH_3^+CH_2CON=CHCOO^- \longrightarrow NH_3^+CH_2CONHCH(OH)COO^- \qquad (4\text{-}10)$$

followed by

$$NH_3^+CH_2CONHCH(OH)COO^- \longrightarrow \ NH_3^+CH_2CONH_2 \ + \ CHOCOO^- \qquad (4\text{-}11a)$$
$$\text{(glycylamide)} \qquad \text{(glyoxylic acid)}$$

$$H^+ \longrightarrow \ NH_3^+CH_2CONH_2 \ + \qquad HCHO \ + \ CO_2 . \qquad (4\text{-}11b)$$
$$\text{(glycylamide)} \qquad \text{(formaldehyde)}$$

An additional source of glycylamide, glyoxylic acid, and formaldehyde is the reaction

$$H_2O_2 \ + \ NH_3^+CH_2CONH\overset{\cdot}{CH}COO^- \longrightarrow NH_3^+CH_2CONHCH(OH)COO^- + OH \ , \qquad (4\text{-}12)$$
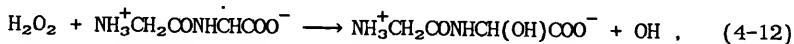
followed by reactions (4-11a) and (4-11b).

Another reaction occurring in irradiated, deoxygenated solutions of glycylglycine is the scavenging of deamination radicals by the solute:

$$\overset{\bullet}{C}H_2CONHCH_2COO^- + NH_3^+CH_2CONHCH_2COO^- \longrightarrow \qquad (4\text{-}13)$$

$$CH_3CONHCH_2COO^- + NH_3^+CH_2CONH\overset{\bullet}{C}HCOO^- \ .$$
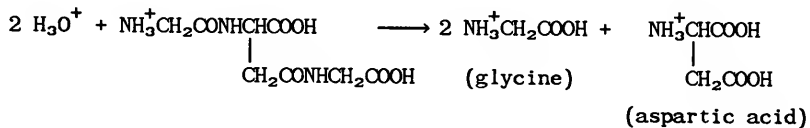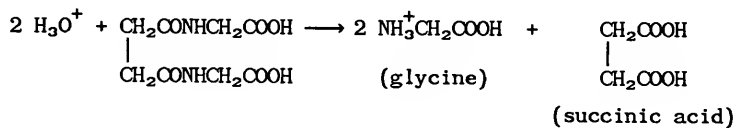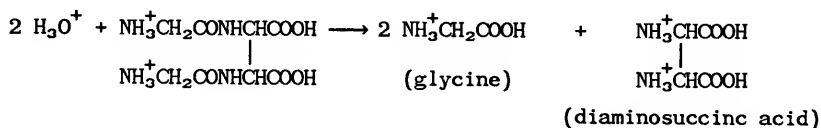(acetylglycine)
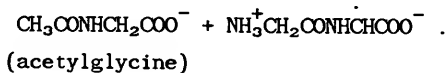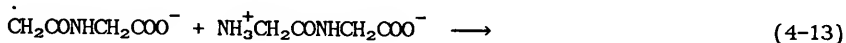
This reaction occurs in competition with reactions (4-8) and (4-9). The result of reaction (4-13) is a conversion of deamination radicals to H-abstraction radicals and acetylglycine.

Chemically-Induced Reactions

Several products are thus formed by irradiating deoxygenated solutions of glycylglycine. Products which can be assayed directly from the irradiated solution include free ammonia from reaction (4-6), glyoxylic acid from reaction (4-11a), formaldehyde and carbon dioxide from reaction (4-11b), and acetylglycine from reaction (4-13). Other products are indirectly assayed by adding strong acid or base to aliquots of the irradiated solution and then measuring various hydrolysis products (Garrison *et al.* 1973). Irradiation products which are indirectly assayed through this technique include those formed in reactions (4-7a), (4-8), and (4-9), and also glycylamide formed in reactions (4-11a) and (4-11b).

In Garrison *et al.* (1973), aliquots of the irradiation solution are made acidic through the addition of 2N HCl, whereby the products of reactions (4-7a), (4-8), and (4-9) undergo the following hydrolysis reactions:

$$2 \ H_3O^+ + NH_3^+CH_2CONHCHCOOH \longrightarrow 2 \ NH_3^+CH_2COOH \quad + \quad NH_3^+CHCOOH$$

with the lower group:

NH₃⁺CH₂CONHCHCOOH under the reactant, (glycine) under the first product, and NH₃⁺CHCOOH under the second product (diaminosuccinc acid).

$$2 \ H_3O^+ + NH_3^+CH_2\underset{|}{CONHCHCOOH} \longrightarrow 2 \ NH_3^+CH_2COOH \quad + \quad NH_3^+\underset{|}{CHCOOH}$$

$$\begin{array}{c} NH_3^+CH_2CONHCHCOOH \\ | \\ NH_3^+CH_2CONHCHCOOH \end{array} \longrightarrow 2\ NH_3^+CH_2COOH \quad + \quad \begin{array}{c} NH_3^+CHCOOH \\ | \\ NH_3^+CHCOOH \end{array}$$

(glycine)   (diaminosuccinc acid)

$$2 \ H_3O^+ + \begin{array}{c} CH_2CONHCH_2COOH \\ | \\ CH_2CONHCH_2COOH \end{array} \longrightarrow 2\ NH_3^+CH_2COOH \ + \ \begin{array}{c} CH_2COOH \\ | \\ CH_2COOH \end{array}$$

(glycine)   (succinic acid)

$$2 \ H_3O^+ + \begin{array}{c} NH_3^+CH_2CONHCHCOOH \\ | \\ CH_2CONHCH_2COOH \end{array} \longrightarrow 2\ NH_3^+CH_2COOH \ + \ \begin{array}{c} NH_3^+CHCOOH \\ | \\ CH_2COOH \end{array} \quad .$$

(glycine)   (aspartic acid)

The yields of the acid precursors formed in reactions (4-7a), (4-8), and (4-9) during irradiation are therefore equal to the yields of the corresponding acids measured within the acidified solution.

The yield of glycylamide formed in reactions (4-11a) and (4-11b) is inferred in Garrison *et al.* (1973) by measuring ammonia released during its hydrolysis at high pH. When 2N NaOH is added to aliquots of the irradiated sample, bound ammonia is released through the reaction:

$$OH^- + \ NH_2CH_2CONH_2 \ \longrightarrow NH_2CH_2COO^- + NH_3 \ .$$

(glycylamide)   (glycine)
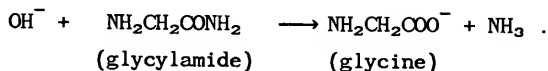
In Garrison *et al.* (1973), this source of ammonia is termed amide ammonia so as to distinguish it from free ammonia produced in reaction (4-6). The term total ammonia refers to the sum of free and amide ammonia.

Rate Constants and Modeling Scheme

The chemistry of secondary radicals produced in deoxygenated solutions is thus described in reactions (4-7) through (4-13). In the simulation code, only the resulting stoichiometry of reactions (4-10), (4-11a), and (4-11b) is considered. In this way, the code scores one glycylamide and also one glyoxylic acid or formaldehyde for every $NH_3^+CH_2CON{=}CHCOO^-$ produced from reaction (4-7b) and for every $NH_3^+CH_2CONHCH(OH)COO^-$ produced in reaction (4-12). Consequently, the simulation code requires rate constants only for reactions (4-7), (4-8), (4-9), (4-12), and (4-13). In addition, the simulation code requires the branching ratio for reactions (4-7a) and (4-7b) and the branching ratio for reactions (4-11a) and (4-11b). Rate constants for the initiating reactions (4-1), (4-2), and (4-6) were discussed previously.

Literature values for secondary radical reactions are limited to only reactions (4-7) and (4-8). In a pulse radiolysis study by Simic *et al.* (1970), k_{4-7} was measured as 3.2×10^8 $M^{-1}s^{-1}$ (pH ~6.0) and k_{4-8} was measured as 9×10^8 $M^{-1}s^{-1}$ (pH 7.0), respectively. Estimates are made for the remaining parameters.

By assuming the rate at which secondary free radicals recombine is fairly uniform, k_{4-9} is estimated at 6×10^8 $M^{-1}s^{-1}$, the average of

k_{4-7} and k_{4-8} given above. In estimating k_{4-12}, one can make a crude assumption that the relative reactivity of the H-abstraction radical (HAR) with H_2O_2 and O_2 is comparable to that of H radicals with H_2O_2 and O_2. Thus,

$$\frac{k_{(H_2O_2 + HAR)}}{k_{(O_2 + HAR)}} = \frac{k_{(H_2O_2 + H)}}{k_{(O_2 + H)}} .$$

where $k_{(H_2O_2 + HAR)}$ is k_{4-12}, $k_{(H_2O_2 + H)}$ is $9.0 \times 10^7 \ M^{-1}s^{-1}$, $k_{(O_2 + H)}$ is $1.8 \times 10^{10} \ M^{-1}s^{-1}$, and $k_{(O_2 + HAR)}$, as estimated in the following section, is $5.5 \times 10^8 \ M^{-1}s^{-1}$. The rate constant k_{4-12} is thus estimated at $2.8 \times 10^6 \ M^{-1}s^{-1}$.

Little information exists as to the value of k_{4-13} other than the statement by Simic that reactions between secondary radicals and solute molecules are "rather slow" (Simic 1983). A value of $1 \times 10^7 \ M^{-1}s^{-1}$ is arbitrarily chosen for k_{4-13} in the simulation code.

By using experimental yields shown in Table 4-1 (p. 71), an estimate of the fraction of reactions (4-7) which result in dimerization [reaction (4-7a)] is obtained by the expression

$$f_{4-7} = \frac{G(\text{diaminosuccinic acid})}{G(\text{diaminosuccinic acid}) + G(\text{glyoxylic acid}) + G(\text{formaldehyde})}.$$

This formulation assumes that the contribution of glyoxylic acid and formaldehyde via reaction (4-12) is small compared to that produced via reaction (4-7b). From the yields in Table 4-1 at 0.05 M and 1 M glycylglycine, the equation above gives f_{4-7} as 0.56 and 0.63, respectively. An average value of 0.60 is used in the simulation model.

Similarly, an estimate of the fraction of reactions (4-11) which produce glyoxylic acid [reaction (4-11a)], as opposed to forming formaldehyde and CO_2 [reaction (4-11b)], is made from the product yields listed in Table 4-1. This fraction is estimated by the expression

$$f_{4-11} = \frac{G(\text{glyoxylic acid})}{G(\text{glyoxylic acid}) + G(\text{formaldehyde})} \ .$$

From the yields in Table 4-1 at 0.05 M and 1 M glycylglycine, the equation above gives f_{4-11} as 0.84 and 0.78, respectively. An average value of 0.81 is used in the simulation model.

As stated in the previous section, the three initiating reactions are treated by pseudo-first-order kinetics in the simulation model. Rate constants used in the model for reactions (4-7), (4-8), (4-9), (4-12), and (4-13) are

$$k_{4-7} = 3.2 \times 10^8 \ M^{-1}s^{-1}$$
$$k_{4-8} = 9 \times 10^8 \ M^{-1}s^{-1}$$
$$k_{4-9} = 6 \times 10^8 \ M^{-1}s^{-1}$$
$$k_{4-12} = 2.8 \times 10^6 \ M^{-1}s^{-1}$$
$$\text{and } k_{4-13} = 1 \times 10^7 \ M^{-1}s^{-1} \quad .$$

Branching ratios for reactions (4-7) and (4-11) are 0.60 and 0.81, respectively. Each of the five reactions above is modeled explicitly at various time points by considering the spatial separation of reactants and their reaction radii. As a first approximation, diffusion coefficients for all secondary free radicals are assumed to equal $1.06 \times 10^{-5} \ cm^2 \ s^{-1}$, the diffusion coefficient of glycine (Weast 1976).

Chemistry in Oxygenated Solution

Reactions During Irradiation

The reactions presented in the previous section continue to occur within irradiated solutions of glycylglycine even in the presence of low concentrations of dissolved oxygen. However, in the presence of O_2 at sufficiently high concentrations, H radicals and hydrated electrons are removed according to the reactions
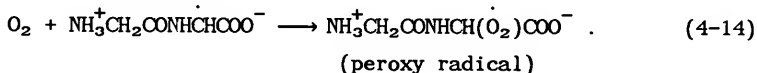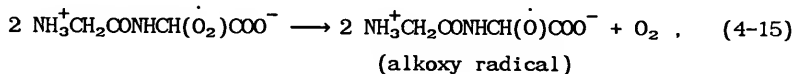
$$H + O_2 \longrightarrow HO_2$$

$$\text{and} \quad e_{aq}^- + O_2 \longrightarrow O_2^- \ .$$
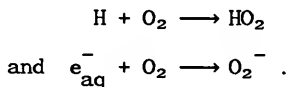
The dominant reaction initiating glycylglycine radiolysis thus becomes H-abstraction by OH radicals:

$$OH + NH_3^+CH_2CONHCH_2COO^- \longrightarrow H_2O + NH_3^+CH_2CONH\overset{\bullet}{C}HCOO^- \ . \qquad (4\text{-}2)$$
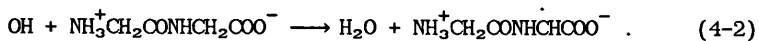
The subsequent chemistry begins with a scavenging of H-abstraction radicals by molecular oxygen via

$$O_2 + NH_3^+CH_2CONH\overset{\bullet}{C}HCOO^- \longrightarrow NH_3^+CH_2CONH\overset{\bullet}{C}H(O_2)COO^- \ . \qquad (4\text{-}14)$$
$$\text{(peroxy radical)}$$

The resulting peroxy radicals react with one another producing alkoxy radicals:

$$2\ NH_3^+CH_2CONH\overset{\bullet}{C}H(O_2)COO^- \longrightarrow 2\ NH_3^+CH_2CONH\overset{\bullet}{C}H(O)COO^- + O_2 \ , \qquad (4\text{-}15)$$
$$\text{(alkoxy radical)}$$

which subsequently react with molecular oxygen according to

$$O_2 + NH_3^+CH_2CONH\overset{\bullet}{C}H(O)COO^- \longrightarrow NH_3^+CH_2CONHCHO + O_2^- + CO_2 \ . \qquad (4\text{-}16)$$
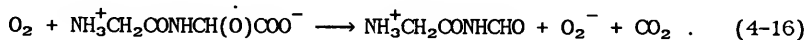
In competition with reaction (4-16), the $(-\overset{\overset{\displaystyle \cdot}{O}}{\underset{|}{C}H-})$ site of the alkoxy radical can react intramolecularly with the C-H bond of the N-terminal α-carbon. The planar structure of the peptide bond forms a "6-member ring" thus enabling an intramolecular hydrogen abstraction to occur:

$$(4-17)$$
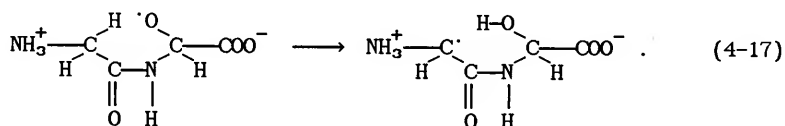
The resulting product can then react with molecular oxygen via

$$O_2 + NH_3^+\overset{\cdot}{C}HCONHCH(OH)COO^- \longrightarrow NH_2^+=CHCONHCH(OH)COO^- + HO_2 \ , \quad (4-18)$$
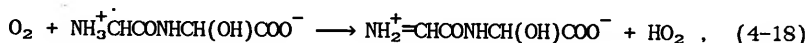
followed by a hydrolysis reaction giving free ammonium ion, glyoxylamide, and glyoxylic acid:

$$H_2O + NH_2^+=CHCONHCH(OH)COO^- \longrightarrow \qquad\qquad (4-19)$$

$$NH_4^+ + \quad CHOCONH_2 \quad + \quad CHOCOO^- \quad .$$
$$\text{(glyoxylamide)} \quad \text{(glyoxylic acid)}$$
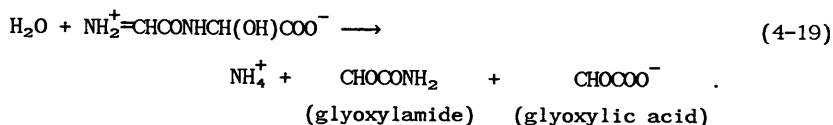
Chemically-Induced Reactions

The terminating reactions for secondary peptide radicals in irradiated, oxygenated solutions of glycylglycine are reactions (4-16) and (4-19). Reaction (4-16) produces O_2^-, CO_2, and the species $NH_3^+CH_2CONHCHO$. Upon the addition of strong base to the irradiated solution, this latter product is hydrolyzed to give glycine, ammonia, and formic acid:

$$2 \ OH^- + NH_2CH_2CONHCHO \longrightarrow NH_2CH_2COO^- + NH_3 + HCOO^- .$$
$$\text{(glycine)} \qquad\qquad \text{(formic acid)}$$
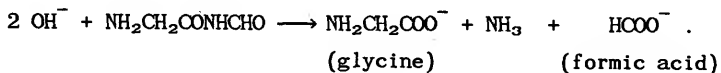
As before, Makada and Garrison (1972) refer to this source of ammonia as amide ammonia so as to distinguish it from the free or unbound ammonia produced in reaction (4-19).

In addition to producing free ammonia, reaction (4-19) also yields glyoxylamide and glyoxylic acid. At high pH, glyoxylamide is hydrolyzed to give additional glyoxylic acid and amide ammonia through the reaction

$$OH^- + CHOCONH_2 \longrightarrow CHOCOO^- + NH_3 .$$
$$\text{(glyoxylamide)} \qquad \text{(glyoxylic acid)}$$
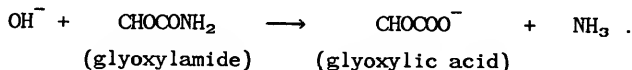
Rate Constants and Modeling Scheme

The primary chemistry of secondary radicals produced in oxygenated solution is thus described in reactions (4-14) through (4-19). In the simulation code, only the resulting stoichiometry of reactions (4-18) and (4-19) is considered. In this manner, the code scores the

production of one free ammonia, one amide ammonia, and two glyoxylic acids (as measured after basic hydrolysis) for every intramolecular reaction (4-17). Thus, only the rate constants for reactions (4-14), (4-15), (4-16), and (4-17) are needed in the simulation code.

A literature search of rate constants was conducted which revealed a range of values useful in estimating k_{4-14} and k_{4-15}. Table 4-4 gives rate constants for the general reaction between molecular oxygen and secondary free radicals. Of the species listed, the one which most closely resembles the glycylglycine radical is the acetylglycylglycine radical as measured by Hayon and Simic (1973). Thus, k_{4-14} is estimated at $5.5 \times 10^8 \ M^{-1}s^{-1}$.

Table 4-5 gives rate constants for the general bimolecular reaction between two peroxy radicals. Of the species listed in this table, the one which most closely represents the peroxyglycylglycine radical is the peroxyacetate radical, $\cdot O_2CH_2COO^-$, as measured by Abramovitch and Rabani (1976). The other listings are for hydroxyl radicals, one is for a cyclic hydrocarbon radical, and the remaining listings are generalizations. Thus, k_{4-15} is estimated at $6.5 \times 10^8 \ M^{-1}s^{-1}$.

The two remaining reactions, (4-16) and (4-17), represent competing reactions for the alkoxy glycylglycine radical, $NH_3^+CH_2CONHCH(O)COO^-$. One can make the assumption that the reaction between O_2 and the alkoxy radical in (4-16) is similar to that between O_2 and the H-abstraction radical in reaction (4-14); thus $k_{4-16} \simeq k_{4-14} \simeq 5.5 \times 10^8 \ M^{-1}s^{-1}$. Given this approximate value for k_{4-16}, one can estimate the value of k_{4-17} using the measured product yields listed in Table 4-2 (p. 72).

Table 4-4

Survey of Rate Constants for Reactions Between
O_2 and Secondary Free Radicals

Radical	k $(M^{-1}s^{-1})$	pH	Reference
Most organic radicals	$\sim 1 \times 10^9$	–	Simic (1983)
$NH_3^+\overset{\cdot}{C}HCOO$	$\sim 1 \times 10^9$	7.9	Abramovitch and Rabani (1976)
$\overset{\cdot}{C}H_2COO^-$	2.1×10^9	8.2	Abramovitch and Rabani (1976)
$(CH_3)_2\overset{\cdot}{C}(OH)$	$\sim 4 \times 10^9$	7.3	Ilan et al. (1976)
$\overset{\cdot}{C}H_2OH$	4.2×10^9	8	Rabani et al. (1974a)
$\overset{\cdot}{C}H_6H_9$	4.9×10^9	7	Rabani et al. (1974b)
$Ac-Gly-NH\overset{\cdot}{C}HCOO^-$	5.5×10^8	5.5	Hayon and Simic (1973)
$CH_3\overset{\cdot}{C}(OH)COO^-$	3.5×10^8	7.3	Hayon and Simic (1973)
$\overset{\cdot}{C}H_2COO^-$	5.0×10^8	4-9	Hayon and Simic (1973)
$CCl_3\overset{\cdot}{C}(OH)_2$	1.0×10^8	5.9	Eriksen et al. (1973)
$NH\overset{\cdot}{C}HCONHCH_2CO$	1.2×10^9	5.0	Hayon and Simic (1971)
$NH\overset{\cdot}{C}(CH_3)CONHCH(CH_3)CO$	1.0×10^9	5.4	Hayon and Simic (1971)
$N(CH_3)\overset{\cdot}{C}HCON(CH_3)CH_2CO$	9.0×10^8	5.2	Hayon and Simic (1971)

Note: Ac and Gly denote an acetyl group and glycine, respectively.
      Horizontal lines indicate bonds within cyclic dipeptides.

Table 4-5

Survey of Rate Constants for Bimolecular Reactions
of Peroxy Radicals

Peroxy Radical	k ($M^{-1}s^{-1}$)	pH	Reference
Most peroxy radicals	$\sim 10^6 - 10^7$	–	Simic (1983)
$\overset{\cdot}{O}_2CH_2COO^-$	6.5×10^8	5.7	Abramovitch and Rabani (1976)
$\overset{\cdot}{O}_2CH_2OH$	1.5×10^8	3	Ilan et al. (1976)
$\overset{\cdot}{O}_2C(CH_3)_2OH$	5.5×10^6	3	Ilan et al. (1976)
$C_6H_9\overset{\cdot}{O}_2$	1.2×10^7	7	Rabani et al. (1974b)
Hydrocarbon and pyrimidyl radicals	$\sim 10^7$	–	Simic (1973)
Hydroxy radicals	$\sim 10^9$	–	Simic (1973)
HOCH$_2\overset{\cdot}{O}_2$	1.85×10^9	6	Downes and Sutton (1973)
CCl$_3\overset{\cdot}{C}O_2(OH)_2$	8.5×10^7	6.6	Eriksen et al. (1973)

Since, after basic hydrolysis, one formic acid is created for every reaction (4-16), and two glyoxylic acids are created for every reaction (4-17), one can write

$$\frac{d[FA]}{dt} = k_{4-16}[AR][O_2]$$

and

$$\frac{d[GA]}{dt} = 2k_{4-17}[AR] \ .$$

where FA, GA, and AR denote formic acid, glyoxylic acid, and the alkoxy glycylglycine radical, respectively. Also, k_{4-16} is a second-order rate constant in units of $M^{-1}s^{-1}$ and k_{4-17} is a first-order rate constant in units of s^{-1}. Upon integration and assuming negligible consumption of dissolved oxygen, one obtains

$$[FA] = k_{4-16}[O_2] \int_0^\infty [AR]dt$$

and

$$[GA] = 2k_{4-17} \int_0^\infty [AR]dt \ .$$

Dividing the expression for [FA] by the expression for [GA] and solving for k_{4-17}, one obtains

$$k_{4-17} = \frac{k_{4-16}[O_2][GA]}{2[FA]} \ .$$

Since [GA]=G(GA)D and [FA]=G(FA)D, where D is the absorbed dose and G is the product G-value,

$$k_{4-17} = \frac{k_{4-16}[O_2]G(GA)}{2G(FA)} .$$

Using $k_{4-16} = 5.5 \times 10^8 \ M^{-1}s^{-1}$, G(formic acid) = 1.6, and G(glyoxylic acid) = 1.9, k_{4-17} can be expressed as $3.27 \times 10^8[O_2] \ s^{-1}$, where $[O_2]$ is the molar concentration of dissolved oxygen.

The rate constants used in modeling the principal reactions occurring in oxygenated, dilute glycylglycine solutions are thus

$$k_{4-3} = 2.2 \times 10^8 \ M^{-1}s^{-1}$$
$$k_{4-14} = 5.5 \times 10^8 \ M^{-1}s^{-1}$$
$$k_{4-15} = 6.5 \times 10^8 \ M^{-1}s^{-1}$$
$$k_{4-16} = 5.5 \times 10^8 \ M^{-1}s^{-1}$$
$$\text{and } k_{4-17} = 3.27 \times 10^8[O_2] \ s^{-1} .$$

In simulating reactions (4-14) and (4-16), the secondary radicals $NH_3^+CH_2CONHCHCOO^-$ and $NH_3^+CH_2CONHCH(O)COO^-$ are given an exponential probability of reaction with O_2 over each simulated time interval. Similarly, each alkoxy radical is allowed an exponential probability of

undergoing the intermolecular reaction (4-17) during these same time intervals. The remaining reactions are modeled explicitly by considering, at each time point, the spatial separation and reaction radii of the reactants.

CHAPTER 5

CALCULATION OF ELECTRON SPECTRA IN IRRADIATED SAMPLES

This chapter presents calculations of electron spectra resulting
from photon irradiation of aqueous solutions. Two calculations are
made--one for 250-kVp X-rays and one for ^{60}Co gamma rays. The former
calculation simulates irradiations conducted at the Oak Ridge National
Laboratory, while the latter simulates irradiations conducted in the
investigations of Garrison (Makada and Garrison 1972; Garrison *et al.*
1973).

The principal distribution of interest is W(E)dE, giving the
fraction of total energy deposition contributed by photon-produced
electrons of initial energy E per energy interval. This distribution is
used in Chapter 7 in the evaluation of Eq. (1-8),

$$G(X,C,\mu s) = \int_0^{E_{max}} \bar{G}(X,C,\mu s,E) \ W(E)dE \ ,\qquad (1-8)$$

giving microsecond yields of various products as functions of
glycylglycine concentration.

98

Calculations for X irradiation

As part of the ORNL project, aqueous solutions of glycylglycine are irradiated with 250-kVp X-rays. The X-ray source used has an inherent filtration of 0.2 mm aluminum and the glycylglycine samples are contained in glass bottles sealed with rubber stoppers. Figure 5-1 shows a schematic diagram of the irradiation geometry. The spectrum of electrons produced within a given sample is found by calculating: (1), the relative fluence spectrum of photons incident upon the bottle, $N_0^f(E)dE$; (2), the relative fluence spectrum of photons attenuated by the bottle and incident upon the water surface, $N(E)dE$; and (3), the transport of photons through the water volume. The electron distribution $W(E)dE$ is tabulated during photon transport.

Calculation of Photon Spectra

When the tungsten target of an X-ray tube is irradiated by electrons accelerated through a potential T_0, the relative energy-fluence spectrum of unfiltered bremsstrahlung photons can be fit by a triangular envelope called Kramers distribution (Kramers 1923; Attix 1986). This distribution is given by the expression
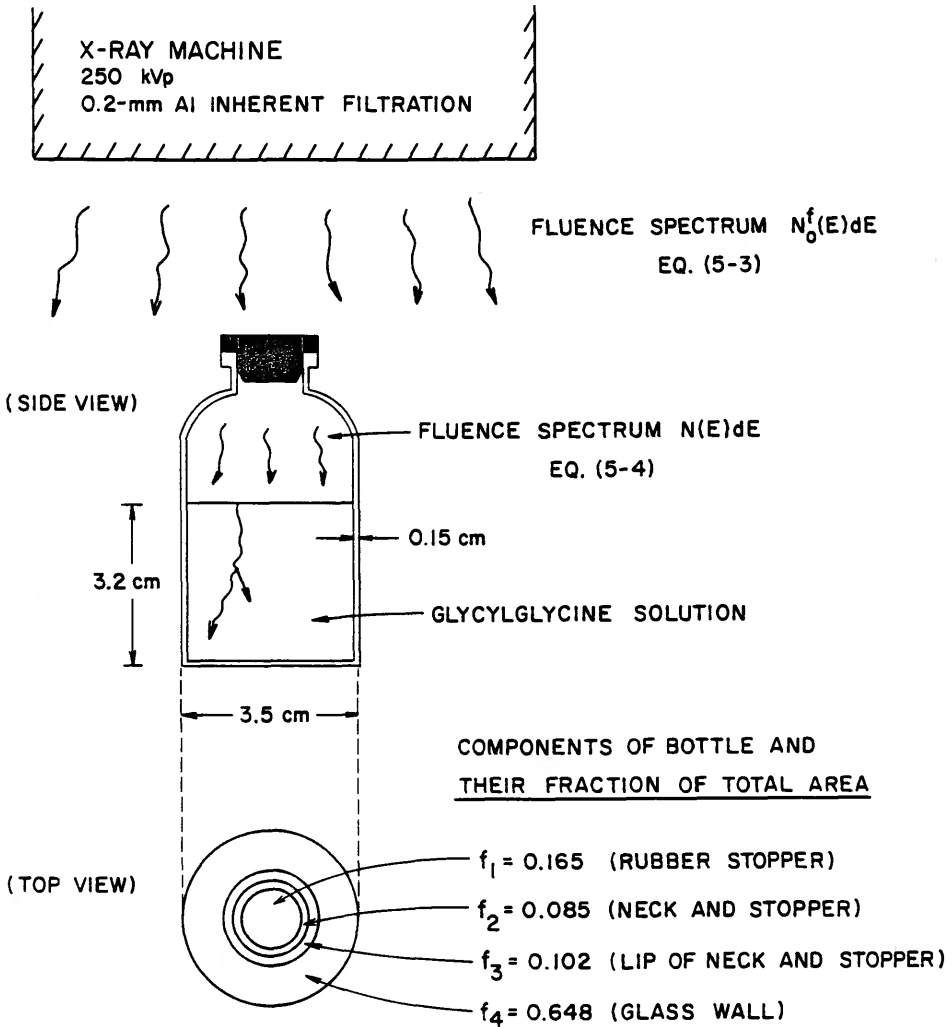
$$I_0^u(E)dE = C(E_m - E)dE , \qquad (5-1)$$

Fig. 5-1. Schematic of irradiation experiments performed at the Biology Division of ORNL. Depicted are the photon fluence spectra $N_0^f(E)dE$ incident upon the sample bottle and $N(E)dE$ incident upon the solution surface.

where $I_0^u(E)dE$ is the energy-fluence at energy E per energy interval,
$E_m=T_0$ is the maximum photon energy, and C is a constant of
proportionality. The relative fluence spectrum of unfiltered photons is
given by

$$N_0^u(E)dE = \frac{C}{E}(E_m - E)dE . \qquad (5\text{-}2)$$

The spectrum of X-rays incident upon each irradiated sample bottle
is obtained by adjusting Eq. (5-2) for any filtration inherent to the
X-ray tube. For the X-ray machine used, this filtration has an
effective value of 0.2 mm aluminum and thus the filtered fluence
spectrum is given by

$$N_0^f(E)dE = \frac{C}{E}(E_m - E) \exp\left\{-\left[\frac{\mu_A(E)}{\rho}\right]\rho x\right\} dE , \qquad (5\text{-}3)$$

where $\dfrac{\mu_A(E)}{\rho}$ is the mass energy-absorption coefficient of aluminum at
photon energy E (Attix 1986), ρ is the density of aluminum in g/cm^3, and
x is the effective thickness of the filter. The spectrum $N_0^f(E)dE$,
normalized to unit area, is shown in Fig. 5-2. Broad-beam geometry is
assumed; therefore, by using energy-absorption coefficients, scattered
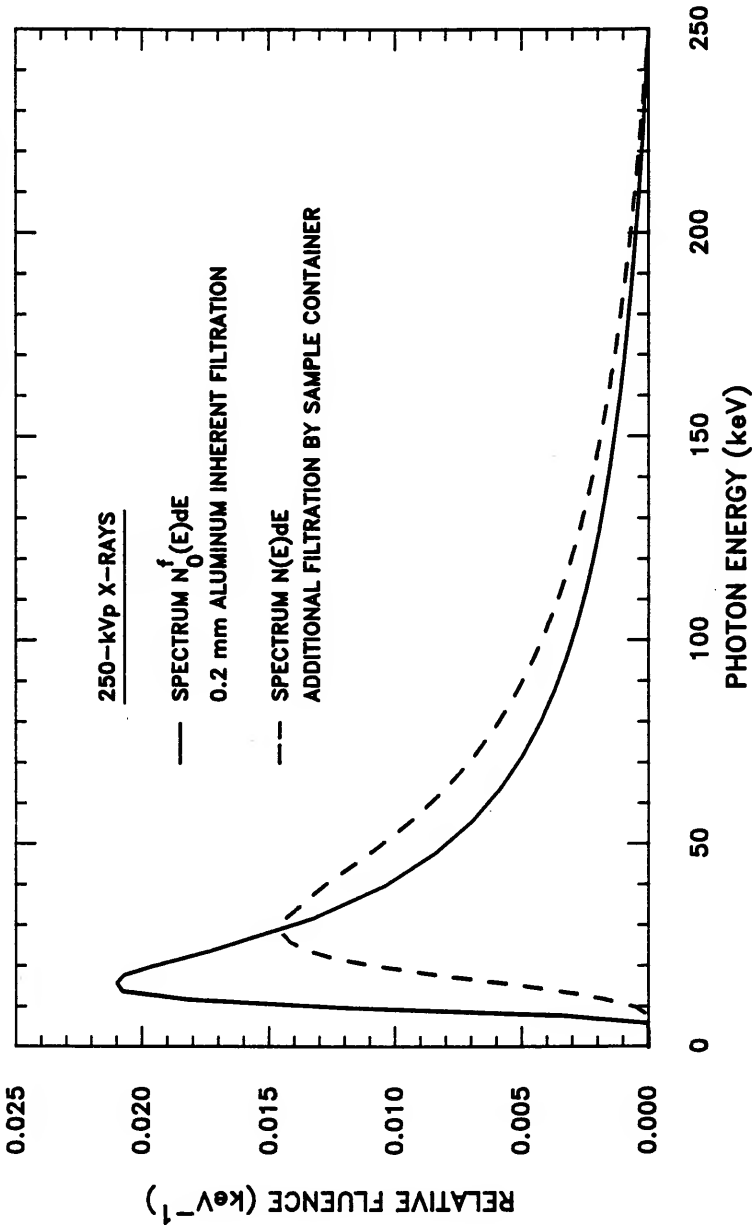as well as uncollided photons contribute to $N_0^f(E)dE$. Good agreement has

Fig. 5-2. Photon fluence spectra $N_0^f(E)dE$ incident upon the sample bottle and $N(E)dE$ incident upon the solution surface. Both are normalized to unit area.

been found between experimental spectra and those predicted by Eq. (5-3) (Villforth *et al.* 1958).

Additional filtration is provided by the glass wall and rubber stopper of the sample container. By approximating the direction of the photon field as normal to the container, photons enter the sample volume having traversed one of four components of the sample bottle: (1) the rubber stopper; (2) the lip of the rubber stopper and the glass neck of the bottle; (3) the lip of the rubber stopper, the lip of the bottle's glass neck, and the glass wall; or, (4) the glass wall of the bottle (see Fig. 5-1). The fluence spectrum of photons reaching the aqueous solution inside the bottle is thus approximated by the expression

$$N(E)dE = N_0^f(E) \sum_i \left\{ f_i \exp -\left[\mu_A^r(E) \ x_i^r + \mu_A^g(E) \ x_i^g \right] \right\} dE, \quad (5-4)$$

where $N_0^f(E)$ is the incident fluence spectrum from Eq. (5-3); f_i is the fraction of photons incident on the bottle which traverse component i; x_i^r and x_i^g are the total thicknesses of rubber and glass, respectively, for component i; and $\mu_A^r(E)$ and $\mu_A^g(E)$ are the linear energy-absorption coefficients for rubber and glass, respectively. Mass energy-absorption coefficients for polyethylene and Pyrex glass are used to estimate $\mu_A^r(E)$ and $\mu_A^g(E)$, respectively (Attix 1986). The normalized spectrum $N(E)dE$ is shown in Fig. 5-2. The small contribution of scattered photons incident

from the sides of sample bottle is neglected in the current calculations.

Photon Transport

The spectrum of electrons produced within the irradiated solution is calculated by simulating individual photon interactions within that solution. Such calculations are made by the Monte Carlo code PHOEL-2 (Turner *et al.* 1979; Turner *et al.* 1980; Todo *et al.* 1982), which was modified here for spatial transport through the water volume.

The program begins by randomly selecting a photon energy E from the incident spectrum N(E)dE and a point of incidence on the water surface. For calculational convenience, all photons are assumed incident normal to the surface. Next, a flight distance is randomly selected and the photon is allowed to undergo either a photoelectric or Compton scattering interaction with a water molecule.

If a photoelectric event occurs, the code determines whether an oxygen K-shell or L-shell vacancy is produced. A K-shell vacancy produces a photoelectron of energy $T=E-BE_K$, where BE_K is the K-shell binding energy in oxygen. Since the fluorescent yield from oxygen is small, a 0.508 keV Auger electron is also produced. An L-shell vacancy results in the production of a photoelectron of energy $T=E-BE_L$, where BE_L is the L-shell binding energy in oxygen.

If a Compton event occurs, an energy T is selected for the scattered electron. As in the case of photoelectric events, an Auger electron is produced as a result of a K-shell vacancy. A new direction

and flight distance is then selected for the scattered photon of energy E'=E-T. The scattered photon is followed through subsequent interactions until it exits the sample bottle. Another photon is then selected from the incident spectrum N(E)dE.

As part of the calculations, the numbers of photon-produced electrons falling within various initial energy bins are tabulated. The resulting frequency distribution of electron energies, normalized to unit area, is shown in Fig. 5-3. The figure also shows contributions by photoelectrons and Compton electrons. The sharp peak in the photoelectron distribution at 0.508 keV is due to the production of Auger electrons.

The electron distribution W(E)dE is obtained by summing initial energies of electrons falling within various initial energy bins. This distribution, normalized to unit area, is shown in Fig. 5-4 along with its photoelectron and Compton-electron components. In this derivation of W(E)dE, all electrons produced within the sample volume are assumed to deposit their full initial energy within the solution.

Calculations for ^{60}Co Gamma Irradiation

In the investigations of Garrison, glycylglycine solutions in sealed Pyrex tubes were irradiated by ^{60}Co gamma rays. By considering the mean free paths of the emitted gamma photons in both glass and water, negligible spectral attenuation is assumed to occur throughout
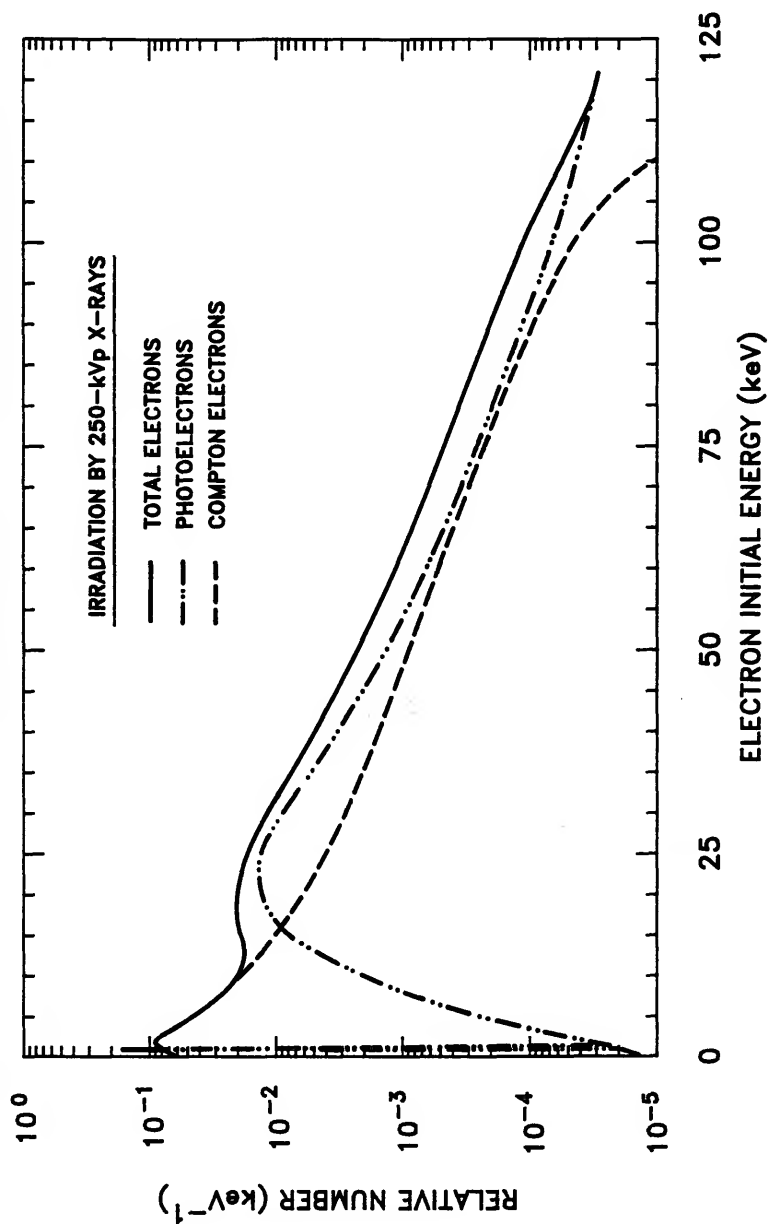
Fig. 5-3. Frequency distribution of electron initial energies produced within glycylglycine solutions during irradiation by 250-kVp X-rays.
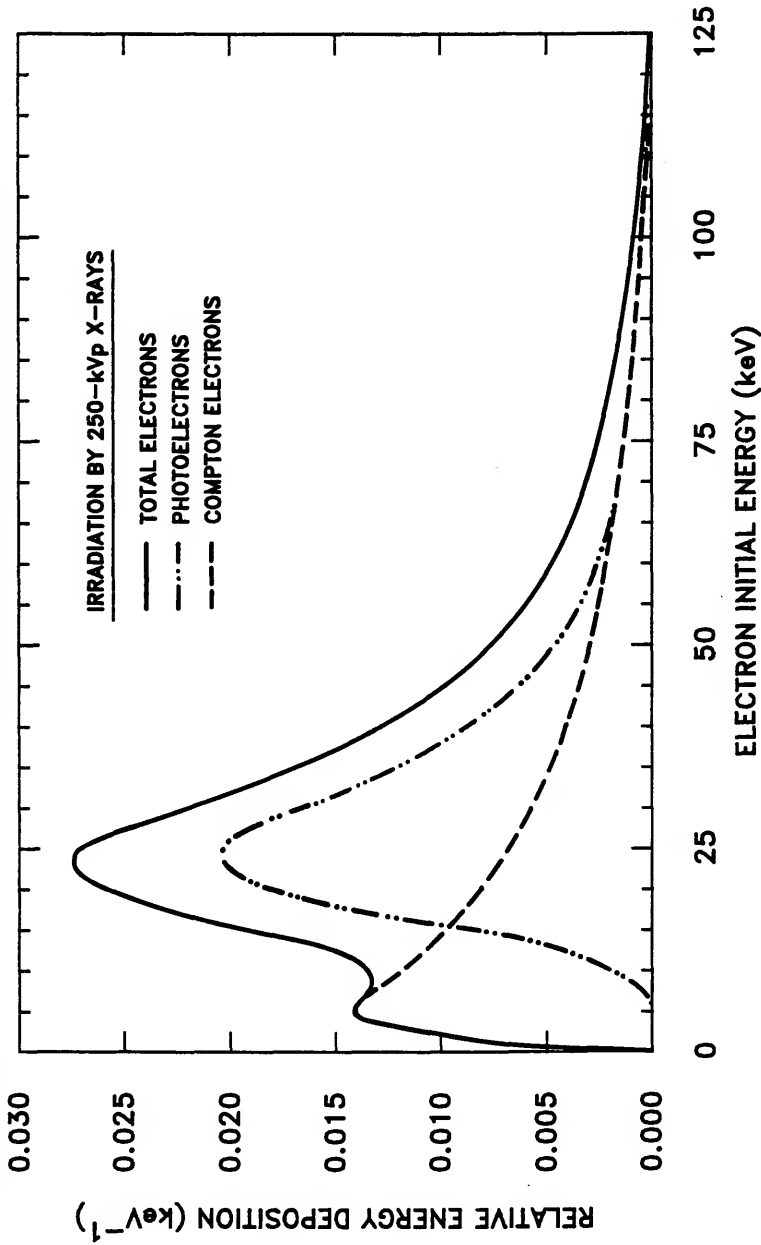
Fig. 5-4. Distribution W(E)dE for X-irradiation giving the fraction of total energy deposition by photon-produced electrons of initial energy E per energy interval. Curve for total electrons is normalized to unit area.

the irradiated sample. Electron spectra for these experiments are thus calculated by the modified version of PHOEL-2 using a bienergetic input spectrum of 1332- and 1173-keV photons.

Figure 5-5 shows the resulting frequency distribution of electron energies, normalized to unit area. A sharp peak at 0.508 keV due to Auger electron production is not shown in this figure. The distribution $W(E)dE$ for ^{60}Co irradiation, normalized to unit area, is shown in Fig. 5-6.
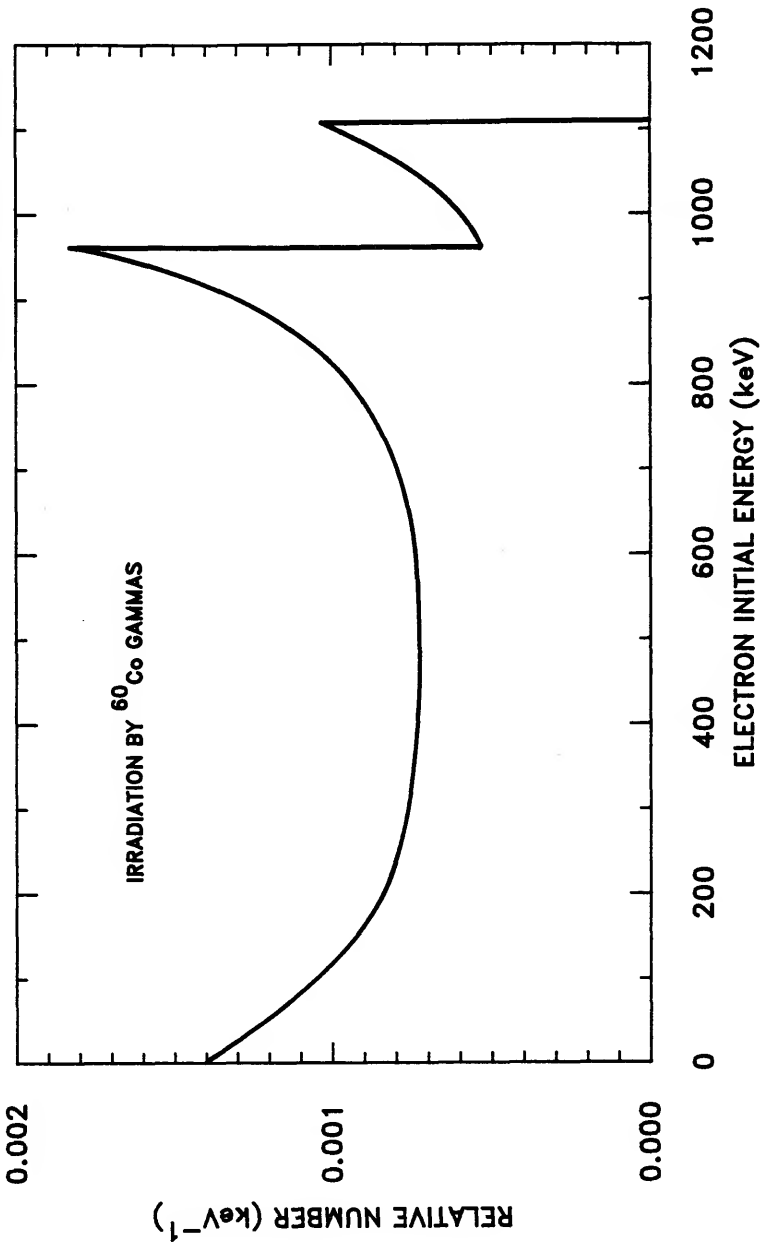
Fig. 5-5. Frequency distribution of electron initial energies produced within glycylglycine solutions during irradiation by ^{60}Co gamma rays.
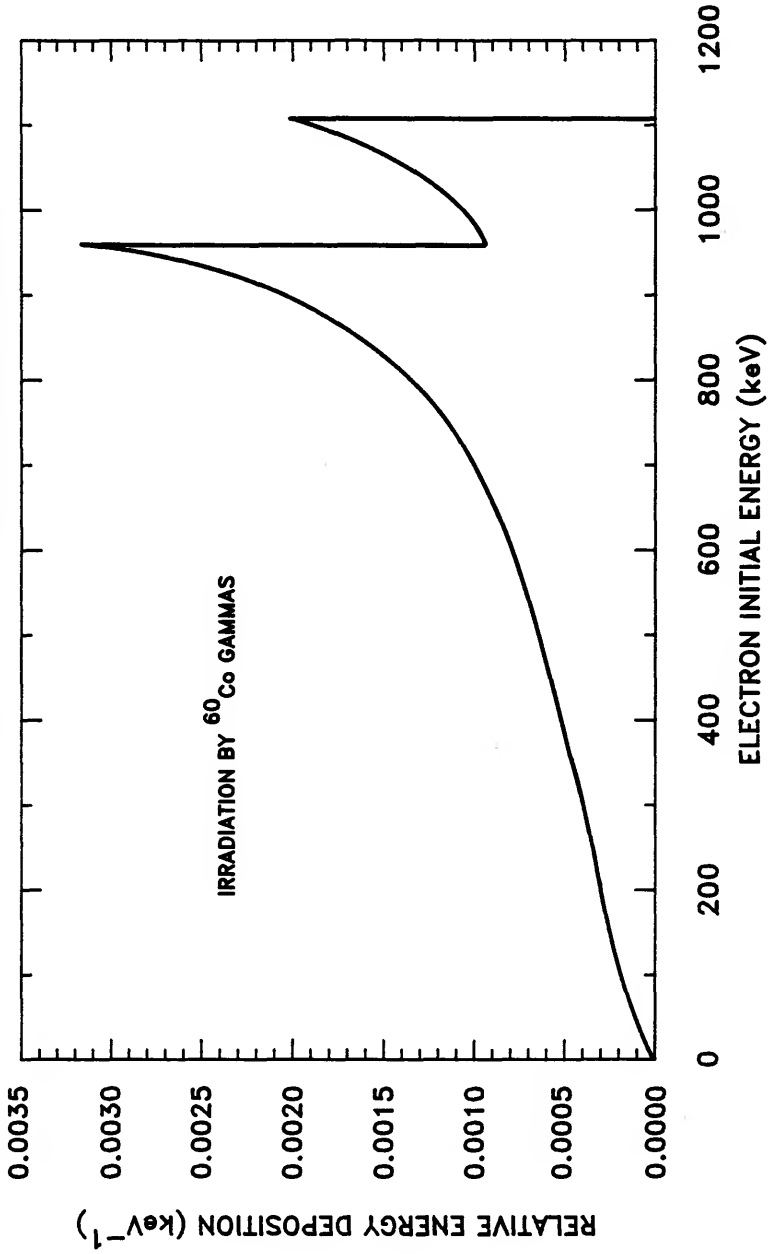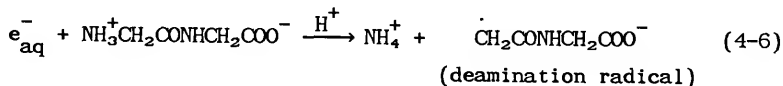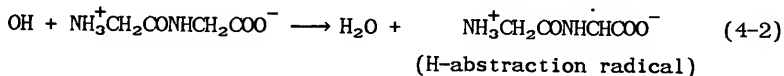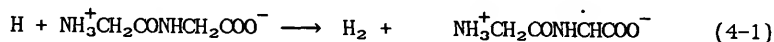
Fig. 5-6. Distribution W(E)dE for ^{60}Co gamma irradiation giving the fraction of total energy deposition by electrons of initial energy E per energy interval. The curve is normalized to unit area.

CHAPTER 6

CALCULATION OF MICROSECOND PRODUCT YIELDS
FOR MONOENERGETIC ELECTRONS

This chapter presents calculated results from the transport and
chemical development of monoenergetic electron tracks in deoxygenated
solutions of glycylglycine. Electron transport is simulated by the
program OREC, while the prechemical stage of glycylglycine radiolysis is
simulated by the modified version of SPCS described in Chapter 3. The
early chemical stage is simulated by the program presented in Chapter 4
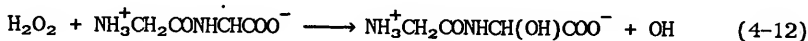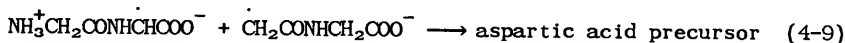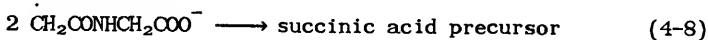for deoxygenated solutions. For reference within this chapter, the
glycylglycine reactions used in the model are given below:

$$H + NH_3^+CH_2CONHCH_2COO^- \longrightarrow H_2 + NH_3^+CH_2CONH\overset{\cdot}{C}HCOO^- \qquad (4-1)$$

$$OH + NH_3^+CH_2CONHCH_2COO^- \longrightarrow H_2O + NH_3^+CH_2CONH\overset{\cdot}{C}HCOO^- \qquad (4-2)$$
$$\text{(H-abstraction radical)}$$

$$e_{aq}^- + NH_3^+CH_2CONHCH_2COO^- \xrightarrow{H^+} NH_4^+ + \overset{\cdot}{C}H_2CONHCH_2COO^- \qquad (4-6)$$
$$\text{(deamination radical)}$$

111

$$2\ \overset{+}{NH_3}CH_2CONH\overset{\cdot}{C}HCOO^- \longrightarrow \text{diaminosuccinic acid precursor} \quad (4\text{-}7a)$$

$$\longrightarrow \overset{+}{NH_3}CH_2CONHCH_2COO^-$$
$$+ \quad (4\text{-}7b)$$
$$\overset{+}{NH_3}CH_2CON{=}CHCOO^-$$

$$2\ \overset{\cdot}{C}H_2CONHCH_2COO^- \longrightarrow \text{succinic acid precursor} \quad (4\text{-}8)$$

$$\overset{+}{NH_3}CH_2CONH\overset{\cdot}{C}HCOO^- + \overset{\cdot}{C}H_2CONHCH_2COO^- \longrightarrow \text{aspartic acid precursor} \quad (4\text{-}9)$$

$$H_2O_2 + \overset{+}{NH_3}CH_2CONH\overset{\cdot}{C}HCOO^- \longrightarrow \overset{+}{NH_3}CH_2CONHCH(OH)COO^- + OH \quad (4\text{-}12)$$

$$\overset{\cdot}{C}H_2CONHCH_2COO^- + \overset{+}{NH_3}CH_2CONHCH_2COO^- \longrightarrow \quad (4\text{-}13)$$
$$\text{acetylglycine} + \overset{+}{NH_3}CH_2CONH\overset{\cdot}{C}HCOO^- \ .$$

As discussed in Chapter 4, both the product $\overset{+}{NH_3}CH_2CON{=}CHCOO^-$ formed in reaction (4-7b) and the product $\overset{+}{NH_3}CH_2CONHCH(OH)COO^-$ formed in reaction (4-12) produce glycylamide, glyoxylic acid, and formaldehyde during subsequent reactions in the irradiated solution.

Calculated results for free ammonia produced in reaction (4-6) are presented first. The influence of both solute concentration and track structure on the dynamics of free ammonia production are discussed. Microsecond yields for other products are presented in the second section of this chapter.

Free Ammonia

Free ammonia is formed through the scavenging of hydrated electrons by the glycylglycine solute. The ability of glycylglycine to scavenge hydrated electrons within the track of a 50-keV primary electron is demonstrated in Fig. 6-1. The top curve shows the calculated time decay of e_{aq}^- within such tracks in pure deoxygenated water. This decay is due to intratrack reactions such as $e_{aq}^- + OH \longrightarrow OH^-$ and $2e_{aq}^- + 2H_2O \longrightarrow H_2 + 2OH^-$. The rate of these reactions gradually decreases with increasing diffusion of the track species over time; the process of diffusion thus accounts for the inflection point observed between 10^{-9} and 10^{-8} s. The decay curve of hydrated electrons in pure water represents the maximum supply of hydrated electrons which would be available for reaction with a glycylglycine solute.

In Fig. 6-1, the curve for the G-value of hydrated electrons in 0.025 M glycylglycine coincides with the pure water curve up until $\sim 3 \times 10^{-9}$ s. This suggests that glycylglycine at 0.025 M is ineffective in competing with intratrack reactions for the supply of hydrated electrons until the track reactants have diffused out to $\sim 3 \times 10^{-9}$ s. After that time, track species become increasingly separated such that solute scavenging becomes more likely than intratrack reactions. Solute scavenging then continues until all hydrated electrons are consumed by one microsecond. At a concentration of 1.2 M, solute scavenging within the track becomes important at an earlier time, $\sim 6 \times 10^{-11}$ s, and all hydrated electrons are scavenged by $\sim 10^{-8}$ s. Since the pure water yield
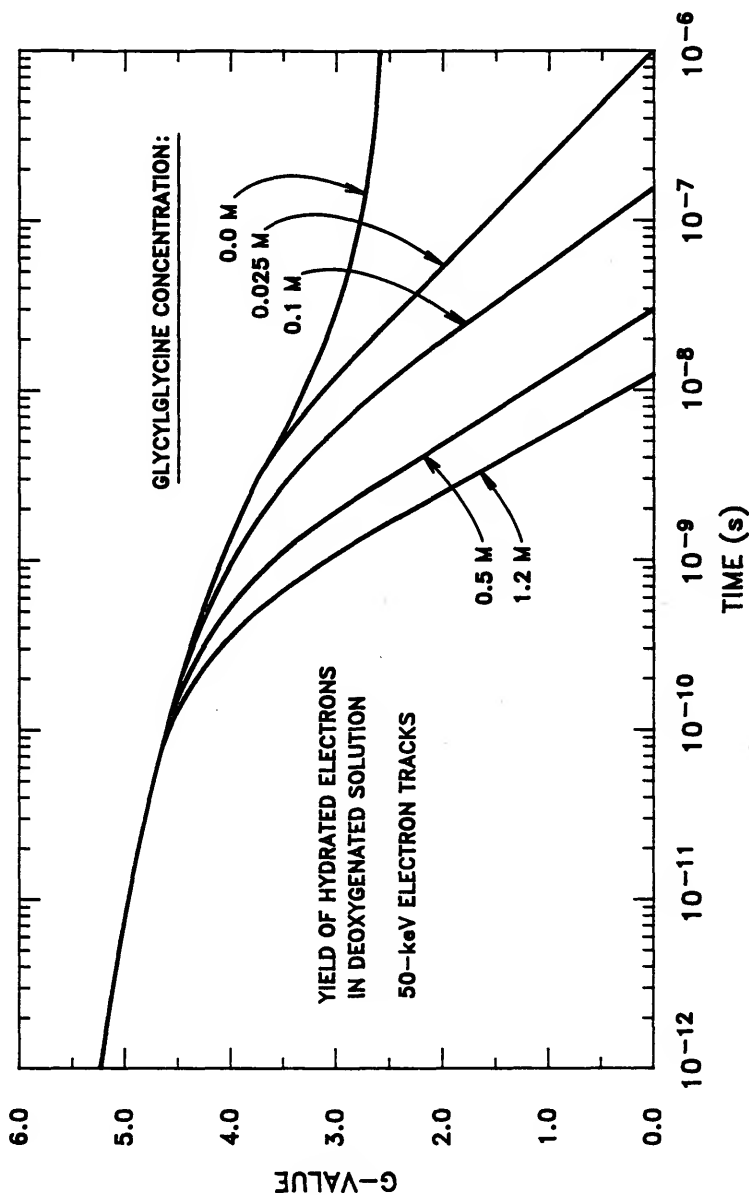
Fig. 6-1. Yield of hydrated electrons calculated for 50-keV electron tracks in deoxygenated glycylglycine solution as a function of time and solute concentration.

of e_{aq}^- is greater at earlier times, and since e_{aq}^- scavenging occurs at earlier times with increasing solute concentration, the total yield of free ammonia is expected to be greater in systems with higher concentrations of glycylglycine.

The yield of free ammonia within 50-keV electron tracks as a function of time and solute concentration is presented in Fig. 6-2. As predicted by Fig. 6-1, increases in solute concentration result in a greater and earlier production of free ammonia within the track.

In modeling the interaction between glycylglycine and the hydrated electron according to reaction (4-6), the intermediate product formed, the electron adduct, is not treated explicitly (see the discussion of initiating reactions in Chapter 4). It is neglected in the simulations mostly because the mean life of the adduct has not be experimentally determined, although it is believed to be very short[1]. The curves in Fig. 6-2 are therefore representative only for an electron adduct whose mean life is infinitely short. If a mean life of the adduct is assumed, these curves would shift forward in time in proportion to the magnitude of that mean life.

The yield of free ammonia within an electron track is also dependent upon the initial energy of the primary electron. Consider the difference between 1-keV and 50-keV electron tracks. The initial picosecond yield of reactive species within these two tracks are essentially the same. However, the stopping power of liquid water for

---

[1]Warren M. Garrison, Lawrence Berkeley Laboratory, University of California, private communication.
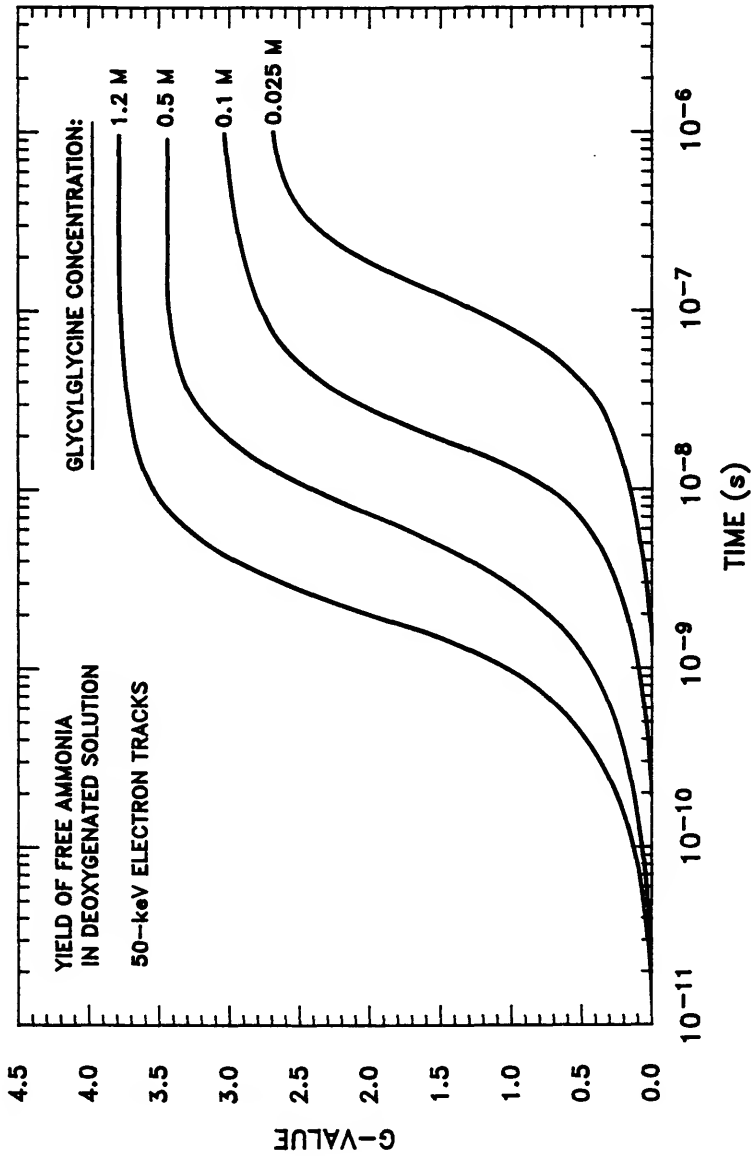
Fig. 6-2. Yield of free ammonia calculated for 50-keV electron tracks in deoxygenated glycylglycine solution as a function of time and solute concentration.

1-keV electrons is ~110 MeV/cm, while the stopping power for 50-keV electrons is ~6 MeV/cm (see Fig. 1-1, p. 7). The initial density of reactive species within 1-keV electron tracks is thus much greater than that within 50-keV tracks.

Figure 6-3 demonstrates the effect of initial track density upon the decay of e_{aq}^- in pure water. The greater initial density of species within 1-keV tracks allows for a greater rate of intratrack reactions compared to the rate within 50-keV tracks. The supply of hydrated electrons available for reaction with glycylglycine at later times is therefore less within 1-keV tracks than within 50-keV tracks. Correspondingly, free ammonia production is expected to be less for 1-keV tracks than for 50-keV tracks at a given value of glycylglycine concentration.

Figure 6-4 shows calculated yields of free ammonia as functions of time for 1-keV and 50-keV electrons and for two concentrations. As predicted, the final yield of free ammonia is less for 1-keV electrons than for 50-keV electrons. The starting time of ammonia production, however, is relatively independent of the electron initial energy.

Figure 6-5 shows calculated microsecond yields of free ammonia at various glycylglycine concentrations and as functions of electron initial energy between 1 keV and 140 keV. For purposes of clarity, curves calculated at 0.05 M, 0.25 M, 0.75 M, and 1.0 M glycylglycine are not shown. As discussed above, the yield of free ammonia increases with increasing electron initial energy and increasing glycylglycine concentration. At one microsecond, all hydrated electrons are
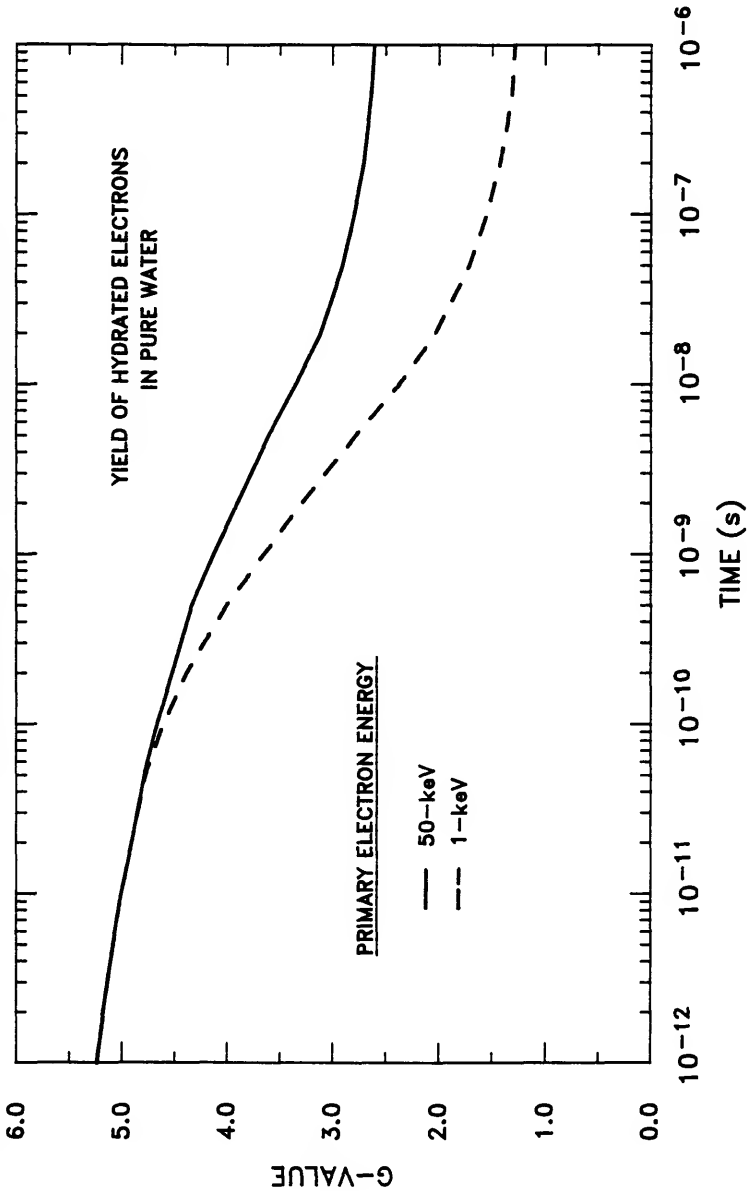
Fig. 6-3. Yield of hydrated electrons in pure water calculated for 1- and 50-keV electron tracks.
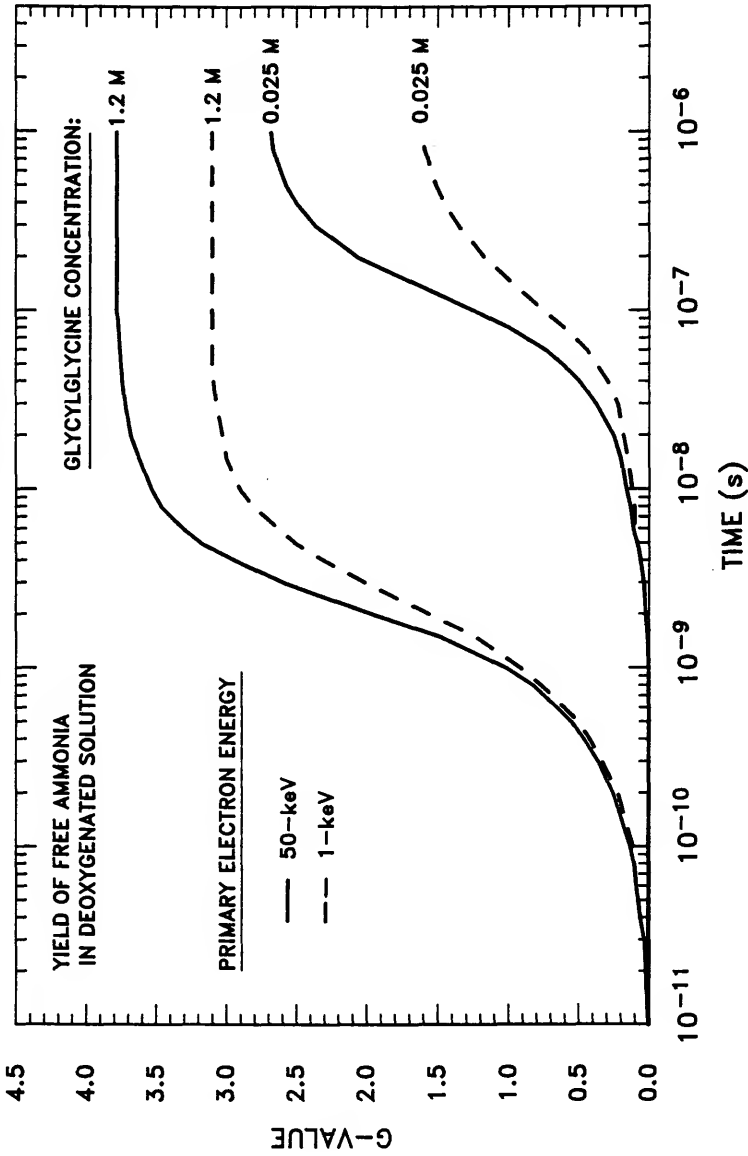
Fig. 6-4. Yield of free ammonia calculated for 1- and 50-keV electron tracks in deoxygenated glycylglycine solution at concentrations of 0.025 M and 1.2 M.
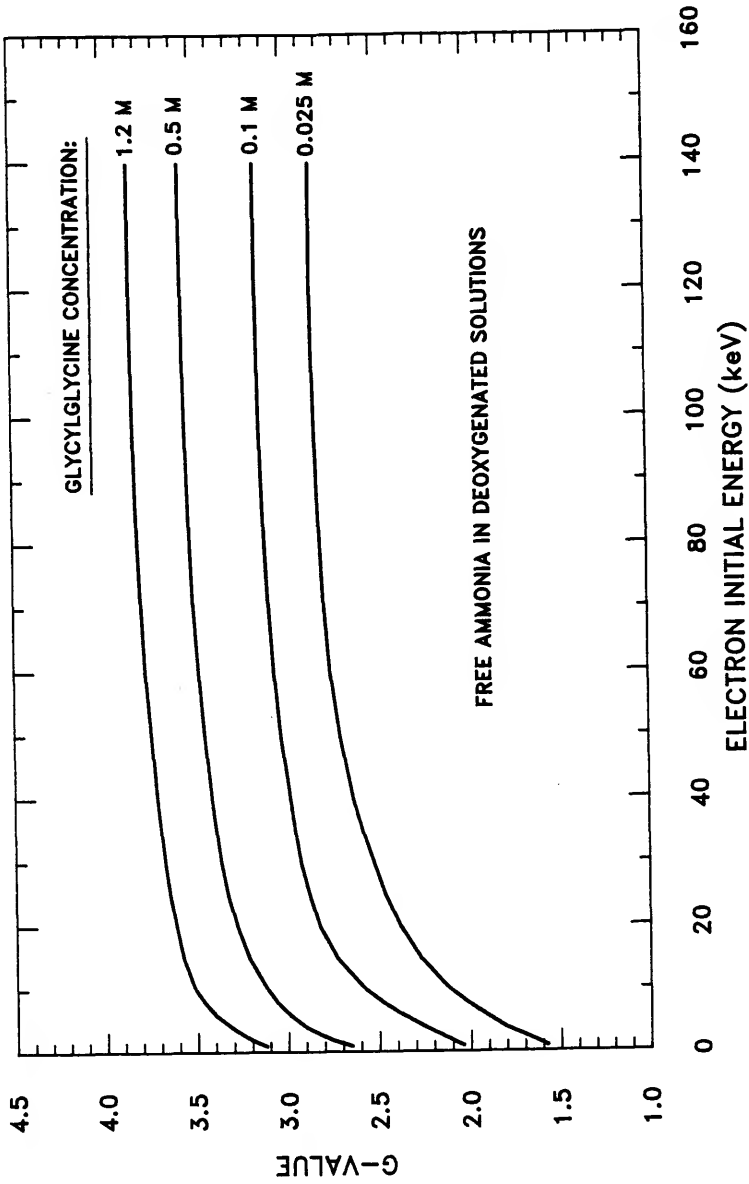
120

Fig. 6-5. Calculated yield of free ammonia in deoxygenated glycylglycine solution as a function of electron initial energy and solute concentration.

scavenged, even at a concentration of 0.025 M. Consequently, these microsecond yields are also the final yields produced within solutions irradiated by electrons of various initial energies.

It is instructive to know the variation of the G-value of free ammonia above 140 keV and below 1 keV. As shown in Fig. 6-5, the G-value of free ammonia approaches a constant value above 100 keV. Since the stopping power of water varies only slightly for electrons between 100 keV and 1 MeV (see Fig. 1-1, p.7), the G-value for free ammonia is expected to remain virtually constant within this energy range.

Certainly, one way of verifying this assumption is to continue the calculations for electrons of greater and greater initial energies. Computer memory and run-time limitations, however, prohibit simulating complete electron tracks of initial energies much greater than 140 keV. As an alternative to full transport of high-energy electrons, free ammonia yields within initial segments of these tracks are investigated. Table 6-1 presents calculated, differential yields of free ammonia produced within initial segments of 100-keV, 300-keV, 500-keV, 700-keV, 900-keV, and 1.1-MeV electrons tracks. Fluctuations in the values shown are attributed to the production of high-energy secondary electrons; the inclusion of these secondary tracks can greatly alter the mean LET, and thus the yield of free ammonia, of the total simulated track segment. Nevertheless, no significant increase in differential yields is observed with increasing primary energy.

Table 6-1

Differential G-values for Free Ammonia Production

Electron Energy (keV)	Glycylglycine Concentration (M)		
	0.025	0.5	1.2
100	2.95 ± 0.09	3.67 ± 0.06	3.92 ± 0.06
300	3.09 ± 0.11	3.27 ± 0.11	3.89 ± 0.08
500	–	3.56 ± 0.08	4.23 ± 0.17
700	3.05 ± 0.13	3.60 ± 0.15	3.95 ± 0.12
900	2.98 ± 0.15	3.68 ± 0.10	4.03 ± 0.10
1100	3.17 ± 0.24	3.73 ± 0.13	4.12 ± 0.11

Figure 6-6 shows the variation of free ammonia yield in 0.5 M glycylglycine solution at electron energies below 1 keV. The total yield of free ammonia is shown to be the sum of ammonia produced by scavenging of secondary electrons within the track and ammonia produced through scavenging the initial primary electron. The curve labeled "primary" is simply a plot of $1/E$, where E is the initial energy of the primary in units of 100 eV. Above 1 keV, the yield of free ammonia is almost entirely due to secondary electrons. As the energy of the primary electron falls below 100 eV, energy loss events begin to favor excitation over ionization and there is a decline the number of secondary electrons produced. At primary energies below 7.4 eV, no secondary electrons are produced and each primary electron produces only one ammonia molecule through reaction (4-6).

Other Products

As shown in reaction (4-6), one deamination radical is created for every free ammonia produced. These secondary radicals are subsequently scavenged by the glycylglycine solute in reaction (4-13), producing acetylglycine and the H-abstraction radical. The latter product is identical to that formed in reactions (4-1) and (4-2). Figure 6-7 presents the microsecond yield of deamination radicals calculated as a function of electron initial energy and solute concentration. As the solute concentration increases, the energy dependence of the yields
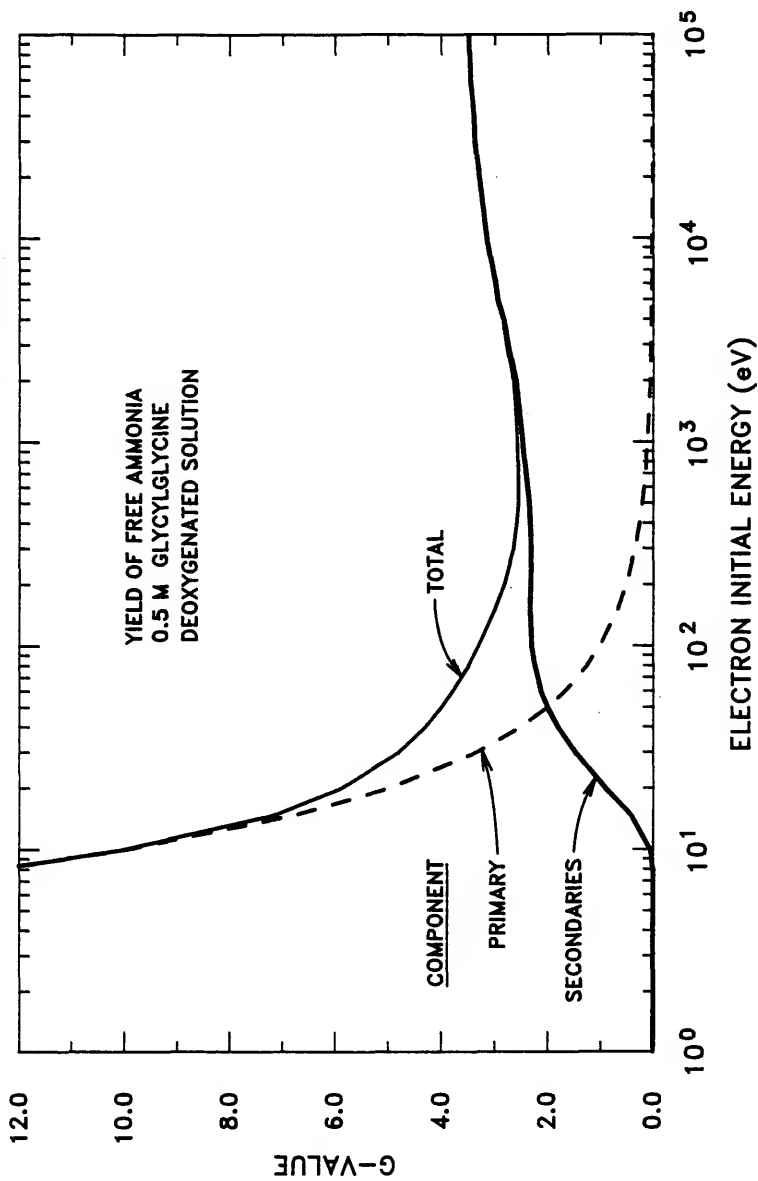
Fig. 6-6. Calculated yield of free ammonia in deoxygenated, 0.5 M glycylglycine solution as a function of electron initial energy from 1 eV to 100 keV.
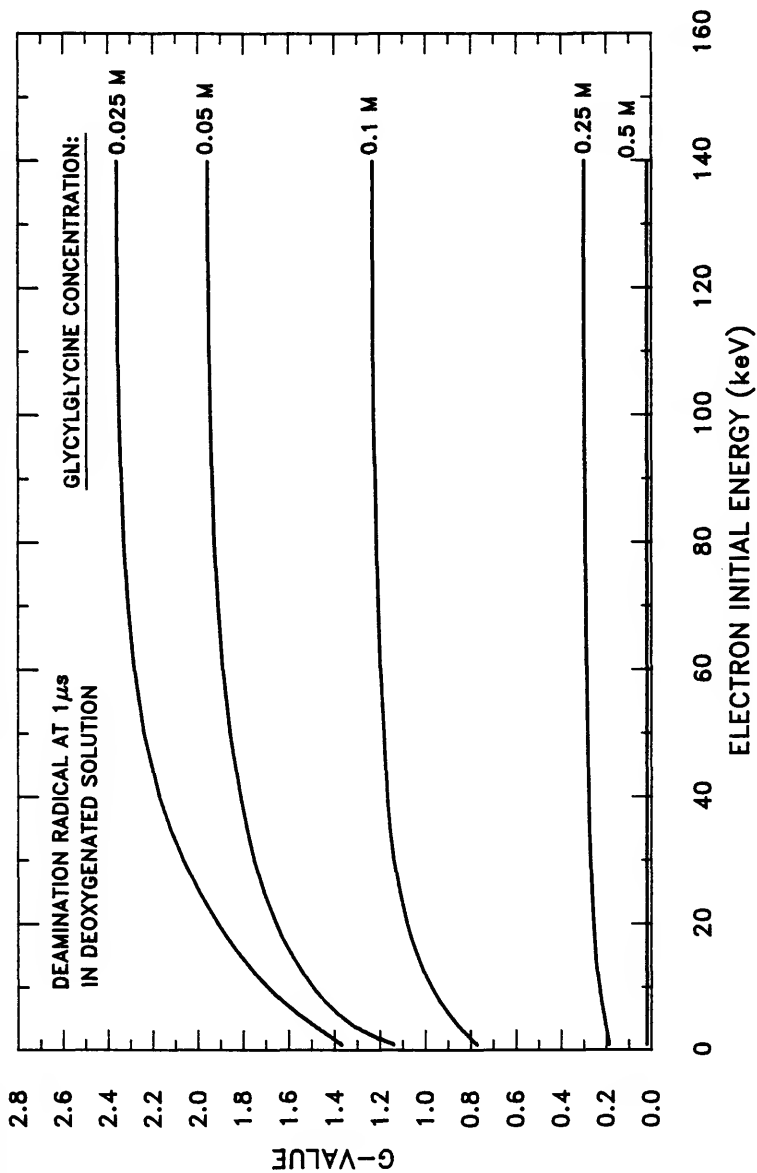
Fig. 6-7. Microsecond yield of deamination radicals in deoxygenated glycylglycine solution as a function of electron initial energy and solute concentration.

decreases. At solute concentrations greater than 0.5 M, all deamination radicals are scavenged by a microsecond. The corresponding curves for the microsecond yield of acetylglycine are presented in Fig. 6-8.

Deamination radicals are also removed through reactions (4-8) and (4-9), the former producing the precursor to succinic acid and the latter producing the precursor to aspartic acid. Calculated microsecond yields of these two products are very small and no energy dependence is demonstrated. Microsecond G-values of succinic acid precursor range from 0.003 at 0.025 M to 0.015 at 1.2 M glycylglycine. Microsecond G-values of aspartic acid precursor range from 0.007 at 0.025 M to 0.062 at 1.2 M glycylglycine.

H-abstraction radicals are produced through solute scavenging of OH and H radicals within the track. Another source is solute scavenging of deamination radicals. The calculated microsecond yield of H-abstraction radicals is presented in Fig. 6-9 as a function of electron initial energy and glycylglycine concentration. As in the case of free ammonia, the microsecond yield of H-abstraction radicals increases with increasing electron initial energy and solute concentration.

H-abstraction radicals are removed via dimerization in reaction (4-7a) or via disproportionation in reaction (4-7b). Reaction (4-7a) produces the precursor to diaminosuccinic acid and reaction (4-7b) produces the intermediate species $NH_3^+CH_2CON=CHCOO^-$. Calculated microsecond yields of these two products are very small and no energy dependence is demonstrated. Microsecond G-values of diaminosuccinic acid precursor range from 0.002 at 0.025 M to 0.055 at 1.2 M
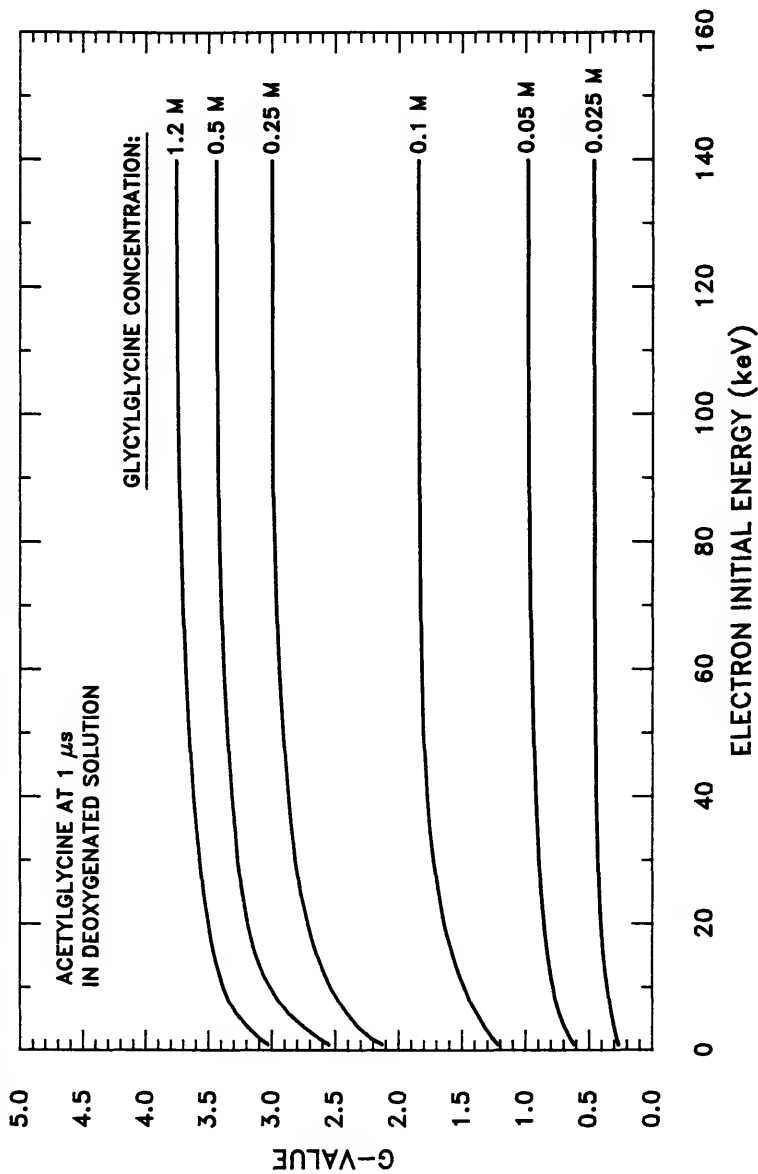
Fig. 6-8. Microsecond yield of acetylglycine in deoxygenated glycylglycine solution as a function of electron initial energy and solute concentration.
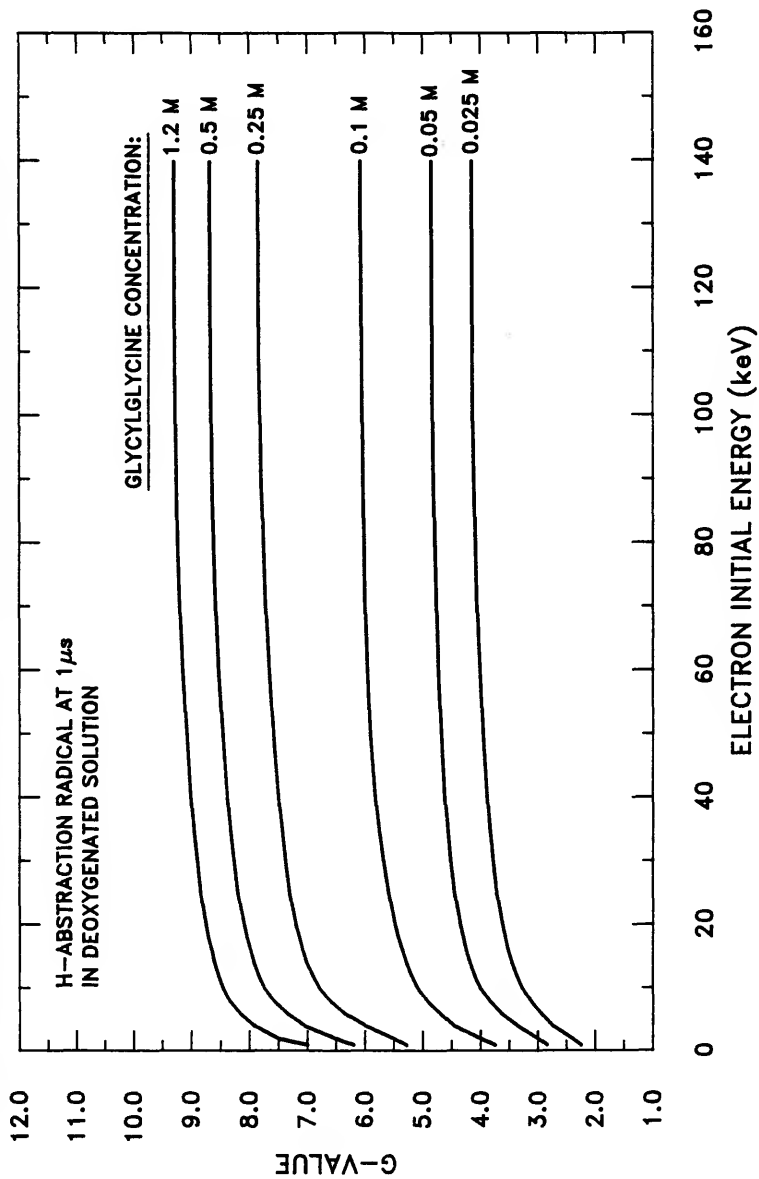
Fig. 6-9. Microsecond yield of H-abstraction radicals in deoxygenated glycylglycine solution as a function of electron initial energy and solute concentration.

glycylglycine. Microsecond G-values of $NH_3^+CH_2CON{=}CHCOO^-$ range from 0.001 at 0.025 M to 0.036 at 1.2 M glycylglycine.

For glycylglycine concentrations greater than 0.025 M, calculations show that all OH radicals and hydrated electrons within electron tracks are completely scavenged by a microsecond. Due to the smaller rate constant for reaction (4-1), a small number of H radicals still remain at a microsecond, even at solute concentrations of 1.2 M. Figure 6-10 shows calculated yields of H radicals as functions of electron initial energy and for various solute concentrations.

Hydrogen peroxide is a final product to consider in deoxygenated solutions. In reacting with H-abstraction radicals via reaction (4-12), H_2O_2 produces the intermediate species $NH_3^+CH_2CONHCH(OH)COO^-$. Calculations at various electron energies and solute concentrations show essentially no production of $NH_3^+CH_2CONHCH(OH)COO^-$ prior to a microsecond.

Figure 6-11 presents calculated yields of hydrogen peroxide as functions of electron initial energy and for various solute concentrations. Hydrogen peroxide is produced primarily through the intratrack reaction $OH + OH \longrightarrow H_2O_2$. Therefore, increases in solute concentration and decreases in track density at higher electron energies would allow greater OH scavenging and a subsequent decline in the production of H_2O_2. Both these effects are demonstrated in Fig. 6-11.
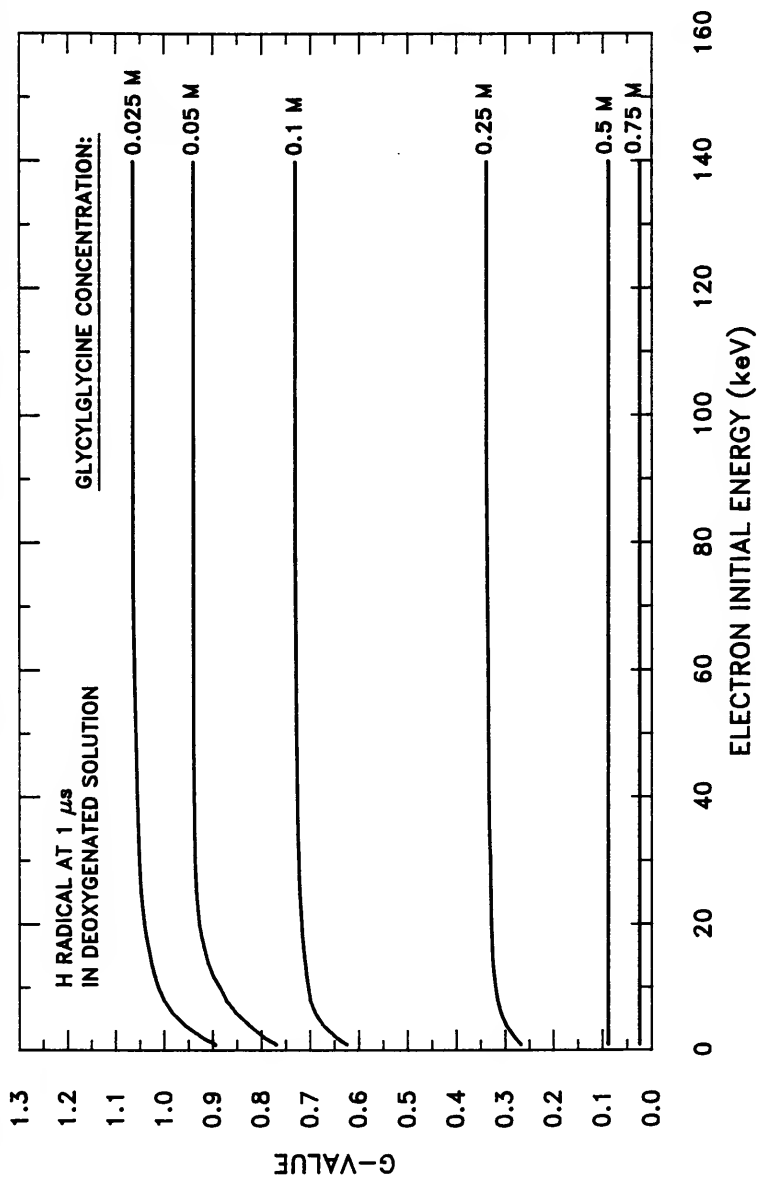
Fig. 6-10. Microsecond yield of H radicals in deoxygenated glycylglycine solution as a function of electron initial energy and solute concentration.
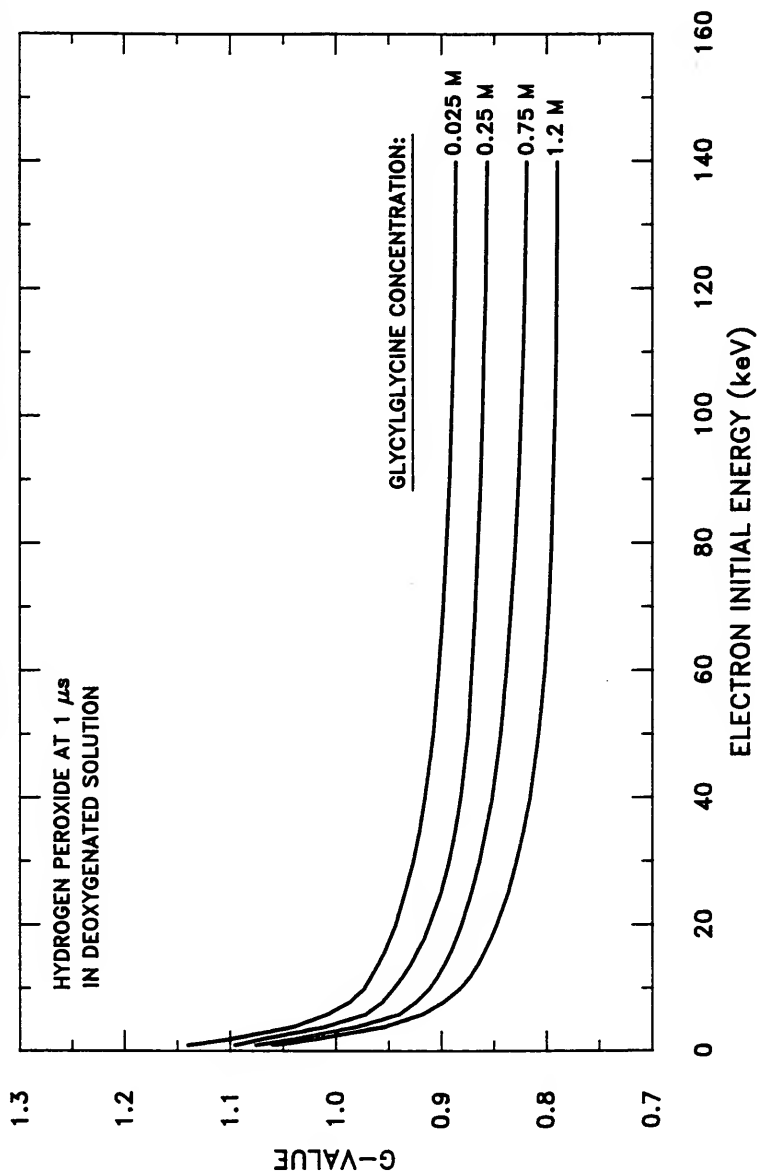
Fig. 6-11. Microsecond yield of hydrogen peroxide in deoxygenated glycylglycine solution as a function of electron initial energy and solute concentration.

CHAPTER 7

CALCULATION OF MICROSECOND PRODUCT YIELDS
IN IRRADIATED SAMPLES

The results of Chapters 5 and 6 are used in this chapter to calculate microsecond product yields for deoxygenated solutions of glycylglycine irradiated either by 250-kVp X-rays or by ^{60}Co gamma rays. These yields are calculated according to Eq. (1-8),

$$G(X,C,\mu s) \quad = \quad \int_0^{E_{max}} \bar{G}(X,C,\mu s,E) \; W(E)dE \; , \qquad (1-8)$$

where E_{max} is the maximum energy of electrons produced within the irradiated system. In water, Compton scattering is the dominant interaction for photon energies greater than 175 keV; therefore, E_{max} is defined as the maximum Compton energy for these two radiation sources. Consequently, E_{max} is 123.6 keV for irradiations by 250-kVp X-rays and is 1117.6 keV for irradiations by ^{60}Co gamma rays.

The distribution W(E)dE represents the fraction of total energy deposition contributed by electrons of initial energy E per energy

132

interval. In Chapter 5, W(E)dE was calculated for (1) 250-kVp X-rays
and the sample container used in this research, and (2) for samples
irradiated by ^{60}Co gamma rays for comparison with measurements by
Garrison et $al.$ (1973). The function $\bar{G}(X,C,\mu s,E)$ represents the average
microsecond G-value of product X as a function of initial electron
energy E and glycylglycine concentration C. In Chapter 6, $\bar{G}(X,C,\mu s,E)$
was calculated for several products, for several solute concentrations,
and for electron energies from 1 keV to 140 keV.

In the first section of this chapter, Eq. (1-8) is evaluated for
free ammonia under both irradiation conditions. Since all free ammonia
is produced within electron tracks prior to a microsecond at
glycylglycine concentrations as low as 0.025 M, the resulting values of
$G(NH_3^f,C,\mu s)$ can be directly compared to measured yields of free ammonia.
The second section of this chapter presents microsecond G-values for
other products.

<u>Free Ammonia</u>

<u>Evaluation of Equation (1-8)</u>

In order to calculate the yield of free ammonia as a function of
glycylglycine concentration and for both irradiation conditions, three
quantities are needed: (1) W(E)dE for 250-kVp X-rays, (2) W(E)dE for
^{60}Co gamma rays, and (3) the function $\bar{G}(NH_3^f,C,\mu s,E)$. In Chapter 5,
W(E)dE was presented in Fig. 5-4 (p. 107) for samples irradiated by
250-kVp X-rays and in Fig. 5-6 (p. 110) for samples irradiated by

^{60}Co gamma rays. Chapter 6 presented $\bar{G}(NH_3^f,C,\mu s,E)$ as shown in Fig. 6-5 (p. 120).

The function $\bar{G}(NH_3^f,C,\mu s,E)$ in Fig. 6-5 is shown only within the energy range 1 keV to 140 keV. In order to evaluate Eq. (1-8), assumptions are made as to the behavior of $\bar{G}(NH_3^f,C,\mu s,E)$ from 0 keV to 1 keV, and from 140 keV to E_{max}. As discussed in Chapter 6, G-values for all products are essentially constant from 100 keV to 1 MeV; values of $\bar{G}(NH_3^f,C,\mu s,E)$ from 140 keV to 1117.6 keV are therefore assumed equal to the value at 140 keV.

As demonstrated in Fig. 6-6, there is much structure in the function $\bar{G}(NH_3^f,C,\mu s,E)$ below 1 keV. This structure need not be treated explicitly, however, in the evaluation of Eq. (1-8). Integrating W(E)dE in Fig. 5-4 (p. 107) from 0 to 1 keV indicates that less than 0.1% of the total energy deposited in the solution is due to primary electrons with initial energies below 1 keV. Figure 5-6 (p. 110) indicates that the percentage is far less in the case of ^{60}Co gamma irradiation. For calculational convenience, the function $\bar{G}(NH_3^f,C,\mu s,E)$ is therefore extrapolated to zero energy for each value of solute concentration C.

With the behavior of $\bar{G}(NH_3^f,C,\mu s,E)$ established over the appropriate energy ranges, Eq. (1-8) is evaluated for both X-ray and ^{60}Co irradiations for the concentration range 0.025 M to 1.2 M glycylglycine. The resulting calculated yields of free ammonia are presented below with discussions concerning (1) differences between calculated yields produced under X and ^{60}Co gamma irradiation, (2) the comparison between calculated and measured yields produced under each irradiation

condition, and (3) the contribution of direct radiation interaction to the production of free ammonia.

Difference in Yields Produced Under X and ^{60}Co gamma Irradiation

Figure 7-1 presents calculated yields of free ammonia for glycylglycine concentrations from 0.025 M to 1.2 M. The solid curves represent the 95% confidence interval for free ammonia yields in simulated irradiations by 250-kVp X-rays. The dashed lines represent the corresponding 95% confidence interval for simulated irradiations by ^{60}Co gamma rays. These confidence intervals represent the statistical fluctuations in G-values calculated for individual electron tracks and are an expected consequence of Monte Carlo sampling in the calculations. Figure 7-1 shows that, at each value of solute concentration and at the 95% confidence level, the yield of free ammonia produced under simulated irradiations by ^{60}Co gamma rays is greater than that produced under simulated irradiations by 250-kVp X-rays.

The difference in calculated free ammonia G-values by the two radiation sources is attributed to the difference in the electron energy distributions produced by these two sources. As an example, one can consider the mean of these distributions which were shown in Fig. 5-4 (p. 107) and in Fig. 5-6 (p. 110) of Chapter 5. The mean initial energy of electrons produced during X irradiation (Fig. 5-4) is 31 keV, while the mean energy produced during ^{60}Co gamma irradiation (Fig. 5-6) is 761 keV. The stopping power of liquid water for electrons of these two energies is 9.44 MeV/cm and 1.91 MeV/cm, respectively. The spectrum of
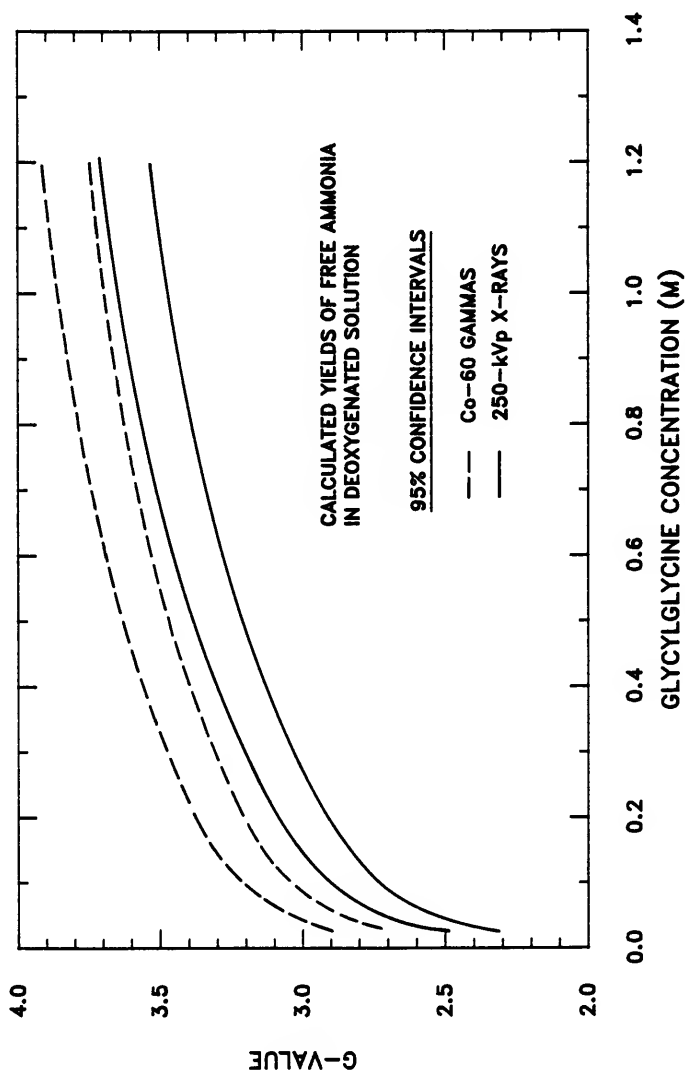
Fig. 7-1. Calculated yield of free ammonia in deoxygenated solution. Solid lines indicate the limits of the 95% confidence interval for simulated irradiations by 250-kVp X-rays. Dashed lines give similar limits for simulated ^{60}Co-gamma irradiations.

electron initial energies is therefore of lower energy and thus higher LET in the case of X irradiation than in the case of ^{60}Co gamma irradiation. As was discussed in the previous chapter, increases in mean LET of electron tracks result in a greater intratrack consumption of hydrated electrons, thus reducing the number available to react with the solute and produce free ammonia.

Comparison Between Calculated and Experimental Yields

For each irradiation condition, a comparison between calculated and experimental yields of free ammonia is an important step in supporting both the reaction mechanisms and calculational techniques of the computer simulations. To make such a comparison, Fig. 7-2 plots the 95% confidence interval for calculated yields of free ammonia under X irradiation. Also shown are measured yields of free ammonia as reported by Yoshida *et al.* (1988). Each point represents the mean and 95% confidence interval of several replicate-sample analyses.

Within the concentration range 0.05 M to 1.2 M, five of seven experimental means fall within the calculation's 95% confidence interval. At 0.05 M, the experimental mean falls just outside the lower confidence limit of the calculations, yet there is substantial overlap between experimental and calculated confidence intervals. At the highest concentration considered, 1.2 M, the experimental mean falls just outside the upper confidence limit of the calculations; still, there is overlap between confidence intervals at this concentration.
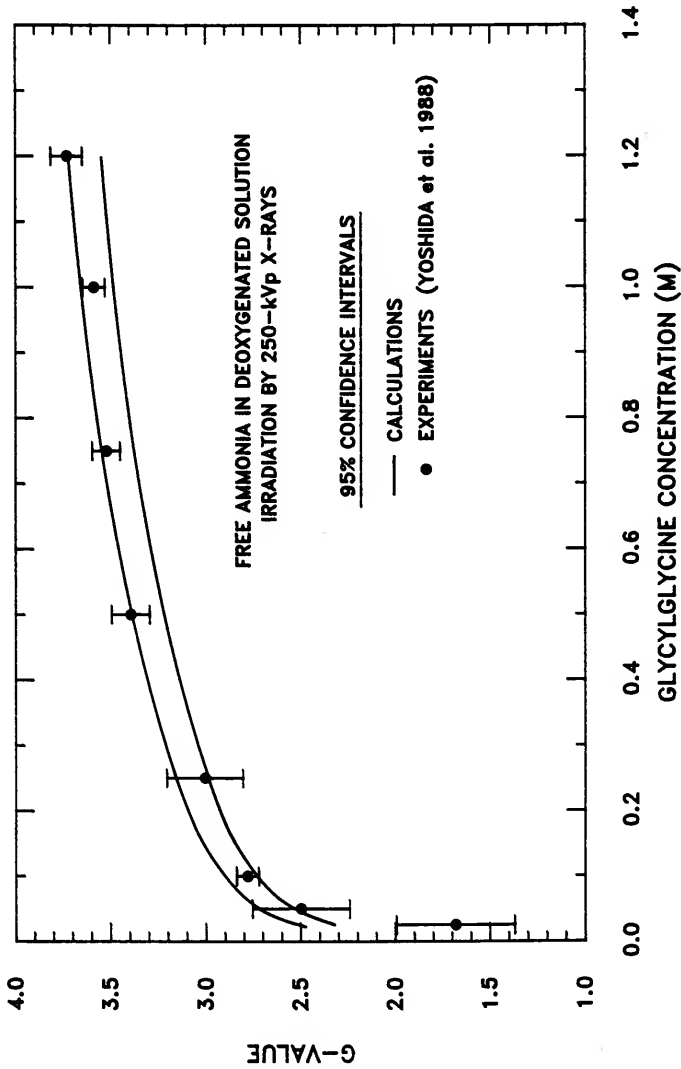
Fig. 7-2. Yield of free ammonia in deoxygenated solution. Solid curve indicates the limits of the 95% confidence interval for calculated yields of free ammonia. Points indicate measured mean yields from Yoshida et al. (1988). Error bars on the points give the 95% confidence interval as determined from replicate analysis.

At a solute concentration of 0.025 M, the simulations overestimate the yield of free ammonia as suggested by experiment. The calculated yield is 1.4 times the experimental yield at that concentration.

For ^{60}Co gamma irradiation, experimental yields of free ammonia are available at only two concentrations. Garrison *et al.* (1973) gives G-values and 95% confidence intervals of 2.8 ± 0.3 at 0.05 M glycylglycine and 3.8 ± 0.4 at 1 M glycylglycine. These confidence intervals are estimated from a reported ±5% reproducibility in the analyses. The corresponding calculated means and 95% confidence intervals shown in Fig. 7-1 for ^{60}Co gamma irradiation are 2.98 ± 0.09 at 0.05 M and 3.78 ± 0.09 at 1.0 M. Therefore, at 0.05 M glycylglycine, the experimental yield of Garrison *et al.* (1973) falls below the lower confidence limit of the calculations, yet there is overlap of confidence intervals. At 1.0 M glycylglycine, there is excellent agreement between experiment and calculations for ^{60}Co gamma irradiations.

Two conclusions are thus drawn from the discussions above. First, there is statistically significant agreement between calculated and measured yields of free ammonia for glycylglycine concentrations of 0.05 M to 1.2 M. Second, the simulation code tends to overestimate the yield of free ammonia at glycylglycine concentrations less than 0.05 M. Support for these conclusions rests primarily on the more extensive experimental data for X irradiations.

Discrepancies at Low Solute Concentrations

In Fig. 7-2, both calculated and experimental yields should
approach zero as the solute concentration approaches zero.
Discrepancies between measurements and calculations below 0.05 M
glycylglycine can be attributed to experimental error, error in
assumptions made within the simulation model, or both. With regard to
the experimental points, measured G-values at 0.025 M glycylglycine
correspond to very low concentrations of ammonia within irradiated
samples--concentrations which are above, but close to, the lower limit
of detection for the spectrophotometric analysis employed. Experimental
error thus increases with decreasing glycylglycine concentration.

Another likely explanation for the discrepancy at low concentration
is found in the manner by which the simulation model allows hydrated
electrons to react with the glycylglycine solute. During the
calculations, each hydrated electron within the track is given an
exponential probability of reacting with a glycylglycine molecule over
each simulated time interval. In this manner, the solute molecules
themselves are not modeled explicitly. The reaction probability used,
P_1, is given by:

$$P_1 = 1 - e^{-kC\Delta t} \ , \hspace{3cm} (7-1)$$

where k is the second-order rate constant for the reaction, Δt is the duration of the time interval, and C is the concentration of glycylglycine. In the calculations, C is assumed constant and equal to the initial solute concentration of the sample.

In situations where the total dose to irradiated sample is very large, however, there may be a substantial depletion of the solute at the end of the experiment and thus C does not remain constant. If this occurs, the use of Eq. (7-1) in the calculations would tend to overestimate hydrated electron scavenging and also free ammonia production.

To explore this possibility, one can consider the experimental point in Fig. 7-2 at 0.025 M for X irradiation. At that concentration, there is ~1.5 x 10^{19} glycylglycine molecules per cm^3 of solution prior to irradiation. The total absorbed dose to samples in these experiments is ~25,000 rads, or ~1.6 x 10^{18} eV/cm^3. Furthermore, Fig. 7-2 shows that G-value for ammonia production at 0.025 M is ~2.5 if one uses the calculated values as a conservative estimate. Thus, the G-value for the consumption of glycylglycine by e_{aq}^- attack is also ~2.5. In the assumption that attacks by OH and H radicals consume approximately the same number of molecules, the total G-value for the consumption of glycylglycine is ~5.0. At the end of the irradiation, the number of molecules consumed per cm^3 of solution is then (1.6 x 10^{18} eV/cm^3) x (5.0 molecules/100 eV), or ~8 x 10^{16} molecules/ cm^3. The percentage of total solute that is depleted is calculated at (8 x 10^{16}/1.5 x 10^{19}) x 100%, or 0.53%. At 1.2 M, the percentage is only 0.011%. The solute

concentration within the bulk solution thus remains essentially constant during these experiments.

Nevertheless, the calculations assume that solute concentrations in the _immediate_ vicinity of electron tracks remain constant between 10^{-12} s and 10^{-6} s. At initially low solute concentrations, depletion of glycylglycine within local track regions may persist at these early times. Use of Eq. (7-1) in these instances would, again, lead to overestimates of hydrated electron scavenging and free ammonia production.

It remains to be seen whether these arguments can explain the discrepancies at low glycylglycine concentrations observed in Fig. 7-2. Modeling individual solute molecules explicitly in the calculations, as is done with the radiogenic track species, would be one method of testing this hypothesis.

Estimate of Ammonia Production by Direct Interaction

The curves shown in Figs. 7-1 and 7-2 were calculated under the assumption that all free ammonia is produced by reactions between the glycylglycine solute and hydrated electrons produced within electron tracks. At high solute concentrations, however, free ammonia could be produced through direct interaction with the molecule by the incident radiation.

A rough estimate of the relative contribution of direct interactions can be made by considering the fractional volume occupied by the molecule in solution. The density of solid glycylglycine is 1.6

g/cm^3 and its molecular weight is 132; the molecular density of solid

glycylglycine is therefore calculated as:

$$N_s = \left[1.6 \ \frac{g}{cm^3} \right] \left[6.023 \times 10^{23} \ \frac{molecules}{mol} \right] \left(\frac{mol}{132 \ g} \right)$$

$$= \ 7.30 \times 10^{21} \ molecules/cm^3.$$

The specific volume of glycylglycine is then 1.37×10^{-22} cm^3/molecule.

The molecular density of glycylglycine in solution is given by:

$$N_w = \left[C \ \frac{mol}{l} \right] \left[\frac{1}{1000 \ cm^3} \right] \left[6.023 \times 10^{23} \ \frac{molecules}{mol} \right]$$

$$= \ 6.023 \times 10^{20} C \ molecules/cm^3 \ of \ solution,$$

where C is the molar concentration of glycylglycine. The fractional

volume occupied by glycylglycine molecules in solution is given by:

$$F_s = \left[1.37 \times 10^{-22} \ \frac{cm^3}{molecule} \right] \left[6.023 \times 10^{20} C \ \frac{molecules}{cm^3 \ soln} \right]$$

$$= \ 0.0825C.$$

At 1.2 M glycylglycine, F_s = 0.099. As a result, approximately 10% of

all electron interactions with the medium involve direct hits to the

glycylglycine molecule. Furthermore, one can make the assumption that

all covalent bonds are equally susceptible to direct interactions and that only a hit to the N–C bond between the amino group and the N–terminal α–carbon results in the release of ammonia. With these assumptions and by noting that glycylglycine has 18 covalent bonds in the zwitterion form, the fraction of all radiation interactions producing free ammonia is estimated at (0.10/18), or 0.0055. The direct action of radiation is therefore not considered a significant source of additional free ammonia, even at a concentration of 1.2 M.

Other Products

Equation (1–8) is used to calculate microsecond yields of other products from the radiolysis of glycylglycine in deoxygenated systems. Figure 7–3 shows the resulting microsecond yield of deamination radicals calculated as a function of glycylglycine concentration from 0.025 M to 1.2 M. Figure 7–4 shows the similar yield for acetylglycine. In both figures, product yields are shown to be higher for ^{60}Co irradiation than for X irradiation. Consider, for the moment, the microsecond yield of these two products and the yield of free ammonia as the solute concentration is slowly increased. As a reference, the yields of these three products are plotted together in Fig. 7–5.

At very low concentrations, a rapid initial increase in the yield of both free ammonia and deamination radicals is expected. At some solute concentration below 0.025 M, solute scavenging of deamination
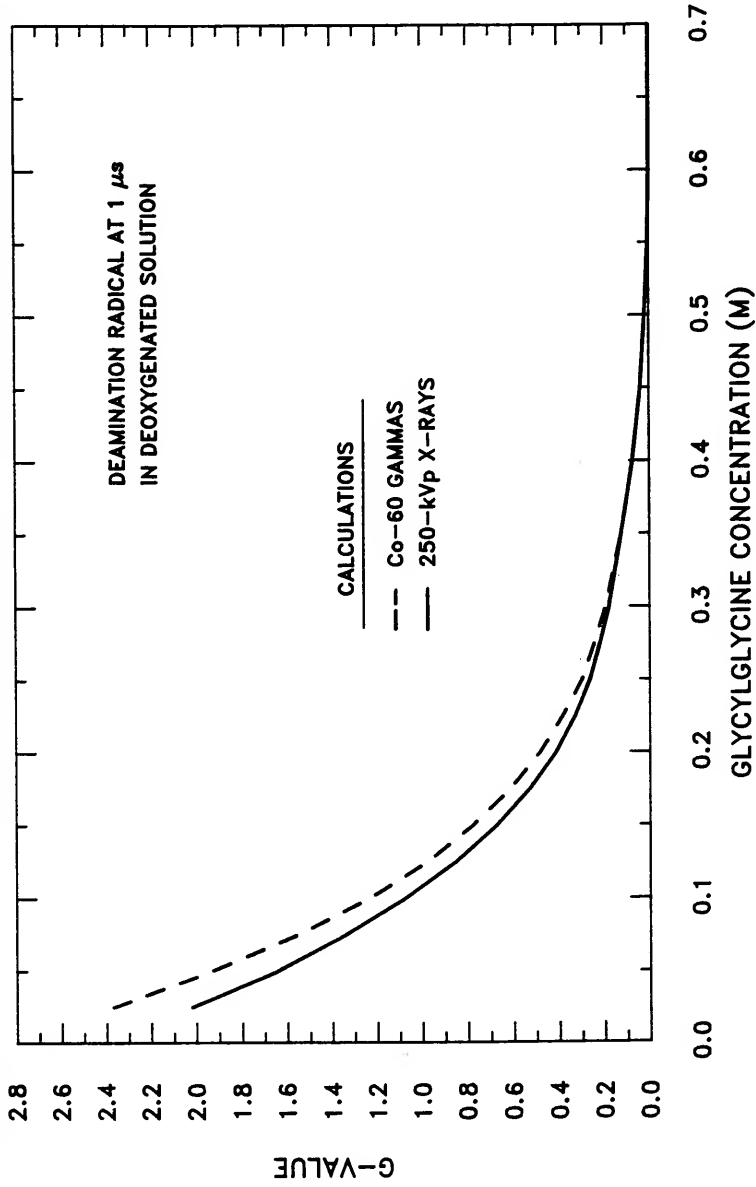
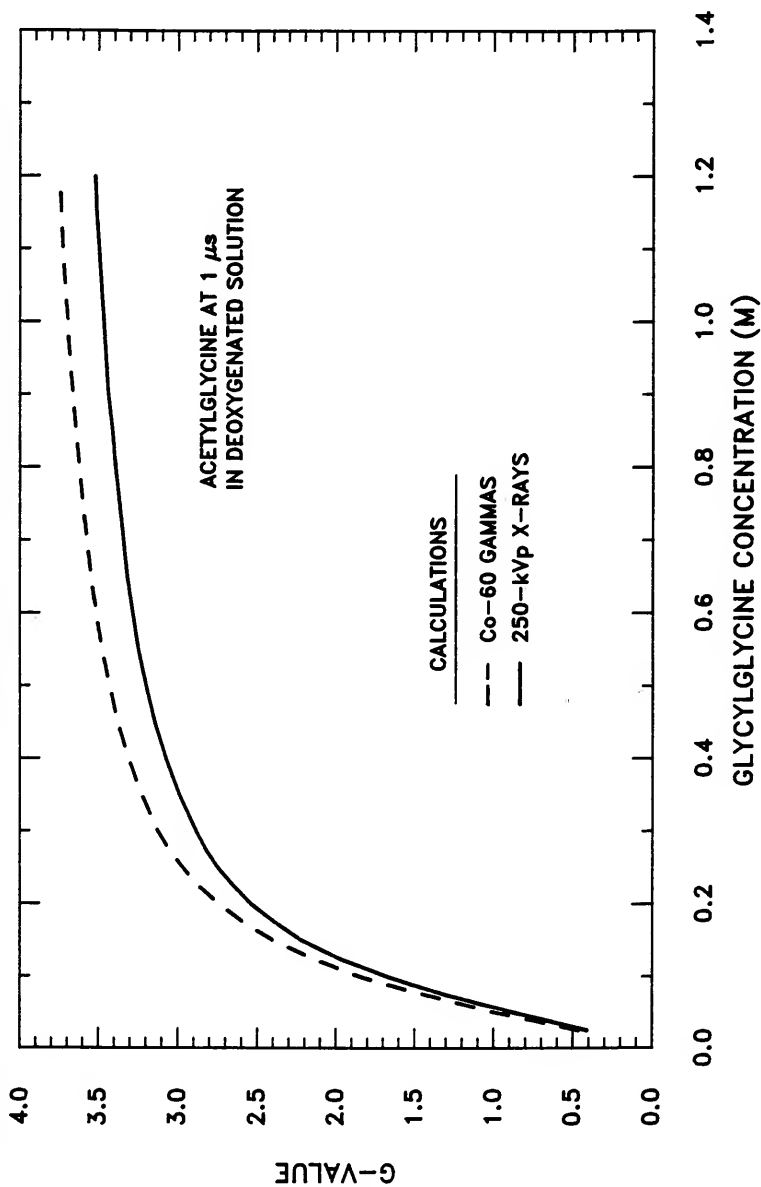Fig. 7-3. Microsecond yield of deamination radicals as a function of glycylglycine concentration.

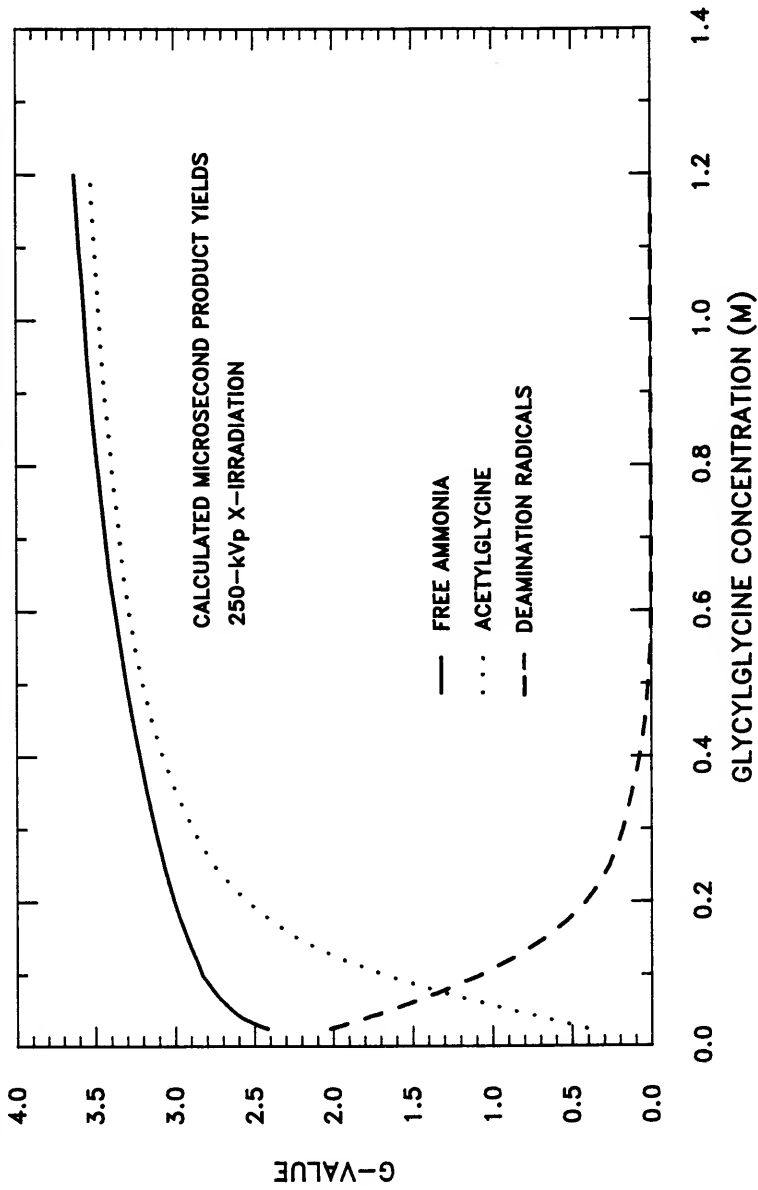Fig. 7-4. Microsecond yield of acetylglycine as a function of glycylglycine concentration.

Fig. 7-5. Microsecond yield of free ammonia, acetylglycine, and deamination radicals as a function of glycylglycine concentration.

radicals by reaction (4-13) (p. 112) occurs prior to a microsecond; correspondingly, there is a fall in the yield of deamination radicals and an increase in the yield of acetylglycine. Further increases in solute concentration continued to reduce the microsecond yield of deamination radicals. At ~0.6 M, no deamination radicals remain at a microsecond and the yield of acetylglycine nearly equals that of free ammonia. The slight difference between the yield of free ammonia and acetylglycine at high concentrations is accounted for by a small number of deamination radicals which, instead of being scavenged by the solute, react with themselves or with H-abstraction radicals to form succinic and aspartic acid precursors, respectively. Microsecond yields of these two acid precursors are shown in Figs. 7-6 and 7-7. No discernible difference is observed between the two radiations sources.

The yield of H-abstraction radicals as a function of solute concentration is plotted in Fig. 7-8 for both X and ^{60}Co irradiation. The effects of track structure and solute concentration on the dynamics of e^-_{aq} scavenging (as discussed in the previous chapter) are the same with regard to OH and H scavenging in the production of H-abstraction radicals. Reactions (4-1) and (4-2) (p. 111), however, are not the only source of H-abstraction radicals. As shown in reaction (4-13) (p. 112), solute scavenging of deamination radicals produces H-abstraction radicals in addition to producing acetylglycine. By subtracting the yield of acetylglycine from the total yield of H-abstraction radicals, one can obtain the fraction of H-abstraction radicals which are due to OH and H scavenging alone. This is shown in Fig. 7-9 for samples under

149

Fig. 7-6. Microsecond yield of succinic acid precursor as a function of glycylglycine concentration.

ASPARTIC ACID PRECURSOR AT 1 μs
IN DEOXYGENATED SOLUTION

G-VALUE

GLYCYLGLYCINE CONCENTRATION (M)
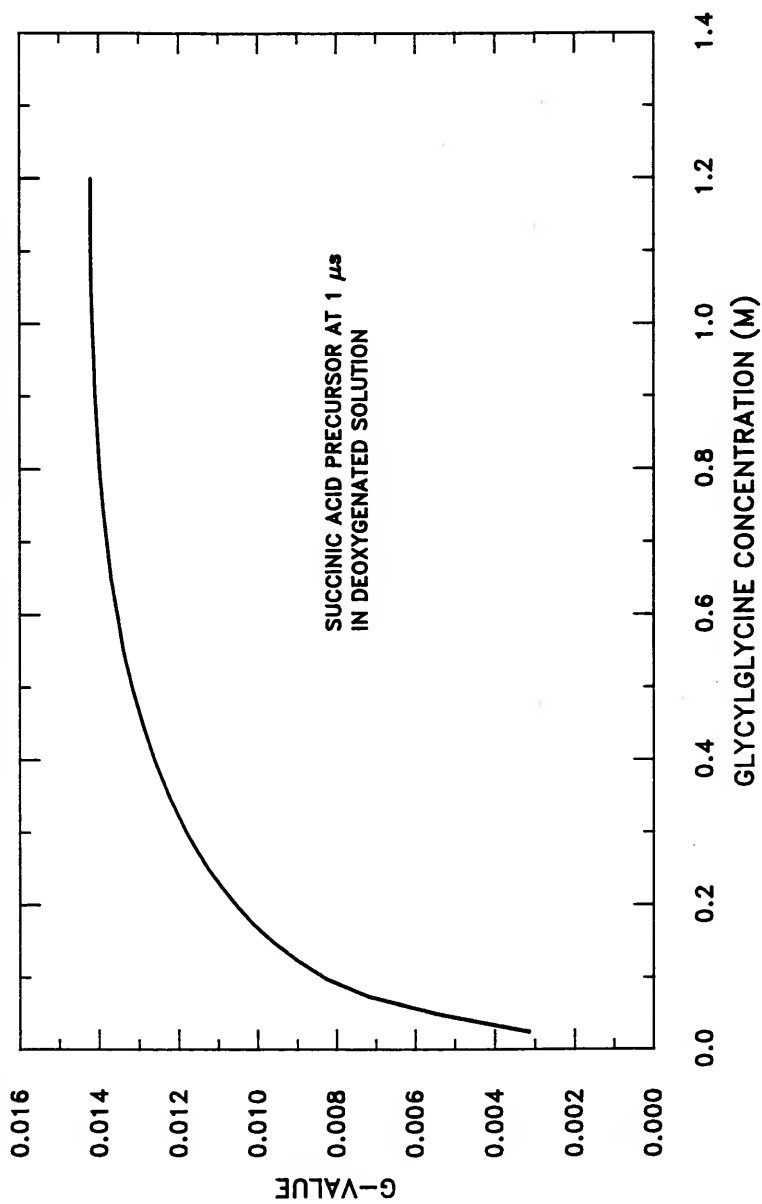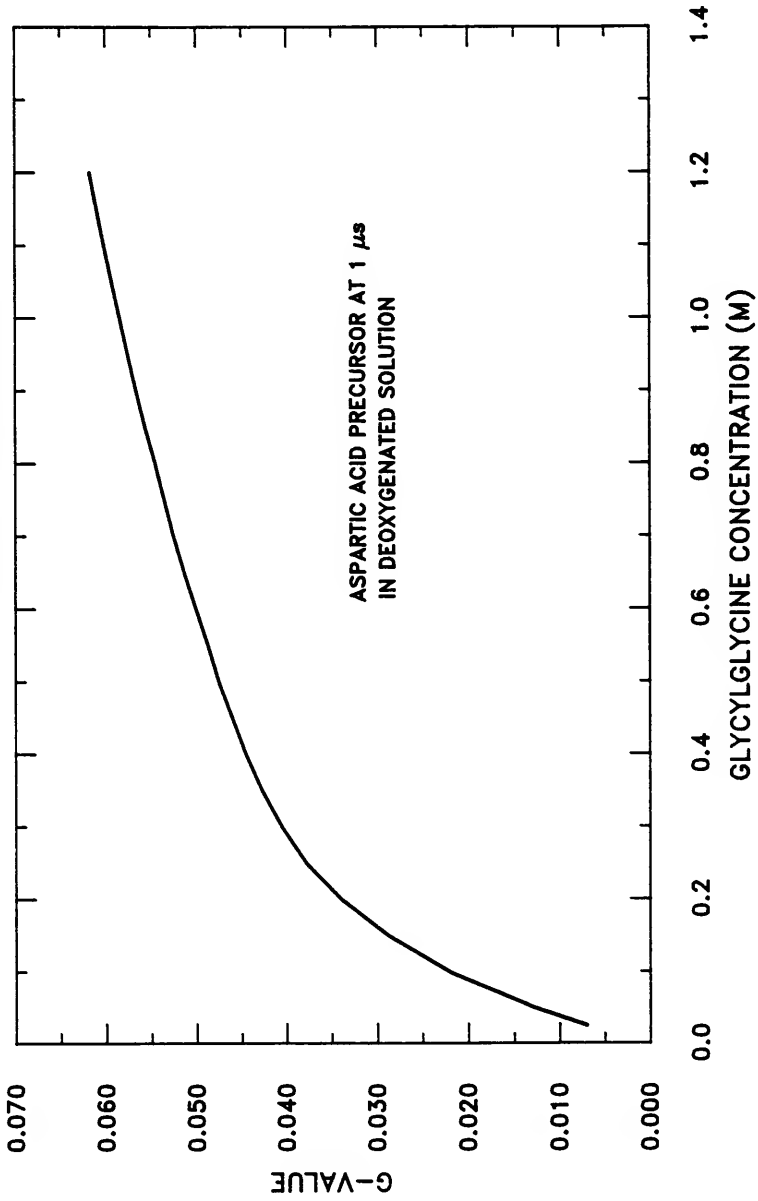
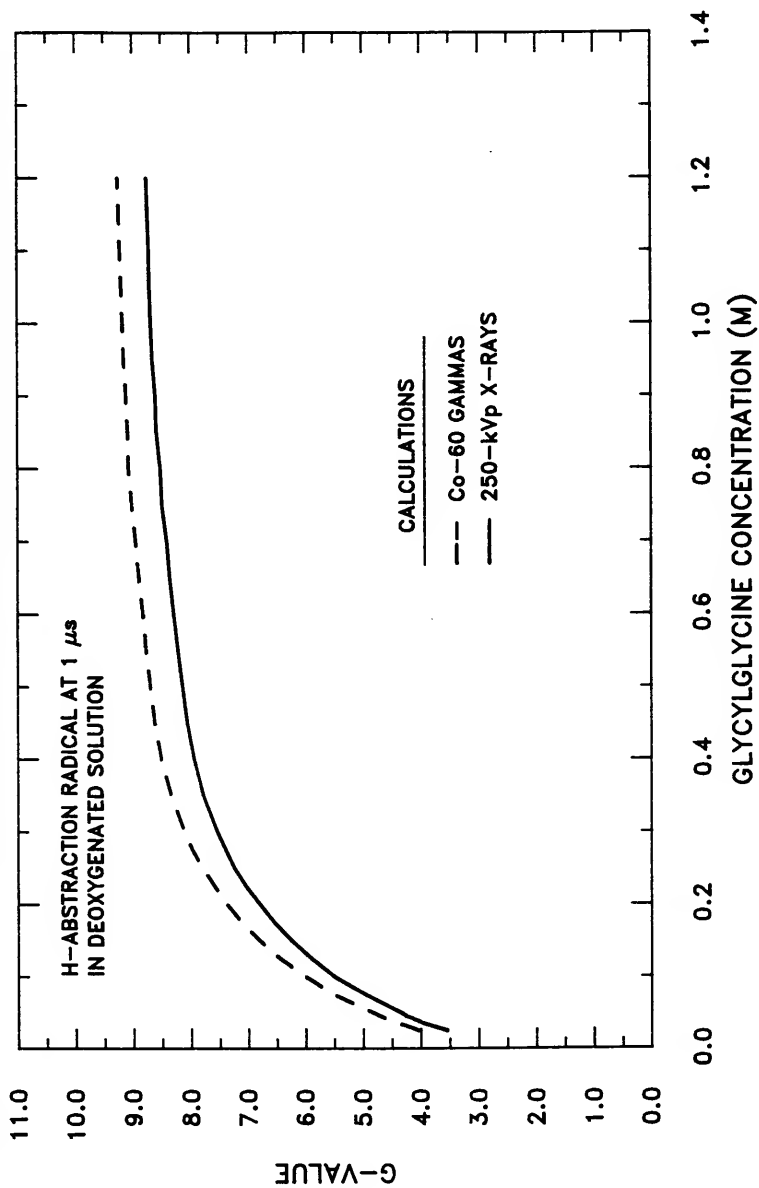Fig. 7-7. Microsecond yield of aspartic acid precursor as a function of glycylglycine concentration.

Fig. 7-8. Microsecond yield of H-abstraction radicals as a function of glycylglycine concentration.
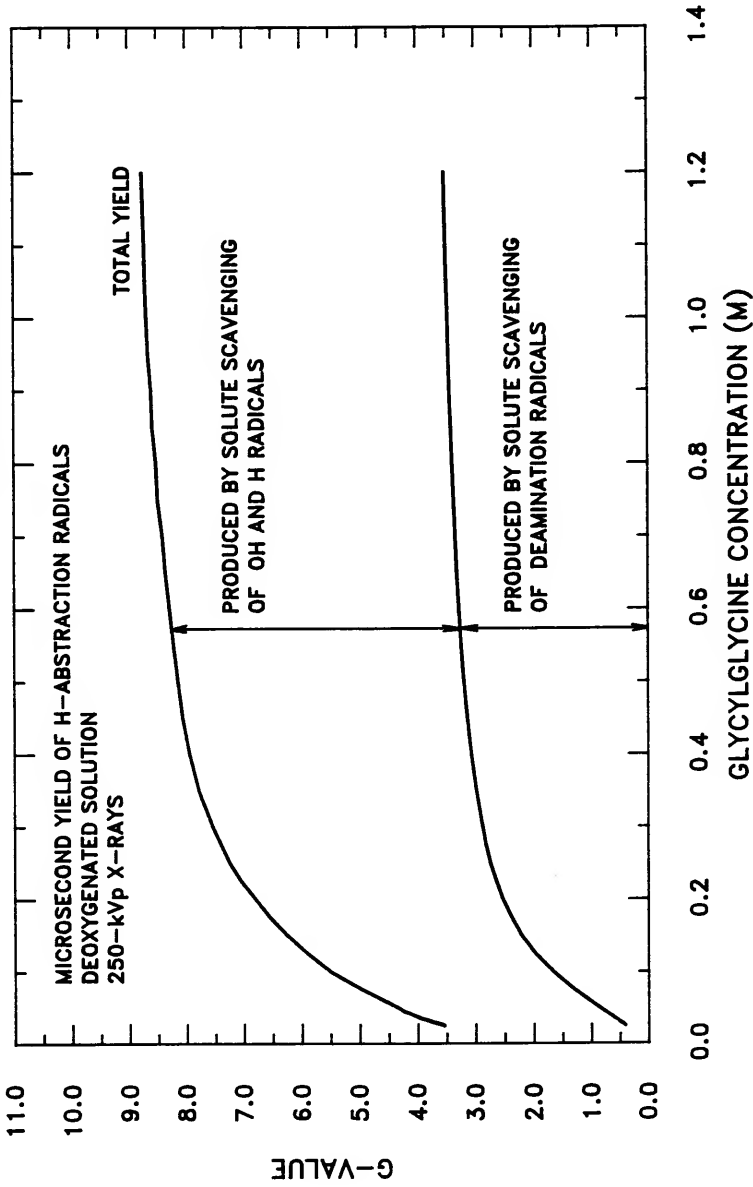
Fig. 7-9.   Partitioning of the microsecond yield of H-abstraction radicals into that produced from OH and H radical attack and that from solute scavenging of deamination radicals.

X irradiation. Roughly 40% of H-abstraction radicals are produced through secondary scavenging of deamination radicals.

Not shown in Fig. 7-9 are the small fraction of H-abstraction radicals which react with deamination radicals to form the aspartic acid precursor, or react with themselves to form either the diaminosuccinic acid precursor via reaction (4-7a) or $NH_3^+CH_2CON\!=\!CHCOO^-$ via reaction (4-7b) (p. 112). Calculated microsecond yields for the latter two products are shown in Figs. 7-10 and 7-11, respectively.

Calculated yields for the H radical at a microsecond are shown in Fig. 7-12. At concentrations below 1.2 M, H radicals are still present at a microsecond. As the solute concentration is decreased, it is expected that a larger fraction of these radicals, although very dilute, will react with one another according to $H + H \longrightarrow H_2$ as opposed to being scavenged by the solute. The rate constants for these two reactions are 1.0×10^{10} M^{-1} s^{-1} and 5.2×10^6 $M^{-1}s^{-1}$, respectively.

The calculated microsecond yield of hydrogen peroxide is shown in Fig. 7-13 as a function of solute concentration for both radiation sources. As discussed in the previous chapter, H_2O_2 yields are less in ^{60}Co-irradiated samples than in X-irradiated samples due to increased OH scavenging in the former system. Hydrogen peroxide is expected to contribute slightly to the yield of glycylamide, glyoxylic acid, and formaldehyde via reaction (4-12) (p. 112).

G-VALUE

GLYCYLGLYCINE CONCENTRATION (M)

DIAMINOSUCCINIC ACID PRECURSOR AT 1 μs IN DEOXYGENATED SOLUTION

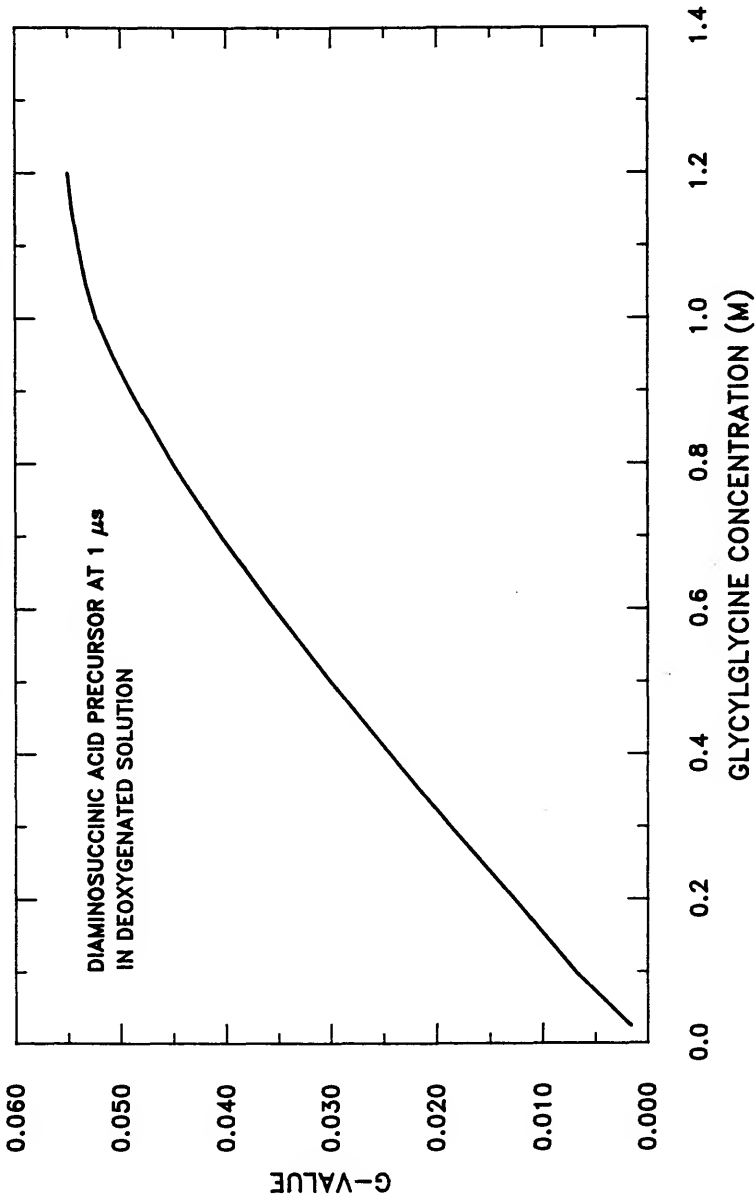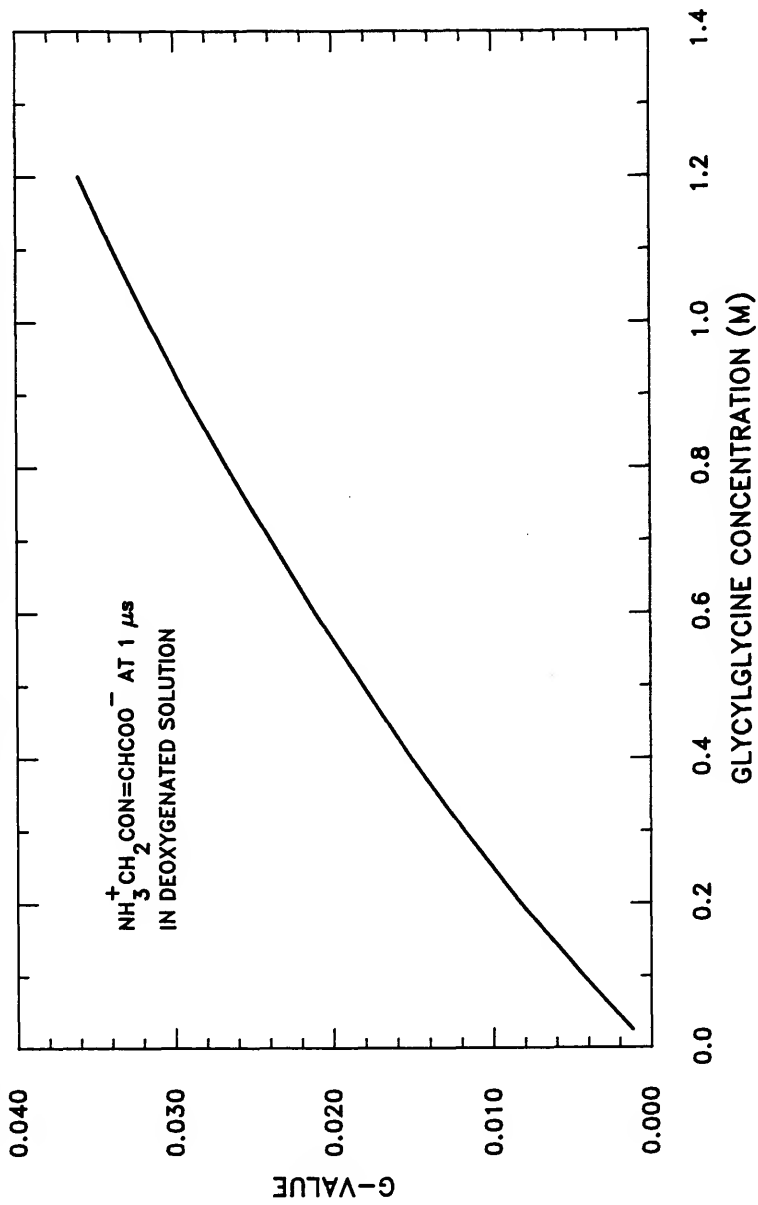Fig. 7-10. Microsecond yield of diaminosuccinc acid precursor as a function of glycylglycine concentration.

Fig. 7-11. Microsecond yield of $NH_3^+CH_2CON=CHOOO^-$ as a function of glycylglycine concentration.
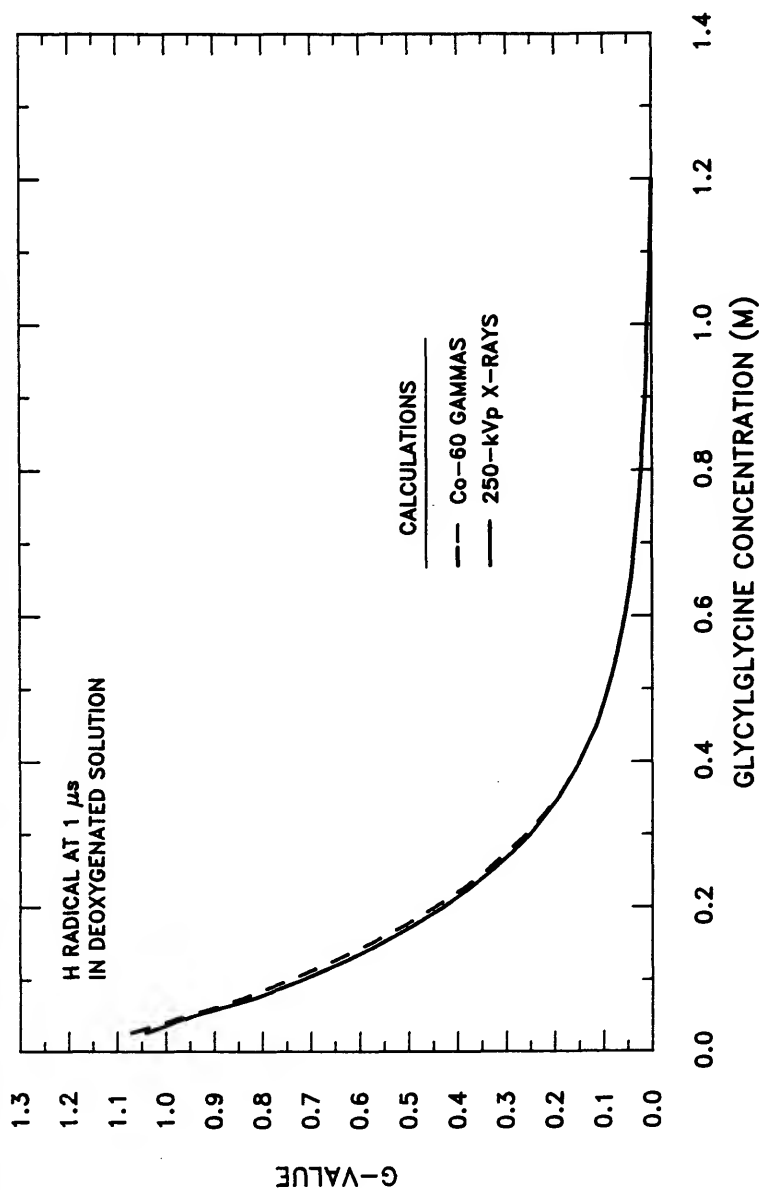
Fig. 7-12. Microsecond yield of H radicals as a function of glycylglycine concentration.
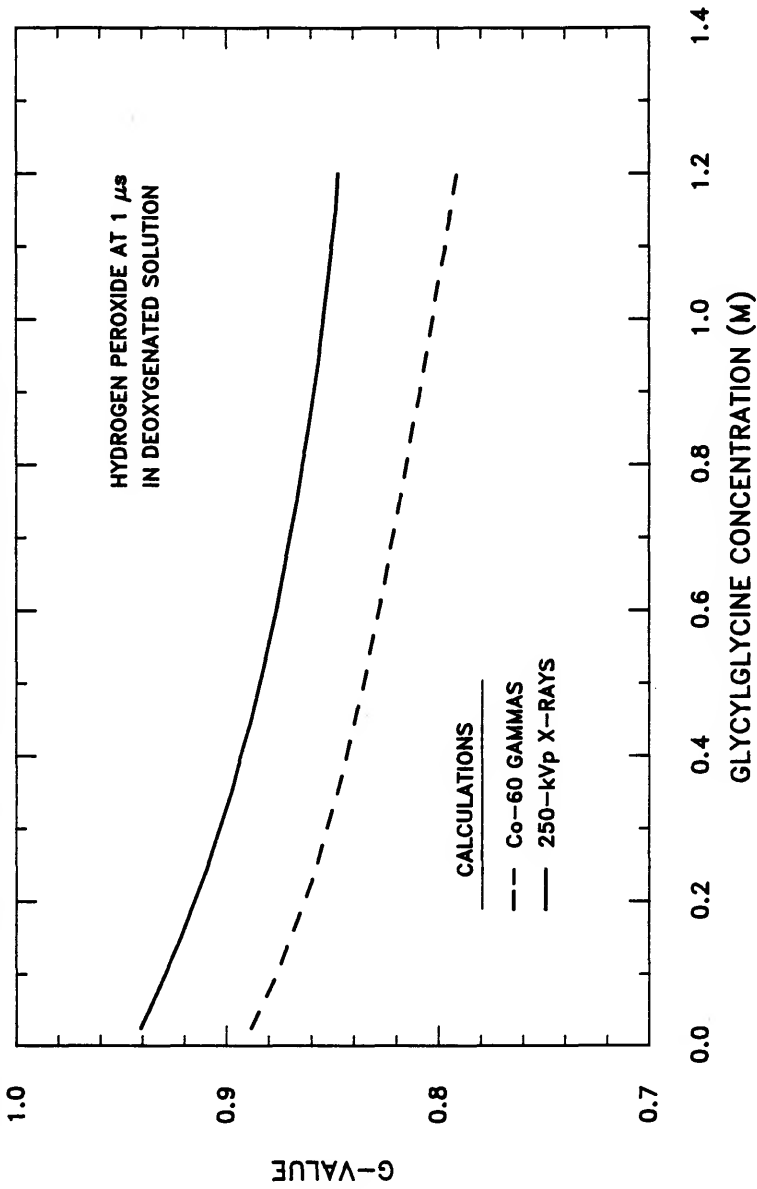
Fig. 7-13. Microsecond yield of hydrogen peroxide as a function of glycylglycine concentration.

CHAPTER 8

SUMMARY, CONCLUSIONS, AND RECOMMENDATIONS

Summary

The objective of this dissertation is to determine the feasibility of studying indirect radiation damage to biomolecules by using detailed Monte Carlo computer simulations. The molecule glycylglycine is chosen for this study primarily because its radiation chemistry is reasonably well characterized, thus limiting the number of unknown parameters in the simulation code. Good agreement between calculated and measured yields of radiolysis products supports the calculational approach and its usefulness in investigating more complex molecules, such as DNA.

This feasibility study involves three tasks. First, a Monte Carlo computer code is developed for simulating the radiolysis of glycylglycine in aqueous solution. Second, this model is used to calculate the yields of various products in systems irradiated either by 250-kVp X-rays or ^{60}Co gamma rays. Third, calculated yields of radiolysis products are compared to measured yields where available.

Development of the simulation model for glycylglycine radiolysis is presented in Chapters 2 through 4. Chapter 2 presents an existing set of computer models, developed at the Oak Ridge National Laboratory

158

(ORNL), which simulate the radiolysis of pure liquid water. Specifically, these codes model the transport of charged particles in liquid water and the formation, diffusion, and chemical reaction of free radicals and other species within their tracks. These calculations model chemical development of an individual charged-particle track up to one microsecond after its creation.

Previous calculations from these codes showed time-dependent yields of hydrated electrons that were not in good agreement with yields measured by pulse radiolysis techniques. Consequently, several modifications are made to the ORNL model as part of this research so as to achieve better agreement. These modifications include a scheme for thermalizing subexcitation electrons and a scheme for adjusting the initial yield of reactant species. These and other modifications are presented in Chapter 3.

Chapter 4 details the simulation code, developed in this research, which models the radiolysis of glycylglycine in both deoxygenated and oxygenated aqueous solutions. In this chapter, the radiation chemistry of both these systems is presented, along with measured or estimated rate constants.

Results of simulated irradiations of aqueous glycylglycine solutions are presented in Chapters 5 through 7. Chapter 5 gives electron energy spectra produced within samples irradiated by 250-kVp X-rays and by ^{60}Co gamma rays. These spectra are calculated by considering the photon spectrum incident upon sample containers, the

filtration of the containers, and the transport of photons through the sample volume.

Chapter 6 reports microsecond yields of various radiolysis products in deoxygenated glycylglycine solutions. These yields are calculated for monoenergetic electrons at various solute concentrations. As discussed in Chapter 7, these energy-dependent, microsecond yields are weighted by the electron energy spectra of Chapter 5 to give microsecond product yields for all major radiolysis products as functions of glycylglycine concentration.

Several end products are formed during the irradiation of deoxygenated glycylglycine solutions. Experimental data are limited to two sources: (1) free and amide ammonia for irradiations by 250-kVp X-rays at eight solute concentrations (Yoshida et al. 1988) and (2) several end products for irradiations by ^{60}Co gamma rays at two solute concentrations (Garrison et al. 1973). Calculations presented in this dissertation give yields of all products at one microsecond for both radiation sources. One of these products, free ammonia, is produced through solute scavenging of hydrated electrons, a process which is complete within one microsecond at solute concentrations as low as 0.025 M. Therefore, experimental support for the simulations in this dissertation rests upon the comparison of calculated and experimental yields of free ammonia.

Conclusions

Four major conclusions can be drawn from the research presented in this dissertation:

1. After modifying the ORNL simulation codes as outlined in Chapter 3, calculated yields of OH radicals and hydrated electrons in pure liquid water are in excellent agreement with yields measured by pulse radiolysis techniques.

2. For glycylglycine concentrations from 0.05 M to 1.0 M and for irradiation by 250-kVp X-rays, calculated yields of free ammonia are in statistically significant agreement with measured yields .

3. Calculated yields of free ammonia exceed measured yields at a glycylglycine concentration of 0.025 M.

4. At the 95% confidence level and at glycylglycine concentrations from 0.025 M to 1.2 M, the yield of free ammonia calculated under simulated irradiations by ^{60}Co gamma rays is greater than that calculated under simulated irradiations by 250-kVp X-rays.

The significance of each conclusion is discussed below, along with an overall assessment of the feasibility study.

Excellent agreement between calculated and experimental yields of OH radicals and hydrated electrons in pure water is demonstrated in Fig. 3-6 (p. 54). Measured yields shown in this figure represent the only experimental data currently available at times less than 10^{-8} s. Such agreement is therefore necessary and significant in supporting these computer simulations of electron energy deposition and radiation chemistry in pure water.

Good agreement between calculated and measured yields of free ammonia, shown in Fig. 7-2 (p. 138), is significant in several respects. First, all parameters in the simulation code are independently selected and no adjustment is made to "fit" the measured yields of Yoshida *et al.* (1988). Therefore, the good agreement shown results from a unique and independent attempt at simulating the events occurring within an irradiated solution of glycylglycine. Second, free ammonia is released as a direct result of solute reactions with hydrated electrons; consequently, agreement between calculated and measured yields of free ammonia at several concentrations gives further evidence that the code correctly simulates the formation, diffusion, and reactions of hydrated electrons. Secondary radicals resulting from H and OH attack do not form measurable end products until the late chemistry of the system ($>10^{-6}$ s) is complete; therefore, definitive conclusions concerning the simulation of these free radicals cannot be made until the yields of

these other products are both calculated and measured over a comparable range of solute concentrations.

Disagreement between calculated and measured yields of free ammonia at 0.025 M glycylglycine suggests that the simulations overestimate reactions between hydrated electrons and the solute at low concentrations (< 0.05 M). As discussed in Chapter 7, this is predicted if appreciable solute depletion does occur at times prior to $\sim 10^{-9}$ s within individual electron tracks. Methods of verifying this hypothesis are outlined in Chapter 7.

Yields of free ammonia produced under simulated irradiations by 250-kVp X-rays and ^{60}Co gamma rays are shown in Fig. 7-1 (p. 136). A statistically significant difference is shown between calculated yields produced by the two radiation sources. Although the measurements of Garrison et al. (1973) at 0.05 M and 1.0 M do suggest higher yields of free ammonia under ^{60}Co irradiation, more data are needed before this difference can be supported experimentally. Nevertheless, these results do demonstrate that the simulations are sensitive to small changes in charged-particle LET.

With regard to the objective of this dissertation, one can definitively state that Monte Carlo computer simulations represent a unique and feasible method of understanding indirect radiation damage at the molecular level. This assertion is supported by the following items. First, the simulations predict yields of free ammonia consistent with experiment over the concentration range 0.05 M to 1.2 M

glycylglycine. This is a necessary and minimum requirement of the feasibility study.

Second, the simulations are able to mechanistically explain several phenomena. For example, the dependence of free ammonia yields on both electron energy and solute concentration is readily understood in terms of track diffusion, track LET, and the competition between intratrack and solute consumption of hydrated electrons. These effects also underlie the difference in the yields produced under simulated irradiations by X-rays and ^{60}Co gamma rays.

Third, these simulations provide information that, in most instances, would be difficult to obtain experimentally. For example, the model readily provides product yields as a function of time during the interval 10^{-12} s to 10^{-6} s within charged-particle tracks. This time interval is important since free radical scavengers exist in high concentration with cells; thus, indirect damage will be highly localized and will be complete well within this time interval.

Recommendations

Research goals necessary to the continued development of this calculational technique can be divided into short-term and long-term objectives. These are discussed separately below.

Short-term Research Objectives

A primary short-term objective is to resolve the disagreement between calculated and measured yields of free ammonia seen at glycylglycine concentrations below 0.05 M. At those low concentrations, treatment of hydrated electron scavenging by pseudo-first-order kinetics could very possibly account for overestimates of free ammonia production. Pseudo-first-order kinetics assumes that at no time during the simulation is the concentration of the solute appreciably depleted. At low solute concentrations and at early times within the chemical development of electron tracks, such depletion may occur. In order to test this hypothesis, simulations should be made whereby solute molecules are treated explicitly in the calculations. Local depletion of the solute, if it does occur, would be modeled and would lower the yield of free ammonia as suggested by experiment.

A second short-term objective is to model the late chemistry stage of glycylglycine radiolysis in deoxygenated solution. In this manner, calculated yields of end products other than free ammonia can be compared to measured yields. Measured products which are currently available include amide ammonia at eight concentrations for X irradiation (Yoshida et al. 1988) and all major products at two concentrations for ^{60}Co gamma irradiation (Garrison et al. 1973).

As an example of how these calculations can be performed, consider a system in which three species (A, B, and C) undergo the following reactions:

$$A + A \longrightarrow B \qquad\qquad (8\text{-}1)$$

$$B + C \longrightarrow D \qquad\qquad (8\text{-}2)$$

$$A + D \longrightarrow E \ . \qquad\qquad (8\text{-}3)$$
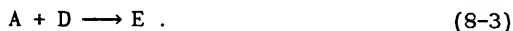
The rates of change in the concentration of these species with time are governed by the following coupled, differential equations:

$$\frac{d[A]}{dt} = -2k_{8\text{-}1}[A]^2 - k_{8\text{-}3}[A][D] + G(A)I$$

$$\frac{d[B]}{dt} = +k_{8\text{-}1}[A]^2 - k_{8\text{-}2}[B][C] + G(B)I$$

$$\frac{d[C]}{dt} = \quad - k_{8\text{-}2}[B][C] + G(C)I$$

$$\frac{d[D]}{dt} = \quad +k_{8\text{-}2}[B][C] - k_{8\text{-}3}[A][D] + G(D)I$$

$$\frac{d[E]}{dt} = \quad +k_{8\text{-}3}[A][D] + G(E)I \ ,$$

where k is the second-order rate constant, [X] is the concentration of product X, G(X) is the microsecond G-value of product X, and I is the dose rate used in the experiment. In Chapter 7, values of G(X) are given for all radiolysis products as functions of glycylglycine concentration. These equations can be solved numerically to give product concentrations as functions of the time following the beginning of the irradiation. Calculated steady-state concentrations would thus

correspond to late-time yields as measured in the laboratory. This approach was used by Chatterjee et $al.$ (1983) for irradiations of pure water systems and showed that steady-state concentrations were achieved some 10 seconds into the irradiation at a dose rate of 400 krad/min.

In order to supplement the data of Yoshida et $al.$ (1988) and Garrison et $al.$ (1973), measurements should be made of other radiolysis products over a wide range of solute concentrations. Such a complete set of experimental data would serve two important purposes. First, it would lend further experimental support to the reaction scheme presented in Chapter 4. Second, it would provide experimental checks on the calculations similar to the results shown in Fig. 7-2 (p. 138) for free ammonia.

For example, if the reactions presented in Chapter 4 are correct, the following two stoichiometric relationships should be met for irradiation of deoxygenated glycylglycine solutions:

$$G(NH_3^f) = G(\text{aspartic acid}) + 2G(\text{succinic acid}) + G(\text{acetylglycine})$$

and

$$G(NH_3^a) = G(\text{glyoxylic acid}) + G(\text{formaldehyde}).$$

These relationships should hold for all values of solute concentration and for both X and ^{60}Co gamma irradiations. If measured yields are not in agreement with these relationships, then the reaction mechanisms

assumed must not be correct and thus the simulation model which incorporates them is no longer valid.

A third short-term research objective is to simulate irradiation by alpha particles. In these calculations, particle transport would be made by the heavy-ion version of OREC. The same physical laws govern diffusion and chemical reaction within both alpha-particle tracks and electron tracks; therefore, chemical development of these simulated alpha-particle tracks would be calculated by the same two programs, SPCS and RADLYS, used and described in this dissertation.

Product yields are expected to differ greatly among samples irradiated by high-LET alpha particles and those irradiated by low-LET photons and electrons. For example, the increased spatial density of species within alpha-particle tracks would result in an increased intratrack consumption of hydrated electrons; thus the yield of free ammonia within alpha-particle tracks would be lower than that within photon-generated electron tracks. The spatial density of secondary peptide radicals would be greater within alpha-particle tracks; thus, the microsecond yield of the precursors to succinic, diaminosuccinic, and aspartic acid would be greater within these tracks than that within electron tracks. Comparison of calculated and experimental product yields for alpha-particle irradiations would be yet another significant test of the Monte Carlo simulations.

Finally, simulations and experiments could be conducted for irradiations of oxygenated solutions of glycylglycine. A Monte Carlo simulation code for this system is presented in the latter part of

Chapter 4. The reaction mechanisms in oxygenated solutions are very different from those occurring in deoxygenated solutions. In addition, the mechanisms presented in Chapter 4 were proposed by Makada and Garrison (1972) only for dilute glycylglycine systems, and thus the model presented in Chapter 4 is possibly limited to dilute solutions.

Long-term Research Objectives

Glycylglycine is investigated in this dissertation because it is a molecule whose radiation chemistry is well characterized. Modeling the irradiation of this molecule thus provides a means of evaluating the Monte Carlo simulation approach. However, as stated in the introduction, a highly desirable, long-term goal is to use this calculational technique to study radiation damage to DNA.

In order to elucidate the physical and chemical mechanisms of radiation-induced damage to DNA, a stepwise investigation would be advisable. These studies should start with attempts at understanding radiation damage to deoxyadenosine-5'-phosphate, deoxyguanosine-5'-phosphate, deoxycytidine-5'-phosphate, and deoxythymidine-5'-phosphate. These molecules are called nucleotides and are the four monomeric units of the DNA molecule. For each nucleotide, aqueous solutions of the molecule would be irradiated and analyzed. Reaction mechanisms would then be proposed to account for the radiation products observed. After incorporating these mechanisms into a Monte Carlo computer code, simulated irradiations would either support or question these reactions.

Once the radiation chemistry of these nucleotides is characterized, subsequent investigations could be made of single-stranded oligonucleotides (short polymers of nucleotides). Eventually, radiation damage to double-stranded oligonucleotides could be studied. Naturally, the ultimate goal of this research would be to understand radiation damage to cellular DNA.

The profession of health physics would benefit greatly from an understanding of the physical and chemical mechanisms of radiation damage to DNA. In the area of risk assessment, such an understanding could aid in the extrapolation of risk estimates for stochastic effects from high to low dose levels. By comparing mechanisms of different radiation types, one would have a better understanding of the relative risk of exposure to various radiation sources.

Understanding mechanisms of radiation damage to DNA can also provide a more fundamental basis for applied dosimetry and microdosimetry. Innovations from this research could result in personnel dosimeters designed as vials of oligonucleotides in aqueous solution. Radiation dose could then be defined as the number of altered molecules per unit mass, a definition of greater biological relevance than its current definition. Furthermore, radiation dose measured by this means would be assessed uniformly for all types of radiation. Consequently, application of the quality factor, with all its inherent uncertainties, would no longer be necessary.

REFERENCES

Adams, G. E., J. W. Boag, J. Currant, and B. D. Michael, Absolute Rate Constants for the Reaction of the Hydroxyl Radical with Organic Compounds. In *Pulse Radiolysis* (M. Ebert, J. P. Keene, A. J. Swallow, and J. H. Baxendale, Eds.). Academic Press, New York, 1965.

Abramovitch, S. and J. Rabani, Pulse Radiolytic Investigations of Peroxy Radicals in Aqueous Solutions of Acetate and Glycine. *J. Phys. Chem.* 80, 1562-1565 (1976).

Anbar, M., M. Bambeneck, and A. B. Ross, *Selected Specific Rates of Reactions of Transients from Water in Aqueous Solution - I. Hydrated Electron.* Report NSRDS-NBS 43, National Standard Reference Data System--National Bureau of Standards, 1973.

Anbar, M., Farhataziz, and A. B. Ross, *Selected Specific Rates of Reactions of Transients from Water in Aqueous Solution - II. Hydrogen Atom.* Report NSRDS-NBS 51, National Standard Reference Data System--National Bureau of Standards, 1975.

Attix, F. H., *Introduction to Radiological Physics and Radiation Dosimetry.* John Wiley & Sons, New York, 1986.

Bader, G., J. Chiasson, L. G. Caron, M. Michaud, G. Perluzzo, and L. Sanche, Absolute Scattering Probabilities for Subexcitation Electrons in Condensed H_2O. *Radiat. Res.* 114, 467-479 (1988).

Bethe, H. A., M. E. Rose, and L. P. Smith, Multiple Scattering of Electrons. *Proc. Am. Phil. Soc.* 78, 573-585 (1938).

Bevington, P. R., *Data Reduction and Error Analysis for the Physical Sciences.* McGraw-Hill, New York, 1969.

Boyd, A. W., M. B. Carver, and R. S. Dixon, Computed and Experimental Product Concentrations in the Radiolysis of Water. *Radiat. Phys. Chem.* 15, 177-185 (1980).

Braams, R., Rate Constants of Hydrated Electron Reactions with Peptides and Proteins. *Radiat. Res.* 31, 8-26 (1967).

171

Burns, W. G., R. May, and K. F. Baverstock, Oxygen as a Product of Water Radiolysis in High-LET Tracks. I. The Origin of the Hydroperoxyl Radical in Water Radiolysis. *Radiat. Res.* <u>86</u>, 1-19 (1981).

Chang, R., *Physical Chemistry with Applications to Biological Systems*, 2nd ed. Macmillan Publishing Co, Inc., New York, 1981.

Chatterjee, A., J. L. Magee, and S. K. Dey, The Role of Homogeneous Reactions in the Radiolysis of Water. *Radiat. Res.* <u>96</u>, 1-19 (1983).

Danjo, A. and H. Nishimura, Elastic Scattering of Electrons from H_2O Molecule. *J. Phys. Soc. Japan* <u>54</u>, 1224-1227 (1985).

Davies, J. V., M. Ebert, and A. J. Swallow, Reactions of the Hydrated Electron with Glycine and Other Amino Acids and Peptides. In *Pulse Radiolysis* (M. Ebert, J. P. Keene, A. J. Swallow, and J. H. Baxendale, Eds.). Academic Press, New York, 1965.

Downes, M. T., and H. C. Sutton, Reactions of the Hydroxy Peroxy Radicals $HOCH_2O_2$ and CH_3CHOHO_2 in Aqueous Solution. *J. Chem. Soc. Faraday Trans. I* <u>69</u>, 263-279 (1973).

Eriksen, T., A. Henglein, and K. Stockhausen, Pulse Radiolytic Oxidation of Chloral Hydrate in Oxygenated and Deoxygenated Aqueous Solution. *J. Chem. Soc. Faraday Trans. I* <u>69</u>, 337-345 (1973).

Farhataziz, and A. B. Ross, *Selected Specific Rates of Reactions of Transients from Water in Aqueous Solution - III. Hydroxyl Radical and Perhydroxyl Radical and Their Radical Ions*. Report NSRDS-NBS 59, National Standard Reference Data System--National Bureau of Standards, 1977.

Fermi, E., *Nuclear Physics*. University of Chicago Press, Chicago, 1949.

Garrison, W. M., Reaction Mechanisms in the Radiolysis of Peptides, Polypeptides, and Proteins. *Chem. Rev.* <u>87</u>, 381-398 (1987).

Garrison, W. M., H. A. Sokol, and W. Bennett-Corniea, Radiation Chemistry of Glycylglycine in Oxygen-Free Systems. *Radiat. Res.* <u>53</u>, 376-384 (1973).

Green, A. E. S., and D. E. Rio, Spatial Aspects of Radiological Physics and Chemistry. In *Proceedings of the Workshop on the Interface Between Radiation Chemistry and Radiation Physics*, pp. 65-72. Report ANL-82-88, Argonne National Laboratory, 1982.

Hamill, W. H., A Model for the Radiolysis of Water. *J. Phys. Chem.* <u>73</u>, 1341-1347 (1969).

Hamm, R. N., J. E. Turner, R. H. Ritchie, and H. A. Wright, Calculation of Heavy-Ion Tracks in Liquid Water. *Radiat. Res.* 104, S20–S26 (1985).

Hamm, R. N., H. A. Wright, R. H. Ritchie, J. E. Turner, and T. P. Turner, Monte Carlo Calculation of Transport of Electrons Through Liquid Water. In *Fifth Symposium on Microdosimetry* (J. Booz, H. G. Ebert, and B. G. R. Smith, Eds.), pp. 1037–1053. Commission of the European Communities, 1976.

Hayon, E., and M. Simic, Pulse Radiolysis Study of Cyclic Peptides in Aqueous Solution. Absorption Spectrum of the Peptide Radical –NHCHCO–. *J. Am. Chem. Soc.* 93, 6781–6786 (1971).

Hayon, E., and M. Simic, Acid–Base Properties of Organic Peroxy Radicals, ·OORH, in Aqueous Solution. *J. Am. Chem. Soc.* 95, 6681–6684 (1973).

Heller Jr., J. M., R. N. Hamm, R. D. Birkhoff, and L. R. Painter, Collective Oscillation in Liquid Water. *J. Chem. Phys.* 60, 3483–3486 (1974).

Hochanadel, C. J., Effects of Cobalt Gamma-Radiation on Water and Aqueous Solutions. *J. Phys. Chem.* 56, 587–594 (1952).

Ilan, Y., J. Rabani, and A. Henglein, Pulse Radiolytic Investigations of Peroxy Radicals Produced from 2-Propanol and Methanol. *J. Phys. Chem.* 80, 1558–1562 (1976).

ICRP, *Recommendations of the International Commission on Radiological Protection.* Report No. 26, International Commission on Radiological Protection, Pergamon Press, Oxford, 1977.

Itikawa, Y., Momentum-Transfer Cross Sections for Electron Collisions with Atoms and Molecules—Revision and Supplement, 1977. *Atomic Data and Nuclear Data Tables* 21, 69–75 (1978).

Jonah, C. D., M. S. Matheson, J. R. Miller, and E. J. Hart, Yield and Decay of the Hydrated Electron from 100 ps to 3 ns. *J. Phys. Chem.* 80, 1267–1270 (1976).

Jonah, C. D., and J. R. Miller, Yield and Decay of the OH Radical from 200 ps to 3 ns. *J. Phys. Chem.* 81, 1974–1976 (1977).

Kramers, H. A., On the Theory of X-ray Absorption and of the Continuous X-ray Spectrum. *Phil. Mag.* 46, 836 (1923).

Logan, S. R., Effects of Temperature on the Rates of Diffusion-Controlled Reactions. *J. Chem. Soc. Faraday Trans.* 63, 1712–1719 (1967).

Makada, H. A., and W. M. Garrison, Radiolytic Oxidation of Peptide Derivatives of Glycine in Aqueous Solution. *Radiat. Res.* 50, 48-55 (1972).

Masuda, T., K. Yoshihara, H. Shinohara, and M. Kondo, Reactivity of Aliphatic Peptides Toward Hydroxyl Radicals in Aqueous Solution. *J. Radiat. Res.* 17, 106-110 (1976).

Mozumder, A., Partially Diffusion-Controlled Reactions of Isolated Pairs in Condensed Media. *J. Chem. Phys.* 69, 1384-1391 (1978).

Neta, P., and R. H. Schuler, Rate Constants for Reaction of Hydrogen Atoms with Compounds of Biochemical Interest. *Radiat. Res.* 47, 612-627 (1971).

Noyes, R. M., Effects of Diffusion Rates on Chemical Kinetics. *Prog. Reaction Kinet.* 1, 129 (1961).

Ogura, H. and W. H. Hamill, Positive Hole Migration in Pulse-Irradiated Water and Heavy Water. *J. Phys. Chem.* 77, 2952-2954 (1973).

Palmer, K. F., and D. Williams, Optical Properties of Water in the Near Infrared. *J. Opt. Soc. Am.* 64, 1107-1110 (1974).

Paretzke, H. G., J. E. Turner, R. N. Hamm, H. A. Wright, and R. H. Ritchie, Calculated Yields and Fluctuations for Electron Degradation in Liquid Water and Water Vapor. *J. Chem. Phys.* 84, 3182-3188 (1986).

Rabani, J., D. Klug-Roth, and A. Henglein, Pulse Radiolytic Investigations of $OHCH_2O_2$ Radicals. *J. Phys. Chem.* 78, 2089-2093 (1974a).

Rabani, J., M. Pick, and M. Simic, Pulse Radiolysis of Cyclopentane in Aqueous Solutions. *J. Phys. Chem.* 78, 1049-1051 (1974b).

Rao, P. S., and E. Hayon, Interaction of Hydrated Electrons with the Peptide Linkage. *J. Phys. Chem.* 78, 1193-1196 (1974).

Ritchie, R. H., Interaction of Charged Particles with a Degenerate Fermi-Dirac Electron Gas. *Phys. Rev.* 114, 644-654 (1959).

Ritchie, R. H., R. N. Hamm, J. E. Turner, and H. A. Wright, The Interaction of Swift Electrons with Liquid Water. In *Sixth Symposium on Microdosimetry* (J. Booz and H. G. Ebert, Eds.), pp. 345-354. Commission of the European Communities, 1978.

Ritchie, R. H., C. J. Tung, V. E. Anderson, and J. C. Ashley, Electron Slowing-Down Spectra in Solids. *Radiat. Res.* 64, 181-204 (1975).

Ross, A. B., *Selected Specific Rates of Reactions of Transients from Water in Aqueous Solution*. Report NSRDS-NBS 43, Supplement, National Standard Reference Data System--National Bureau of Standards, 1975.

Scholes, G., P. Shaw, R. L. Willson, and M. Ebert, Pulse Radiolysis Studies of Aqueous Solutions of Nucleic Acids and Related Substances. In *Pulse Radiolysis* (M. Ebert, J. P. Keene, A. J. Swallow, and J. H. Baxendale, Eds.). Academic Press, New York, 1965.

Simic, M., The Chemistry of Peroxy Radicals and Its Implication to Radiation Biology. In *Fast Processes in Radiation Chemistry and Biology, Proceedings of the Fifth L H Gray Conference* (G. E. Adams, E. M. Fielden, and B. D. Michael, Eds.). John Wiley & Sons, New York, 1973.

Simic, M. G., Radiation Chemistry of Water-Soluble Food Components. In *Preservation of Food by Ionizing Radiation* (E. S. Josephson and M. S. Peterson, Eds.). Chemical Rubber Company, Boca Raton, 1983.

Simic, M., and E. Hayon, Reductive Deamination of Oligopeptides by Solvated Electrons in Aqueous Solution. *Radiat. Res.* 48, 244-255 (1971).

Simic, M., P. Neta, and E. Hayon, Selectivity in the Reactions of e_{aq}^{-} and OH Radicals with Simple Peptides in Aqueous Solution. Optical Absorption Spectra of Intermediates. *J. Am. Chem. Soc.* 92, 4763-4768 (1970).

Sinclair, W. K., and R. J. M. Fry, Mechanisms of Radiation Interaction with DNA: Potential Implications for Radiation Protection. *Radiat. Res.* 112, 407-417 (1987).

Smoluchowski, M. von, Three Discourses on Diffusion, Brownian Movements, and the Coagulation of Colloid Particles. *Phys. Zeits.* 17, 557-571, 585-599 (1916).

Sonntag, C. von, *The Chemical Basis of Radiation Biology*. Taylor & Francis, London, 1987.

Spinks, J. W. T., and R. J. Woods, *An Introduction to Radiation Chemistry*. John Wiley & Sons, New York, 1976.

Sumiyoshi, T., and M. Katayama, The Yield of Hydrated Electrons at 30 Picoseconds. *Chem. Letters*, 1887-1890 (1982).

Tal, Y., and M. Faraggi, The Reaction of the Hydrated Electron with Amino Acids, Peptides, and Proteins in Aqueous Solution I. Factors Affecting the Rate Constants. *Radiat. Res.* 62, 337-346 (1975).

Tan, K. H., C. E. Brion, Ph. E. van der Leeuw, and M. J. van der Wiel, Absolute Oscillator Strengths (10 - 60 eV) for the Photoabsorption, Photoionisation and Fragmentation of H_2O. *Chem. Phys.* <u>29</u>, 299–309 (1978).

Todo, A. S., G. Hiromoto, J. E. Turner, R. N. Hamm, and H. A. Wright, Monte Carlo Calculations of Initial Energies of Electrons in Water Irradiated by Photons with Energies up to 1 GeV. *Health Phys.* <u>43</u>, 845–852 (1982).

Turner, J. E., R. N. Hamm, M. L. Souleyrette, D. E. Martz, T. A. Rhea, and D. W. Schmidt, Calculations for Beta Dosimetry Using Monte Carlo Code, OREC, for Electron Transport in Water. *Health Phys.* In press (1988a).

Turner, J. E., R. N. Hamm, H. A. Wright, J. T. Modolo, and G. M. A. A. Sordi, *User's Manual for PHOEL-2, A Monte Carlo Computer Code for Calculating Energies of Photoelectrons and Compton Electrons in Water*. Report ORNL/TM-6954, Oak Ridge National Laboratory, 1979.

Turner, J. E., R. N. Hamm, H. A. Wright, J. T. Modolo, and G. M. A. A. Sordi, Monte Carlo Calculation of Initial Energies of Compton Electrons and Photoelectrons in Water Irradiated by Photons with Energies up to 2 MeV. *Health Phys.* <u>39</u>, 49–55 (1980).

Turner, J. E., R. N. Hamm, H. A. Wright, R. H. Ritchie, J. L. Magee, A. Chatterjee, and Wesley E. Bolch, Studies to Link the Basic Radiation Physics and Chemistry of Liquid Water. *Radiat. Phys. Chem.* In press (1988b).

Turner, J. E., J. L. Magee, R. N. Hamm, A. Chatterjee, H. A. Wright, and R. H. Ritchie, Early Events in Irradiated Water. In *Seventh Symposium on Microdosimetry* (J. Booz, H. G. Ebert, and H. D. Hartfiel, Eds.), pp. 507–520. Commission of the European Communities, 1981.

Turner, J. E., J. L. Magee, H. A. Wright, A. Chatterjee, R. N. Hamm, and R. H. Ritchie, Physical and Chemical Development of Electron Tracks in Liquid Water. *Radiat. Res.* <u>96</u>, 437–449 (1983).

Upton, A. C., The Biological Effects of Low-Level Ionizing Radiation. *Scientific Am.* <u>246</u>, 41–49 (1982).

Villforth, J. C., R. D. Birkoff, and H. H. Hubbell, Jr., *Comparison of Theoretical and Experimental Filtered X-Ray Spectra*. Report ORNL-2529, Oak Ridge National Laboratory, 1958.

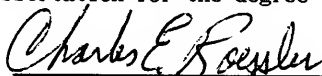Weast, R. C., *Handbook of Chemistry and Physics*, 57th ed. CRC Press, Cleveland, 1976.

Weinberg, A. M., and E. P. Wigner, *The Physical Theory of Neutron Chain Reactors*. University of Chicago Press, Chicago, 1958.

Willix, R. L. S., and W. M. Garrison, Chemistry of the Hydrated Electron in Oxygen-Free Solutions of Amino Acids, Peptides, and Related Compounds. *Radiat. Res.* 32, 452-462 (1967).

Wright, H. A., R. N. Hamm, J. E. Turner, J. L. Magee, and A. Chatterjee, Physical and Chemical Events that Follow the Passage of a Charged Particle in Liquid Water. In *Fourth Radiopharmaceutical Dosimetry Symposium*. Oak Ridge Associated Universities, 1985a.

Wright, H. A., C. E. Klots, R. N. Hamm, W. E. Bolch, and J. E. Turner, Computer Simulation of Chemical Reactions in Charged-Particle Tracks. Abstract Em-5, *36th Annual Meeting of the Radiation Research Society*, Philadelphia, Pennsylvania, April 16-21, 1988.

Wright, H. A., J. L. Magee, R. N. Hamm, A. Chatterjee, J. E. Turner, and C. E. Klots, Calculations of Physical and Chemical Reactions Produced in Irradiated Water Containing DNA. *Radiat. Prot. Dos.* 13, 133-136 (1985b).

Wright, H. A., J. E. Turner, R. N. Hamm, R. H. Ritchie, J. L. Magee, and A. Chatterjee, Physical and Chemical Evolution of an Electron Track in Liquid Water. In *Eighth Symposium on Microdosimetry* (J. Booz and H. G. Ebert, Eds.), pp. 101-109. Commission of the European Communities, 1983.

Yoshida, H., K. B. Jacobson, W. E. Bolch, and J. E. Turner, Radiation Chemistry of Glycylglycine: Measurements of Products. Abstract Em-11, *36th Annual Meeting of the Radiation Research Society*, Philadelphia, Pennsylvania, April 16-21, 1988.

Zoloratev, V. M., and A. V. Demin, Optical Constants of Water Over a Broad Range of Wavelengths, 0.1 Å - 1 m. *Opt. Spectrosc. (USSR)* 43, 157-161 (1977).

BIOGRAPHICAL SKETCH

Wesley E. Bolch was born in San Antonio, Texas, on March 16, 1961. He has lived in Gainesville, Florida, since 1967 where he graduated from Buchholz High School in 1979. He then entered the University of Florida that same year and received a Bachelor of Science in Engineering degree from the Department of Environmental Engineering Sciences in 1984.
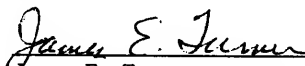
During that same year, Wesley entered the department's graduate program in health physics under a U.S. Department of Energy Health Physics Fellowship. He performed research in the area of neutron dosimetry and received his master's degree in May of 1986. His doctoral research in the area of microdosimetry was performed full-time at the Health and Safety Research Division of the Oak Ridge National Laboratory. He is a member of the Health Physics Society, the Radiation Research Society, and the American Nuclear Society.

I certify that I have read this study and that in my opinion it conforms to acceptable standards of scholarly presentation and is fully adequate, in scope and quality, as a dissertation for the degree of Doctor of Philosophy.

Charles E. Roessler, Chair
Professor of Environmental
Engineering Sciences

I certify that I have read this study and that in my opinion it conforms to acceptable standards of scholarly presentation and is fully adequate, in scope and quality, as a dissertation for the degree of Doctor of Philosophy.
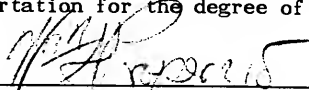
James E. Turner
Professor of Environmental
Engineering Sciences

I certify that I have read this study and that in my opinion it conforms to acceptable standards of scholarly presentation and is fully adequate, in scope and quality, as a dissertation for the degree of Doctor of Philosophy.

Joseph J. Delfino
Professor of Environmental
Engineering Sciences

I certify that I have read this study and that in my opinion it conforms to acceptable standards of scholarly presentation and is fully adequate, in scope and quality, as a dissertation for the degree of Doctor of Philosophy.

William S. Properzio
Associate Professor of
Environmental Engineering
Sciences

I certify that I have read this study and that in my opinion it conforms to acceptable standards of scholarly presentation and is fully adequate, in scope and quality, as a dissertation for the degree of Doctor of Philosophy.

Genevieve S. Roessler
Associate Professor of Nuclear
    Engineering Sciences

I certify that I have read this study and that in my opinion it conforms to acceptable standards of scholarly presentation and is fully adequate, in scope and quality, as a dissertation for the degree of Doctor of Philosophy.

Phillip M. Achey
Professor of Microbiology and
    Cell Science

This dissertation was submitted to the Graduate Faculty of the College of Engineering and to the Graduate School and was accepted as partial fulfillment of the requirements for the degree of Doctor of Philosophy.

August 1988

Dean, College of Engineering

Dean, Graduate School